# Durham E-Theses

## *Luminescence spectroscopy of cdte/cds based photovoltaic devices and associated materials*

Potter, Mark David George

**How to cite:**

Potter, Mark David George (2000) *Luminescence spectroscopy of cdte/cds based photovoltaic devices and associated materials*, Durham theses, Durham University. Available at Durham E-Theses Online: http://etheses.dur.ac.uk/4607/

**Use policy**

The full-text may be used and/or reproduced, and given to third parties in any format or medium, without prior permission or charge, for personal research or study, educational, or not-for-profit purposes provided that:

- a full bibliographic reference is made to the original source
- a link is made to the metadata record in Durham E-Theses
- the full-text is not changed in any way

The full-text must not be sold in any format or medium without the formal permission of the copyright holders.

Please consult the full Durham E-Theses policy for further details.

Academic Support Office, Durham University, University Office, Old Elvet, Durham DH1 3HP
e-mail: e-theses.admin@dur.ac.uk Tel: +44 0191 334 6107
http://etheses.dur.ac.uk

# Luminescence Spectroscopy of CdTe/CdS Based Photovoltaic Devices And Associated Materials

By Mark David George Potter

Submitted for the Degree of Ph.D.

University of Durham,

Department of Physics, 2000

**The copyright of this thesis rests with the author. No quotation from it should be published in any form, including Electronic and the Internet, without the author's prior written consent. All information derived from this thesis must be acknowledged appropriately.**

1 9 SEP 2001

I hereby declare that the work contained within this thesis is my own work and nothing that is a result of collaboration unless otherwise stated. No part of this work has been submitted for a degree or other qualification at this or any other university

The copyright of this thesis rests with the author. No quotation from it should be published without his prior written consent and information derived from it should be acknowledged.

# Abstract

This thesis contains primarily a study of CdTe/CdS heterojunction solar cells, chiefly using photoluminescence spectroscopy. These solar cells show a good potential for commercial power generation in the near future and are of interest to several major companies. A vital but little understood step in the manufacturing process is annealing the cells in the presence of chlorine prior to back contact application. Studies are performed on a selection of thin film CdTe/CdS cells subjected to $CdCl_2$ anneals of different duration. A chemical bevel etch was used to study the spectra at different depths into the sample and laser intensity and sample temperature variations to identify the mechanisms behind the observed photoluminescence peaks. Evidence was found for the $CdCl_2$ anneal promoting sulphur diffusion and subsequent grain boundary passivation in the CdTe, leading to increased minority carrier lifetimes and device efficiencies. Attempts to obtain electroluminescence from the CdTe/CdS solar cells were made. By using current pulses electroluminescence was obtained in the 780-850nm range with discernible spectral features.

Photoluminesence (PL) studies were also performed on a single crystal of CdTe grown to an unprecedented size of approx. 5 cm diameter at Durham university by a multi-tube seeded vapour method of crystal growth. Much higher resolution spectra were obtained for this than for the solar cells. Several peaks were identified and the mechanisms responsible were theorised. By taking slices of the crystal boule the PL spectra at different points throughout the bulk of the crystal were determined. A series of high quality ion-implanted CdTe crystals were also studied by intensity and temperature dependent PL in order to obtain a better understanding of the effects of known concentrations of known impurities on the PL spectra of CdTe. Specific PL features associated with certain dopants were observed.

# Index


| | | |
|---|---|---|
| | **Abstract** | ...3 |
| | **Index** | ...4 |
| 1 | **Introduction** | ...7 |
| | 1.1 CdTe based devices and applications | ...7 |
| | 1.2 Overview of my work | ...8 |
| | 1.3 References | ...9 |
| 2 | **Theory** | ...10 |
| | 2.1 Of semiconductors | ...10 |
| | 2.2 Of crystals and lattices | ...10 |
| | 2.3 Of Bloch theory and the reciprocal lattice | ...12 |
| | 2.4 Of real semiconductors | ...17 |
| | 2.5 Of optical effects | ...21 |
| | 2.6 Of phonons and excitons | ...26 |
| | 2.7 Of junctions and semiconductor devices | ...29 |
| | 2.8 Of photoluminescence spectroscopy | ...32 |
| | 2.9 Bibliography | ...35 |
| | 2.10 References | ...35 |
| 3 | **Experimental** | ...36 |
| | 3.1 Apparatus setup – photoluminescence | ...36 |
| | 3.2 Electroluminescence | ...39 |
| | 3.3 Sample mounting | ...39 |

| | | |
|---|---|---|
| | 3.4 Equipment calibration | ...40 |
| 4 | **Studies of a Single Crystal Boule of CdTe** | ...43 |
| | 4.1 Introduction | ...43 |
| | 4.2 Experimental | ...44 |
| | 4.3 Results and discussion | ...46 |
| | 4.4 Conclusions | ...60 |
| | 4.5 References | ...60 |
| 5 | **Studies of Bevelled CdTe/CdS Solar Cells** | ...63 |
| | 5.1 Introduction | ...63 |
| | 5.1.1 Thin film cells | ...65 |
| | 5.2 Experimental | ...69 |
| | 5.2.1 Device preparation | ...69 |
| | 5.2.2 Bevel etching | ...71 |
| | 5.3 Results and discussion | ...73 |
| | 5.3.1 Electrical characterisation | ...75 |
| | 5.3.2 Spatially resolved photoluminescence | ...75 |
| | 5.3.3 Temperature and intensity dependent photoluminescence | ...88 |
| | 5.3.4 Time resolved photoluminescence | ...92 |
| | 5.3.5 Electroluminescence | ...94 |
| | 5.4 Conclusions | ...95 |
| | 5.5 References | ...96 |
| 6 | **Studies of Ion Beam Implanted CdTe** | ...102 |
| | 6.1 Introduction | ...102 |

6.2 Experimental ...102

6.3 Results and discussion ...104

6.4 Conclusions ...119

6.5 References ...119

7 **Summary** ...121

7.1 Polycrystalline material ...121

7.2 Single crystal material ...122

7.3 Suggestions for future study ...123

7.4 references ...123

**Acknowledgements** ...124

**Appendices** ...125

# 1 Introduction

We live in an age of electrical technology. As far back as records go man has known of the terrible power of lightening, but since the discovery of electrical induction by Faraday in 1831 it has played an increasing role in the technological development of the human race. Our communications, transportation, entertainment trade and economy increasingly depend on the manipulation of this nebulous force. Central to the recent boom in consumer electronics, most notably in the field of information technology, is the ease with which electrical charge can be manipulated on an increasingly microscopic scale. The ubiquitous "silicon chip" is the mainstay of all modern computing devices and arguably one of the most important technological achievements of modern times. The key to the fine control over electricity is in the use of semiconductors. These are (as is discussed in more detail in the theory section) materials with properties between those of an insulator and a conductor, whose conductivity and other electrical characteristics can be influenced in a variety of ways including temperature, applied fields and currents, irradiation and chemical doping. Due to their electronic bandgaps, semiconductors also generally have a strong interaction with electromagnetic radiation. These factors allow the fabrication of a huge range of useful devices such as diodes, transistors, sensors and photovoltaic junctions. The homogeneous crystalline nature of semiconductors makes them suitable for miniaturisation, principally down to the size of the smallest lattice repeat units, but in practice limited by the resolution of the lithography used to define the devices.

## 1.1 CdTe Based Devices/Applications

CdTe, a II-VI semiconductor with a bandgap in the near infra red regime, has several current and potential applications in the fields of electronics and optics. One of its most potentially important applications in the next few years will be in the production of ploycrystalline thin film CdTe/CdS photovoltaic cells. CdTe has a very high optical absorption coefficient ($>10^4$cm$^{-1}$) due to its high atomic number and low bandgap and in its polycrystalline form (grain sizes of the order of microns typically), it can be deposited in thin films (8-10μm) with sufficient quality to form p-n junction devices. A detailed discussion of these devices will be saved for chapter 5 but suffice to say that moderate efficiencies (>10%) combined with low materials usage due to the thin film nature of the cells makes CdTe/CdS an attractive proposition for future large area terrestrial solar power applications.

High quality single crystal CdTe has uses in the area of radiation detection. Again due to its high absorption coefficient it makes a good solid state detector for high energy radiation such as X rays and Gamma rays, as is discussed in chapter 4. CdTe is also used as a substrate for the growth of $Hg_xCd_{1-x}Te$, which has a wide variety of applications in infra red detectors, lasers and LEDs.

The near infra red bandgap of CdTe means that it is a good transmitter for longwave radiation. With transmission of 60-70% for a wavelength range from 1-28μm[1] , it is a potentially useful material for infra-red windows and other optical components. Unlike some other infra-red optical transmitters CdTe is unaffected by atmospheric moisture.

In addition to these applications, CdTe has a number of properties which, while not currently greatly exploited commercially have potential for development. It exhibits thermoeletric properties which make it suitable for use in peltier effect coolers, though its efficiency in this role is only a fraction of a percent of that of the best materials. Under excitation by an electron beam, CdTe has been observed to lase at low temperatures, along with several other II-VI compounds. Attempts to create diode injection lasers using CdTe and CdTe/ZnTe junctions have resulted in spontaneous emission [1] , implying that lasing is possible. CdTe also exhibits the Gunn effect: when a DC voltage is applied across a randomly oriented sample it emits microwave radiation.

### 1.2 Overview of My Work

The principle concern of this thesis is the characterisation of the II-VI semiconductor cadmium telluride, though in the course of the work some analysis is also done on cadmium sulphide, another II-VI semiconductor used in conjunction with CdTe in solar cells. Using photoluminescence (PL) spectroscopy as the principal investigative tool, it is hoped that insight will be gained into the nature of the CdTe in various forms that are used in its principal applications, and the influence of the processing techniques on those properties. Since PL is highly sensitive to the presence of defects and impurities within the crystal lattice, and it is these that define the vital electrical characteristics of the CdTe, the analysis should be directly relevant to the manufacturers of such devices. The variation of PL emission with changes in temperature and illumination intensity, as well as with time on a nanosecond scale, is also influenced by the defect states responsible for the PL emission, and so all these techniques will be applied to further characterise the samples. Two main forms of CdTe will be studied in this thesis. The first is high purity single crystal CdTe, as used to manufacture radiation detectors both directly and as a substrate for the

growth of HgCdTe. In this case the manufacturing aim it to get as close as possible to a defect free crystal of CdTe, in order to have maximum electrical resistance and long carrier lifetimes. Medium/high resolution PL will be used to observe and characterise any sub-bandgap emission due to defects. Due to the spatial resolution of the PL being limited by the size of the laser spot used to excite the luminescence, in this case approximately 0.5mm, readings can be taken at an array of positions throughout a single CdTe crystal (single crystals can be grown up to several cm in diameter [2]) in order to detect any inhomogenieties in it due to the growth technique. Access to positions in the centre of the crystal can be obtained by cleaving. Also, intentionally doped monocrystalline samples will be studied in order to characterise the behaviour of specific dopants.

The second form of CdTe we will deal with is polycrystalline CdTe, as used in the manufacture of thin film photovoltaics. This is known to be a less pure form of CdTe with many structural defects and so only low-resolution photoluminescence will be applied due to the tendency of high defect concentrations and the polycrystalline nature of the material (grain sizes of the order of microns mean that the laser beam probes thousands of grains simultaneously, and each grain may have different properties) tend to broaden out the PL emission peaks. Since in this case the samples studied will be partially completed devices, the polycrystalline CdS layer will also be probed. The use of a chemical bevel will allow PL access below the surface of the CdTe in this case as the thinness of the devices (~10μm) makes cleaving impractical. The effects of varying $CdCl_2$ anneals (a vital step in the manufacturing process) on both materials will be studied. In addition to PL characterisation, attempts will be made to obtain electroluminescence (EL) from the samples in order to evaluate its worth as an analytical technique for CdTe/CdS solar cells and to obtain characteristic emission from the electrical p-n junction of the devices.

### 1.3 References


1. Ray, B., *II-VI Compounds.* 1969: Pergamon Press.
2. Aitken, N.M., *et al.*, *Characterisation of cadmium telluride bulk crystals grown by a novel "multi-tube" vapour growth technique.* Journal of Crystal Growth, 1999. **199**(Pt2): p. 984-987.

# 2 Theory

The theory provided here assumes some degree of familiarity with solid state physics and does not give complete proofs. For a more thorough treatment of the theories behind my work I recommend consulting a good specialised textbook such as Kittel[1], Ray[2], Kazowski[3], Bube[4], Perkowitz[5] or Seeger[6].

## 2.1 Of Semiconductors

A semiconductor can be defined in perhaps its crudest sense (and there are other definitions) as a material with an electrical resistance somewhere between that of a metal ($\sim 10^7 Sm^{-1}$) and that of an insulator ($\sim 10^{-8} Sm^{-1}$). The electrical transport properties of semiconductors vary greatly depending upon the makeup of the semiconductor, any impurities present in it and the temperature. Because of the relative ease with which differences in their transport properties can be made, semiconductors are the primary materials used in modern electronics. Integrated circuits, transistors, diodes, photovoltaics and radiation sensors are all efficiently manufactured from semiconductors.

Semiconductors normally incorporate elements from groups II to VI in appropriate stochiometric combinations to satisfy the valency of the atoms involved, eg. CdTe, GaAs, Si. As we will see below, due to their electronic structure semiconductors have strong and well defined interactions with electromagnetic radiation of optical or near optical wavelengths.

## 2.2 Of Crystals and Lattices

All semiconductors consist of regular arrangements of atoms in repeating units. This is known as a crystal lattice and is responsible for many of the unique properties of semiconductors. These repeating units can have several structures. The most common structure for compound semiconductors is the Zincblende lattice (see figure 2.1).

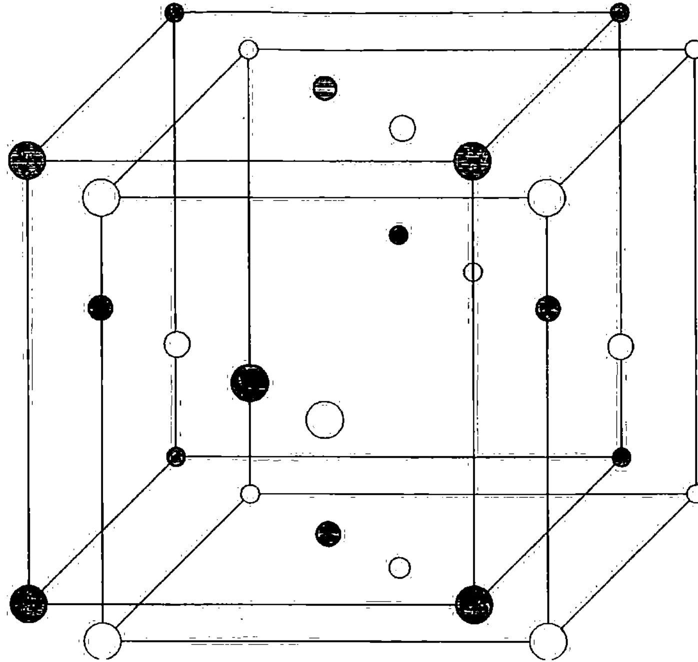

Figure 2.1: A zincblende crystal lattice

The atoms are arranged in a regular repeating structure. From a physical point of view, this means that the physical environment experienced by an electron and therefore the properties of the semiconductor at any given point are the same as those at any other point which is separated from the first by a lattice vector composed of integer numbers of the unit vectors of the basic repeat unit. For semiconductor theory it is convenient and realistic to assume an effectively infinite lattice. This array of discrete points, which appear to have the same arrangement when viewed from any other lattice point, is known as a Bravais lattice. The smallest repeating unit of a crystal lattice is known as the basis, and the smallest set of vectors connecting repeating points on the lattice are known as the primitive translation vectors. The smallest repeating unit can be found by drawing lines from one lattice point to all its near neighbours, and bisecting these lines perpendicularly with planes. The smallest volume enclosed by these plains is known as the Wigner-Seitz cell (see figure 2.2).

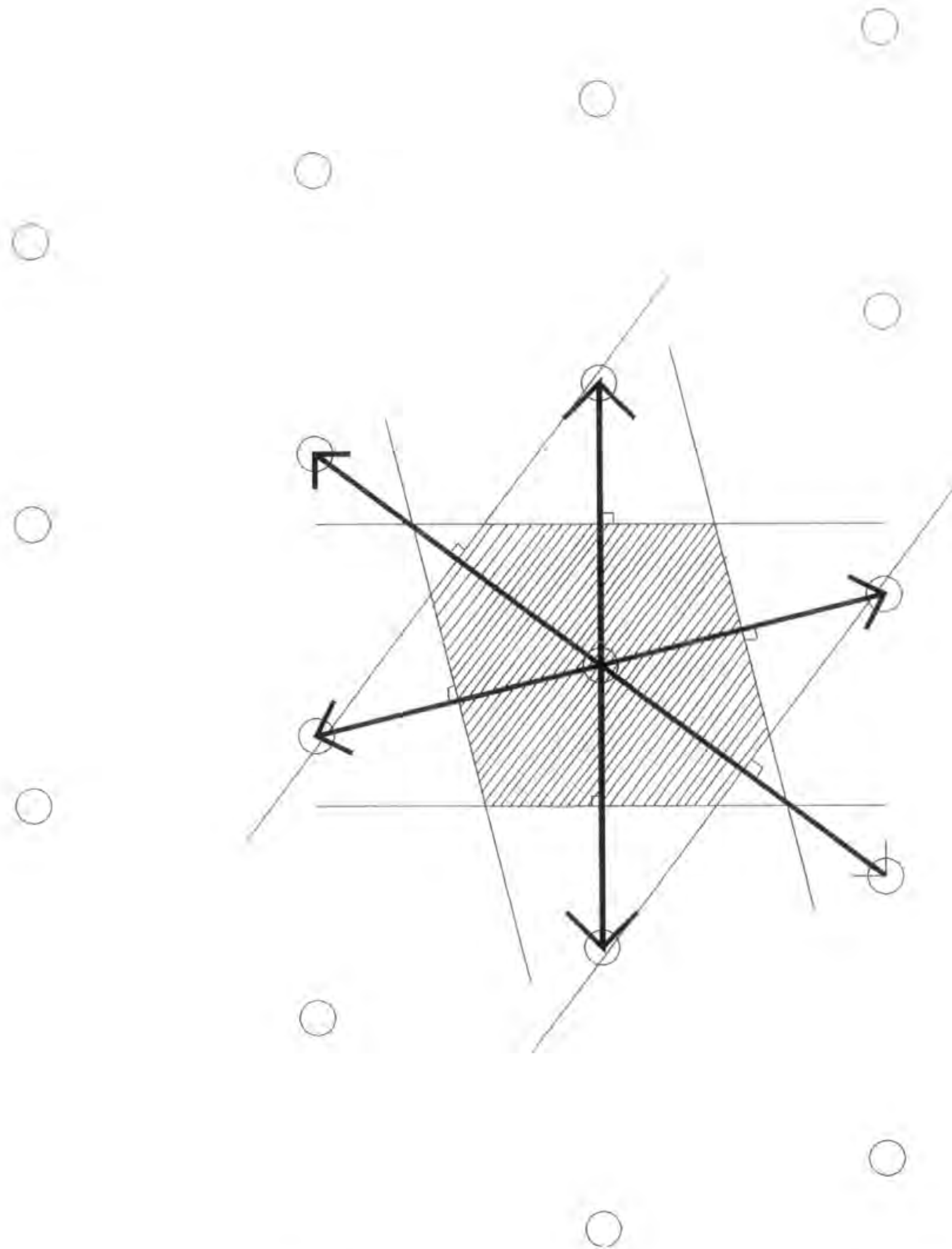

Figure 2.2: The Wigner-Seitz cell in 2 dimensions (hexagonal point lattice).

### 2.3 Of Bloch Theory and the Reciprocal Lattice

If the physical properties of a crystal lattice are the same in every unit cell, we can write this as:

$f(\underline{r}) = f(\underline{r}+\underline{R})$ where $\underline{R} = u_1\underline{a}_1 + u_2\underline{a}_2 + u_3\underline{a}_3$ (2.1)

Where f is any physical function, $\underline{r}$ is the position of any point in the crystal; $\underline{a}_1$, $\underline{a}_2$ and $\underline{a}_3$ are the primitive translation vectors and $u_1$, $u_2$ and $u_3$ are integers.

Any such regular, repeating function can be expressed as a Fourier series, using:

$$f(\underline{r}) = \sum_{mx,my,mz} A e^{i\underline{g}.\underline{r}} \tag{2.2}$$

$$\text{Where } \underline{g} = \frac{2\pi m_x \hat{\underline{x}}}{|\underline{a1}|} + \frac{2\pi m_y \hat{\underline{y}}}{|\underline{a2}|} + \frac{2\pi m_z \hat{\underline{z}}}{|\underline{a3}|} \tag{2.3}$$

NB. For the above to be true the co-ordinate system must be chosen along the lines of the primitive translation vectors. This also requires that the primitive vectors are mutually orthogonal, which is not always the case in real crystals. A more rigorous definition of $\underline{g}$ for an arbitrary set of primitive translation vectors is:

$\underline{g} = m_1\underline{b}_1 + m_2\underline{b}_2 + m_3\underline{b}_3$

Where $m_1$, $m_2$ and $m_3$ are integers, and (2.4)

$$\underline{b}_i = 2\pi \frac{\underline{a}_j \times \underline{a}_k}{\underline{a}_i \cdot (\underline{a}_j \times \underline{a}_k)} \tag{2.5}$$

Likewise, we find that

$$\underline{a}_i = 2\pi \frac{\underline{b}_j \times \underline{b}_k}{\underline{b}_i \cdot (\underline{b}_j \times \underline{b}_k)} \tag{2.6}$$

With i,j,k cyclic 1,2,3.

It can easily be shown that $\underline{R}.\underline{g}=2m\pi$, satisfying (2.1) when applied to (2.2), satisfying the condition for a periodic lattice.

This set of vectors g are known as reciprocal lattice vectors and define the reciprocal lattice, which like the crystal lattice is periodic, with a lattice spacing of 2π/a (a=crystal lattice parameter for a simple crystal). The primitive cell for the reciprocal lattice, called the first Brillouin zone, can be found using the same method as described above for finding the Weigner-Seitz cell.

The planes that form the edges of the unit cell in reciprocal space can be conveniently defined by Miller Indices. These are normals to the lattice planes in reciprocal space chosen so that the ratio of primitive vectors is integral. In the simple (primitive) cubic example (a simple cubic Bravais lattice gives rise to a simple cubic reciprocal lattice) the miller indices of a face of the cube would be (100). (110) would define a plane diagonal across the centre of the cube, and (111) would define a plane that is not parallel or normal to any face of the cube.

The Schrodinger equation can be used to describe electrons in a crystal potential:

$$\left[-\frac{\hbar^2}{2m}\nabla^2 + V(\underline{r})\right]\psi(\underline{r}) = E(\underline{r}) \tag{2.7}$$

A periodic potential in the crystal can be represented by the Fourier series:

$$V(\underline{r}) = \sum_m V_{(g_m)} e^{ig_m \cdot \underline{r}} \tag{2.8}$$

In order to satisfy periodicity of the wavefunction:

$$\psi(\underline{r}) = \psi(\underline{r} + \underline{R}) \tag{2.9}$$

It can be shown mathematically that the solution to the Schrodinger equation is:

$$\psi(\underline{r}) = \sum_m C_{(g_m)} e^{ig_m \cdot \underline{r}} e^{ik.\underline{r}} \tag{2.10}$$

This is known as the Bloch wavefunction and consists of two parts. The first part (as shown here) is periodic with the same period as the lattice spacing. The second part is the wavefunction for a free electron and defines the momentum of the electron via $\underline{p}=h\underline{k}/2\pi$. The values of the coefficients $C_{(gm)}$ are

dependent upon the periodic potential of the crystal. In the simple case of no periodic potential the solutions can be represented in an E-K diagram as shown:

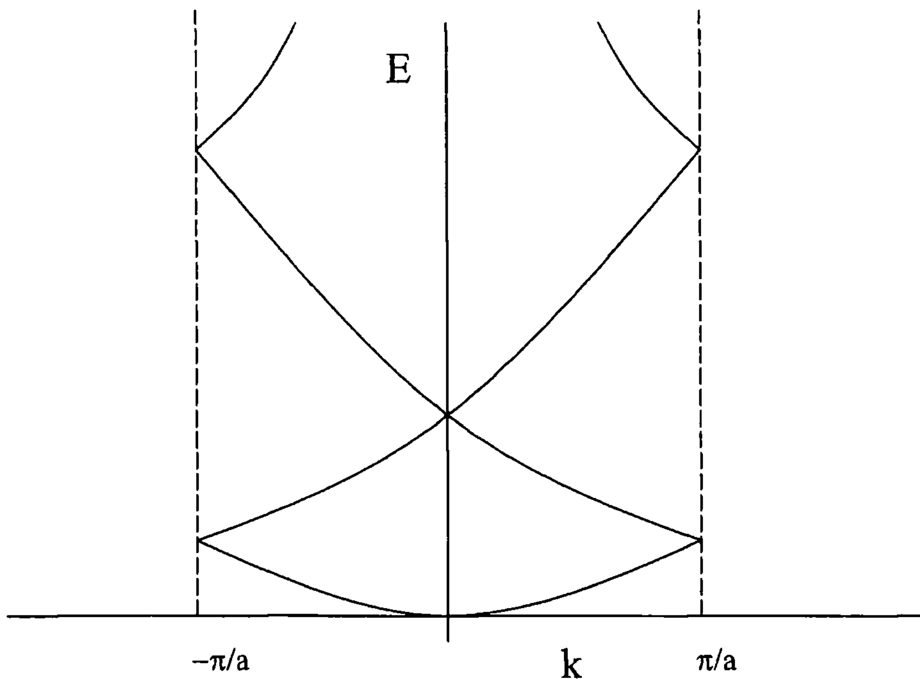


Figure 2.3: Bloch solutions to the Schrodinger equation in a periodic lattice with no periodic potential. (reduced scheme)

Since these solutions repeat every $2\pi/a$ in k-space we can obtain all useful information from these solutions by studying them only in the range $-\pi/a \leq k \leq \pi/a$. This region is called the first Brillouin zone. The figure above shows that there should be solutions to the Schrodinger equation for all values of E. However, to make our model more realistic for a crystalline material we must allow for the periodic potential of the lattice affecting the solutions.

Taking equation (2.8), we can neglect the m=0 term as this refers to the average potential of the lattice, which is not relevant to calculating the periodic perturbation.

If we assume that the perturbation is small, we can take equation (2.10) as representing the wavefunction with $C_{(g_m)} = 0$ for m>0 and $C_{(g_m)} \sim 1$ for m=0 (small perturbation theory).

We can then put (2.8) and (2.10) into the Schrodinger equation (2.7). Taking out a normalising factor from C of $1/(V_g^{1/2})$ we get:

$$\frac{1}{\sqrt{V_g}}\sum_m\left(\frac{\hbar^2}{2m}(k+g_m)^2 - E_{(k)} + \sum_l V_{(g_l)}e^{ig_l\cdot r}\right)D_{(g_m)}e^{i(k+g_m)\cdot r} = 0$$

(2.11)

Where D is the re-normalised form of C. This can be simplified by integrating over $V_g$ to

$$\left(\frac{\hbar^2}{2m}(k+g_n)^2 - E_{(k)}\right)D_{(g_n)}\sum_m V(g_n - g_m)D_{(g_m)} = 0$$

(2.12)

Approximating

$$E = \frac{\hbar^2 k^2}{2m}$$

And $D_{(0)}=1$, $D_{(>0)}=0$

We get:

$$D_{(g_n)} \approx \frac{-v(g_n)}{\frac{\hbar^2}{2m}\left[(k+g_n)^2 - k^2\right]}$$

(2.13)

It can be clearly seen that D becomes significant when $(k+g_n)^2=k^2$ for some value of $g_m=g_p$. This corresponds to approaching the edge of the Brillouin Zones. If we substitute this back into equation (2.12) we find that D(0) and $D(g_p)$ become the only significant terms. We thus have non-trivial solutions when $g_n=0$ and $g_m=g_p$:

$$\left(\frac{\hbar^2}{2m}k^2 - E_{(k)}\right)D_{(0)} + V(-g_p)D_{(g_p)} = 0$$

(2.14)

Also when $g_m=0$ and $g_n=g_p$:

$$\left(\frac{\hbar^2}{2m}(k+g_p)^2 - E_{(k)}\right)D_{(g_p)} + V(g_p)D_{(0)} = 0$$

(2.15)

Solving these two equations for $E_{(k)}$ gives us:

$$E = \frac{\hbar^2 k^2}{2m} \pm \left|V(g_p)\right|$$

$$(2.16)$$

Thus as we approach the zone boundaries there is a splitting in the energy levels dependent upon the periodic potential of the lattice. This can be represented on an E-k diagram as shown in figure 2.4:

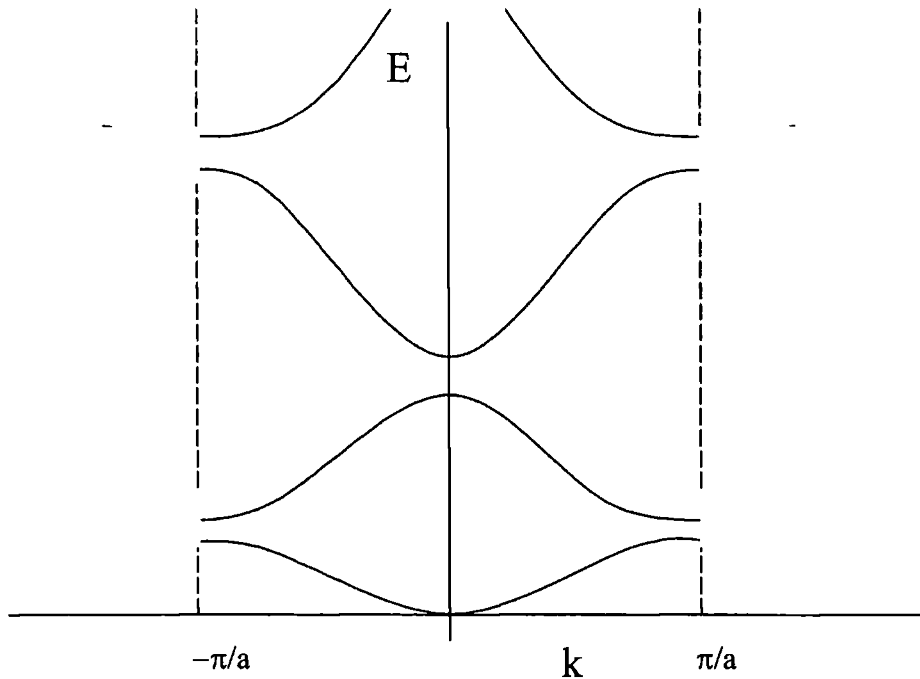


Figure 2.4: Bloch solutions in a periodic lattice with a weak periodic potential. (reduced scheme)

It can clearly be seen that there are regions of reciprocal space in which no solutions to the Schrodinger equation exist. These are known as bandgaps. In the case of a semiconductor the fermi level of the electrons lies within a bandgap, which accounts for the electrical properties of the semiconductor.

### 2.4 Of Real Semiconductors

In reality, the bandstructure of semiconductors is much more complex than we have considered here. In three dimensions the E-k diagram looks much different due to the intrinsic anisotropy of any crystal lattice. Also the periodic potential cannot be entirely approximated as a weak perturbation and splitting of bands occurs due to the spin-orbit interaction of the electrons. The real bandstructure of a typical semiconductor would look something like this:

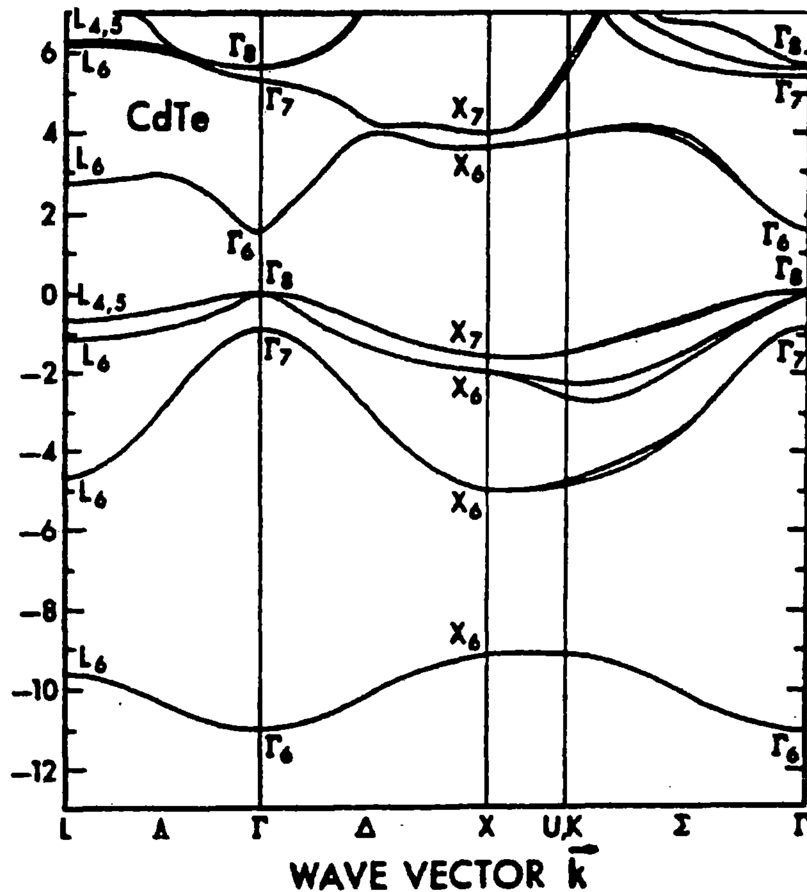


Figure 2.5: The bandstructure of Cadmium Telluride[1].

In the above figure convenient symmetry points in reciprocal space are used to allow a representative diagram of the energy levels to be drawn. The Γ point refers to the centre of the first Brillouin zone, where k=0 in any direction. The L point refers to the zone boundary with Miller indices [111], and the X point refers to the zone boundary with indices [100].

It is worth noting the splitting of the valence band in the region between the L point and the zone centre into two bands joining at the Γ point. The different curvatures of these bands give rise to "light holes" and "heavy holes". Transitions between the light and heavy hole bands can be important in some electronic processes such as Auger recombination (see later).

At very low temperatures approaching zero Kelvin, the electrons in any solid settle to their lowest states, filling the energy bands up to the Fermi energy. In this state a semiconductor will have a whole number of energy bands filled, with energy bands above the fermi level being completely empty. The highest filled energy band is known as the valence band, and the first empty energy band is the conduction band. In this state current flow is impossible as there are no unoccupied states for electrons to

move between within the limits of their thermal energy. As the temperature increases however, some electrons are excited thermally above the bandgap from the valence band to the conduction band. Electrons in the conduction band are free to move throughout the semiconductor as there are many free states in the conduction band for the electrons to move between. Also the liberation of electrons from the valence band leaves unoccupied states which valence band electrons can move into, allowing a flow of charge in the valence band as well (in this case it is normally considered as a flow of empty states or holes in the opposite direction to that of the electron migration). Thus as the temperature increases the conductivity increases, the opposite trend to metals. The electrons and holes move through the semiconductor with effective masses dependent upon the curvature of the energy bands in reciprocal space:

$$\frac{1}{m^*} = \frac{1}{\hbar^2} \frac{\partial^2 E}{\partial k^2} \tag{2.17}$$

In pure semiconductors this effect is very small at practical temperatures, limiting the uses of semiconductors. However, the increase of conductivity with temperature can be greatly enhanced by the process of doping. This involves substituting atoms of greater or lesser valency than the normal semiconductor atoms into the crystal lattice. From the point of view of the real lattice this means that the substitutional atoms will either donate an extra electron to the crystal lattice which will be free to conduct (known as n-type doping with a substitutional atom of greater valency) or remove an electron from the crystal lattice creating a hole which will be free to conduct (known as p-type doping with a substitutional atom of lesser valency).

From the point of view of energy bands the substitutional atoms create energy states within the bandgap close to a band edge. With only minimal thermal excitation electrons can be excited from the valence band to an acceptor level creating a hole which is free to carry current. Likewise electrons can be excited from a donor level to the conduction band to carry a current.

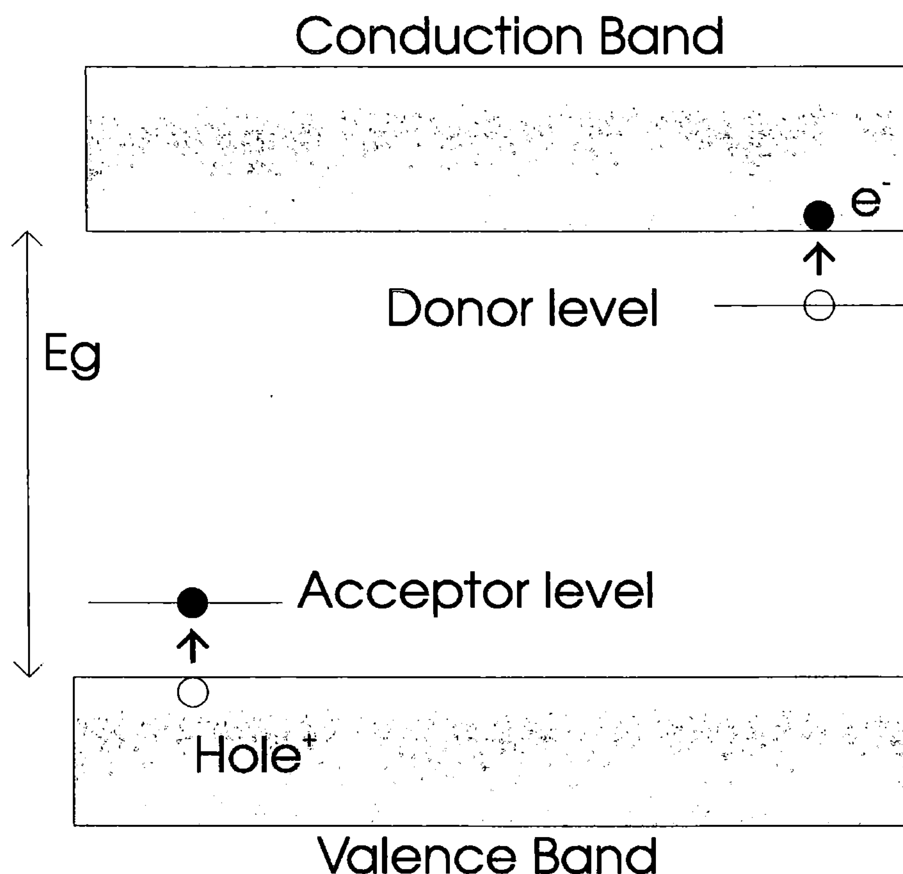


Figure 2.6: Donor and Acceptor impurity levels in a semiconductor.

Looking at the energy bands created by shallow donors and acceptors in more detail, they can be found to consist of a series of hydrogen like energy levels. Binding energies can be calculated from the hydrogenic model using the effective mass of the electron/hole and come to the order of tens of meV. Some types of impurity, typically substitutional transition metals or lattice defects, can cause impurity bands near the centre of the bandgap. These are known as deep level traps and tend to reduce conductivity and luminescence in semiconductors by absorbing free electrons or holes, which cannot be easily thermally excited back into the conduction or valence bands.

### 2.5 Of Optical Effects

Electrons bound to any atomic structure can undergo three processes in their interaction with photons: Absorption, spontaneous emission and stimulated emission.

Absorption occurs when a photon excites an electron from its current energy level to a higher level. The energy increase of the electron is equal to the photon energy as the photon is entirely absorbed in this process. In the case of semiconductors photons of energy less than the bandgap of the semiconductor are not normally absorbed as there are no states within the bandgap for electrons in the valence band to be excited to. The exception is at specific energies where electrons are excited to and from impurity levels within the bandgap, and so absorption spectroscopy is a useful tool to determine the existence and energy levels of impurity bands within a semiconductor. Absorption of photons with energy $>E_g$ can occur freely in *direct gap* semiconductors. These are semiconductors in which the minima of the conduction band as displayed on an E-k diagram occurs at the same k-value as the maxima of the valence band, since photons have negligible momentum compared to electrons and so can only directly cause vertical transitions on an E-k diagram due to conservation of momentum. In the case of *indirect gap* semiconductors the conduction band minima is displaced in k-space, so electronic transitions from the valence band to the conduction band require a significant $\Delta\mathbf{k}$, which cannot be met by a photon so a *phonon* (see later) is required to interact with the electron in order to conserve momentum. The requirement of two waveforms simultaneously interacting with the electron severely reduces the bandgap absorption of indirect bandgap semiconductors. However, when the photon energies become equal or greater than the Γ point bandgap direct absorption can occur in indirect bandgap semiconductors.

On a macroscopic scale the absorption of light occurs as an exponential drop in intensity as the light penetrates into the material according to the Beer Lambert law:

$$I = I_0 e^{-\alpha_{(\varpi)} x} \tag{2.18}$$

Where the coefficient of absorption α can be determined from Fermi's golden rule.

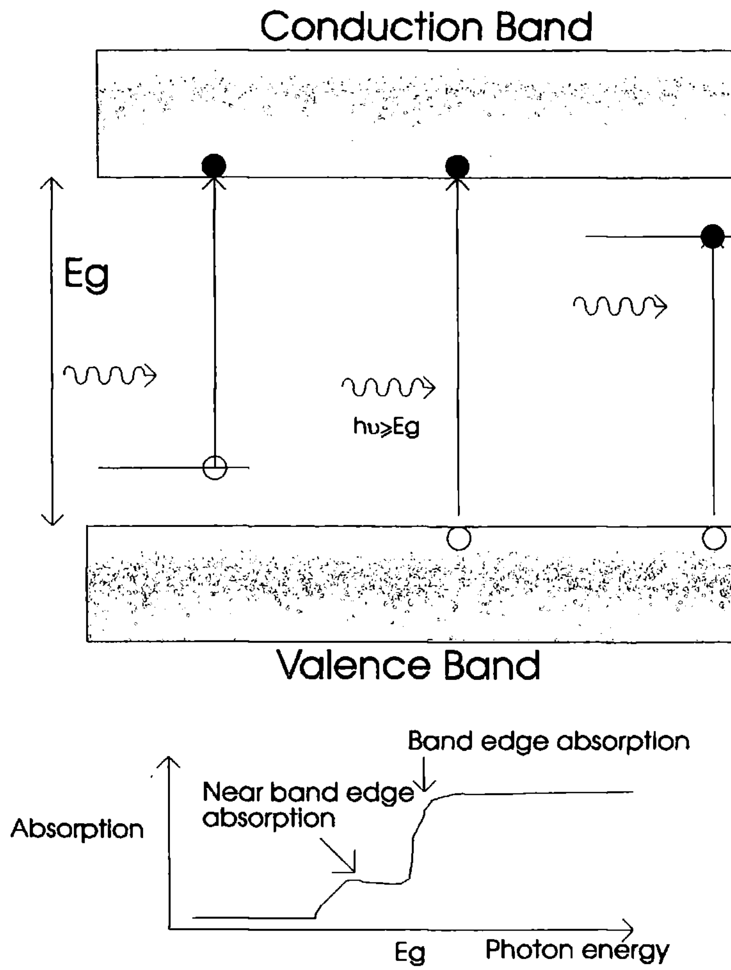


Figure 2.7: Optical absorption in a semiconductor.

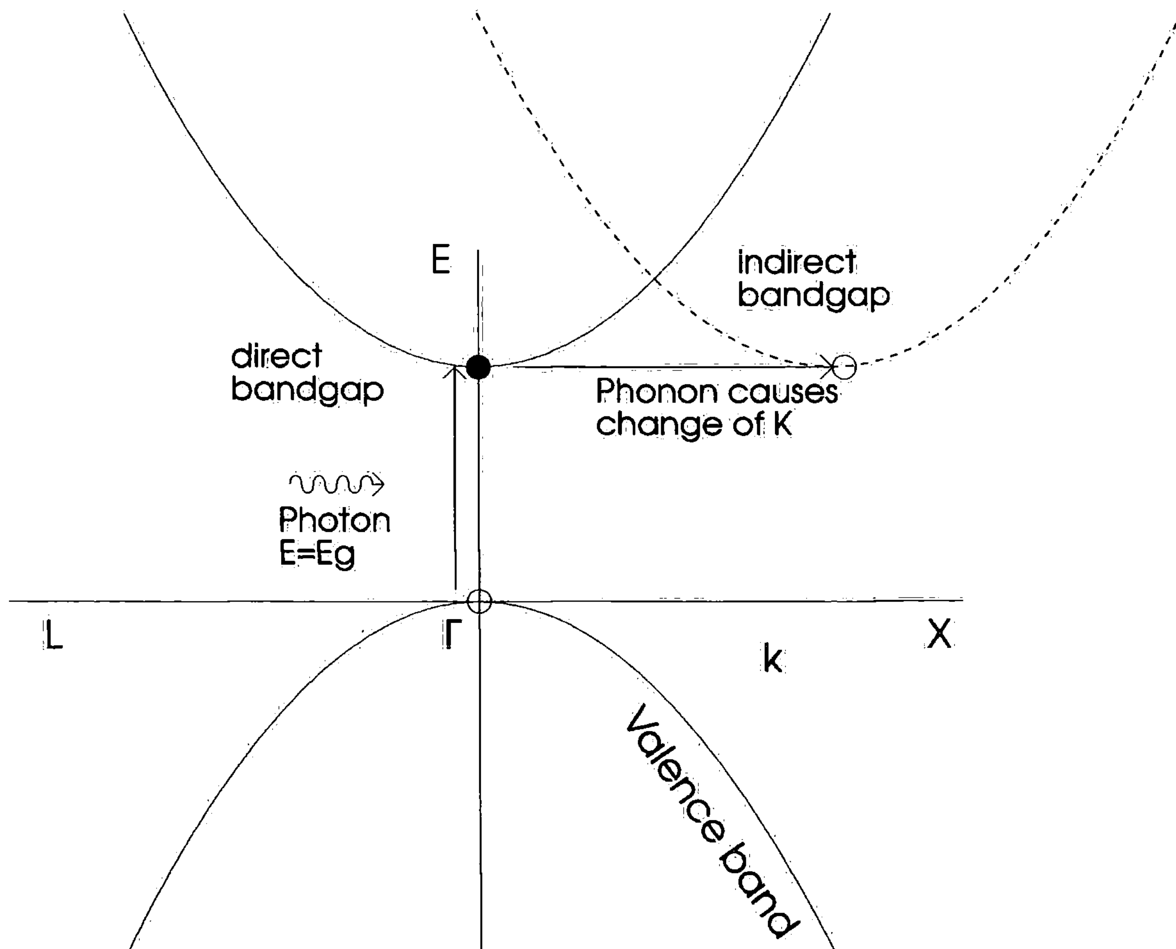


Figure 2.8: Direct and indirect bandgap semiconductor absorption.

Spontaneous emission occurs when an electron drops from a higher energy state to a lower one, giving off a photon of energy equal to the drop in energy of the electron. As with absorption, the energies of the photons involved are dependent upon the bandgap of the semiconductor and on the energy levels of any dopants in the semiconductor.

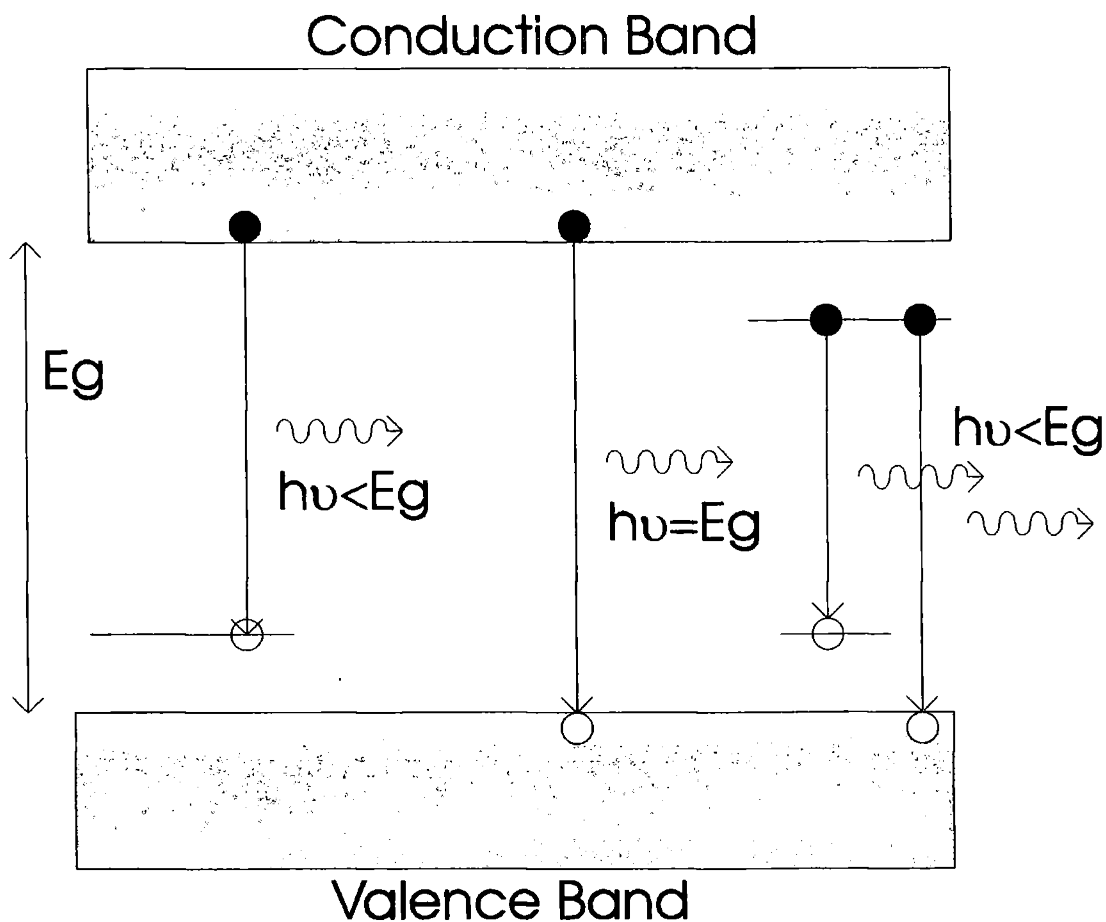


Figure 2.9: Spontaneous emission in a semiconductor

Stimulated emission occurs when a photon, of energy equal to a specific optical transition in the semiconductor, passes close to an excited electron, causing it to undergo the optical transition, losing energy and creating a second photon of the same phase, energy and polarisation as the first. This process is most relevant to semiconductor lasers and requires a carefully maintained population inversion if the process is to be self-propagating. It is of little direct use in characterisation.

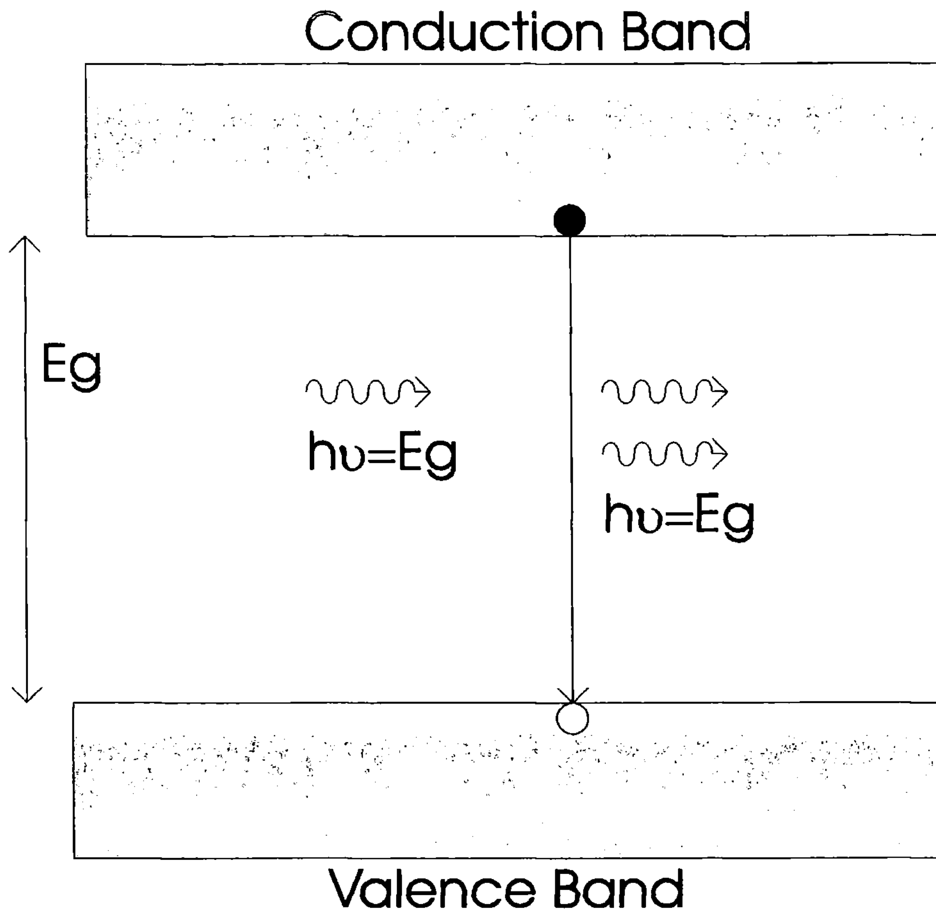


Figure 2.10: Stimulated emission in a semiconductor.

Although not a radiative recombination mechanism, Auger recombination should be mentioned here since it is a significant recombination mechanism in semiconductors which competes with radiative processes. It occurs when an electron moves from the conduction to the valence band to recombine with a hole, and instead of emitting a photon it either promotes another conduction band electron into a higher energy state or moves a hole from the heavy hole valence band to the light hole valence band such that energy and wavevector are conserved (see figure 2.11). In n-type material Auger processes involving three electrons and one hole are more probable; likewise in p-type material the heavy hole-light hole transition is more probable. Auger recombination has a thermal activation energy dependent upon the bandgap of the material so it becomes a more dominant mechanism in narrow-gap semiconductors. In semiconductors with relatively large bandgaps such as CdTe auger processes are not dominant.

Figure 2.11: Auger recombination.

**2.6 Of Phonons and Excitons**

Phonons are thermally induced vibrations in the crystal lattice of a semiconductor or other crystalline structure. They have much lower energies but higher wavevectors than photons, thus phonon interactions are described on E-k diagrams as near horizontal movements of electrons (see figure 2.8). Phonons can be described as solutions to the equation for a series of coupled harmonic oscillators:

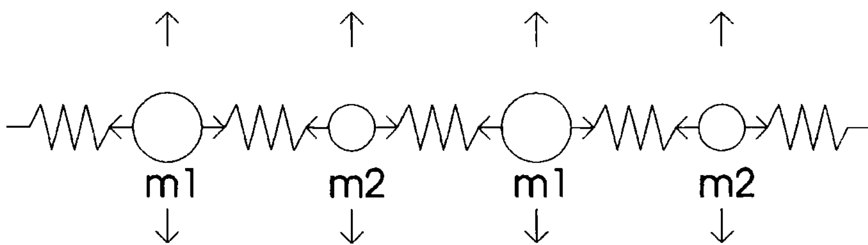


Figure 2.12: Vibrating linked atoms causing phonons.

Taking only one dimension (from which three-dimensional solutions can be easily extrapolated) we have for the 2nth atom in a diatomic chain:

$$m_1 \frac{d^2 U_{2n}}{dt^2} = \beta(U_{2n+1} + U_{2n-1} + 2U_{2n})$$

Where $U_{2n}$ is the displacement of the 2nth atom in the chain. (2.19)

m is the mass of the atom and β is a function.

Also for the (2n+1)th atom:

$$m_2 \frac{d^2 U_{2n+1}}{dt^2} = \beta(U_{2n+2} + U_{2n} + 2U_{2n+1})$$

(2.20)

The solution to these equations can be written as a travelling wave of form:

$$u_{2n} = u_a e^{i(2nqa - \varpi t)}$$

(2.21)

And:

$$u_{2n+1} = u_b e^{i((2n+1)qa - \varpi t)}$$

(2.22)

Solutions can be found for ω by using the determinants of the simultaneous equations of motion for the oscillators. This gives:

$$\varpi = \sqrt{\beta\left(\frac{1}{m_1} + \frac{1}{m_2}\right) \pm \sqrt{\left(\frac{1}{m_1} + \frac{1}{m_2}\right)^2 - \frac{4\sin^2(qa)}{m_1 m_2}}}$$

(2.23)

Since the energy of the phonon depends upon its frequency $\omega$, which is a function of wavevector q, we can draw an E-q diagram for phonons. It can be seen from equations 2.21 and 2.22 that the E-q relation is repeated every $q=2\pi/a$ and so can be represented in 2D and 3D by the first Brillouin zone in the same way as the solutions for the electron energy levels.

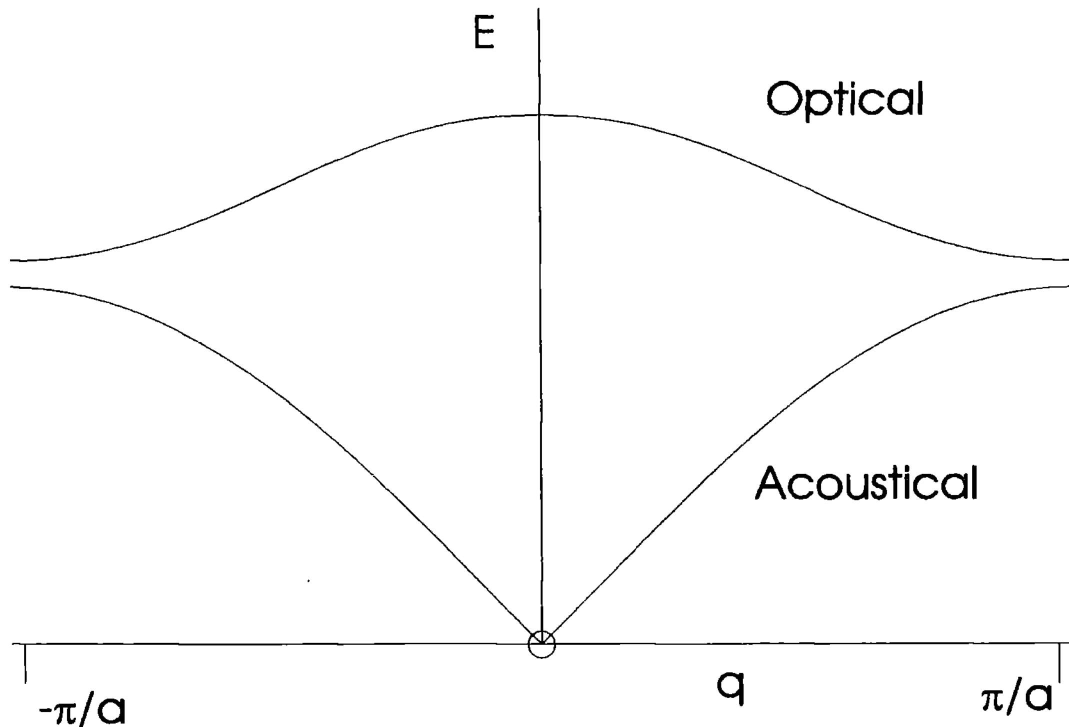


Figure 2.13: E-q diagram for phonons.

The two possible solutions for each q value in equation (2.22) lead to the two modes shown in figure 2.13, acoustic and optical. Physically acoustic modes involve all adjacent atoms oscillating in phase with each other whereas optical modes involve adjacent atoms being totally out of phase with each other, thus making all atoms of the same mass in phase. A further splitting of phonon modes occurs by considering that longitudinally oscillating phonons will have a different E-q relationship to transverse phonons. In real three-dimensional semiconductors anisotropy may further split the transverse phonon modes.

As optical branch phonons have a finite energy as q=0 is approached on an E-q diagram they are able to couple with photons and excitons (see below). For the purposes of high resolution photoluminescence this can lead to the creation of phonon replicas of excitonic luminescence features with energies lower than the primary feature by a set amount dependent upon the crystal structure of the semiconductor.

Free excitons occur when a free electron in the conduction band becomes bound to a hole in the valence band via the coulomb attraction, forming a loosely bound electron-hole pair with some similar properties to a hydrogen atom. The binding energy of the exciton can be approximated from the hydrogenic model[7] as:

$$E_{ex}(n,k) = Eg - \frac{13.6\mu}{m_o\varepsilon^2 n^2} + \frac{\hbar^2 k^2}{2M}$$

(2.24)

Where μ is the reduced mass, M and k are the net mass and wavevector of the exciton and n is its principal quantum number.

Excitons can be spatially bound in the vicinity of a neutral or ionised donor or acceptor impurity. The perturbation to the crystal potential caused by the impurity acts to localise the exciton. The binding energies of excitons, typically between 1 meV and 200 meV, do not substantially change the optical transition energies observed in most semiconductors. However, the exciton binding does have a substantial effect on the transition probabilities for electron-hole pairs. At low temperatures and in semiconductors relatively free of deep level traps, excitonic effects dominate the near bandgap optical properties due to the high probability of exciton formation from the semiconductors free charge carriers. However, due to the aforementioned small binding energies, excitons are easily dissociated by thermal processes or distortions in the crystal lattice and so are not observed at room temperature or in very impure semiconductors.

### 2.7 Of Junctions and Semiconductor Devices

When a p-type semiconductor comes into direct contact with an n-type semiconductor, a p-n junction is formed. In the region of this junction, free electrons from the n-type semiconductor move across the junction to fill the holes in the p-type semiconductor. This causes an equilibrium condition where there are no free charge carriers near the junction, and there is a strong electrostatic potential across it. The p-n junction forms the basis for most of the important semiconductor devices including diodes, transistors and photovoltaics.

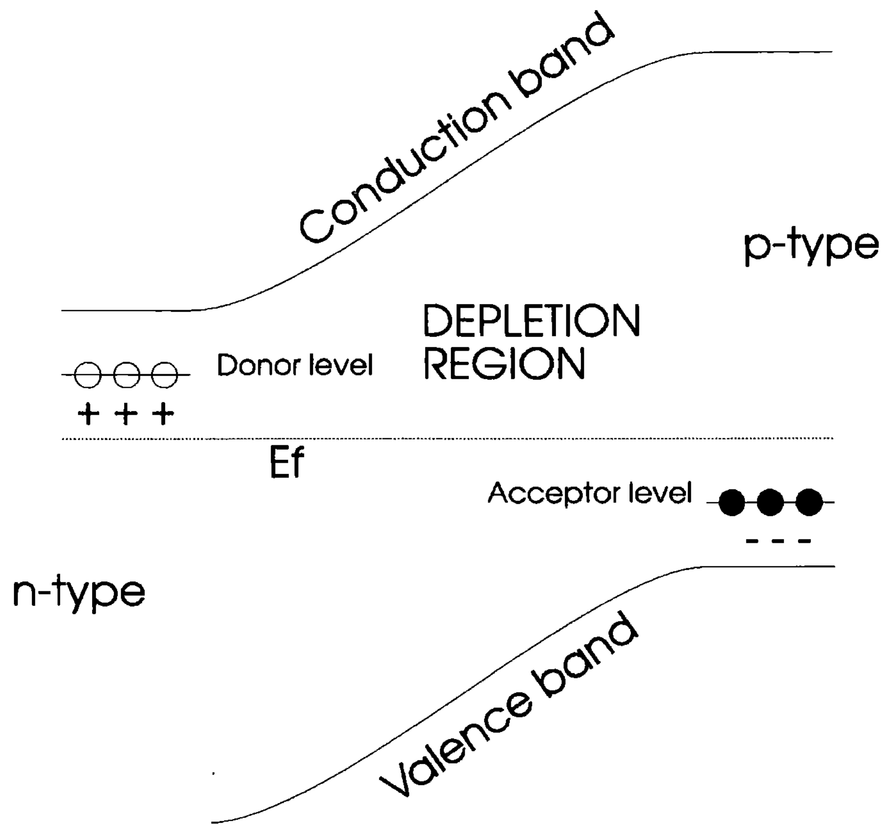


Figure 2.11: A p-n junction from an energy band viewpoint

Junctions can be sub-divided into homojunctions (a single piece of semiconductor with different doping applied to different parts) or heterojunctions (two different semiconductors in direct contact). Any basic p-n junction will have the clearly identifiable electrical characteristic of non-ohmic current flow. When a potential V is applied to the junction in such a direction as to tend to move electrons from the n-type material to the p-type material (forward bias), the internal field is reduced and current will flow through the junction in a non-ohmic fashion:

$$J = J_s\left(e^{\frac{eV}{kT}} - 1\right) \tag{2.25}$$

Where $J_s$ is the minority carrier drift current, given by;

$$J_s = \frac{eD_p p_{n0}}{L_p} + \frac{eD_n n_{p0}}{L_n} \tag{2.26}$$

Where $D_p$ and $D_n$ are the hole and electron diffusion coefficients, $L_p$ and $L_n$ are the carrier drift lengths and $p_{n0}$ and $n_{p0}$ are the equilibrium minority carrier concentrations in the n and p type regions respectively.

If the direction of the applied potential is reversed so that it attempts to force electrons through from the p-type material to the n-type (reverse bias), the internal field is increased and current will not flow until a limiting potential is reached (breakdown voltage, Vb) at which point the applied field overcomes the internal field and current flows.

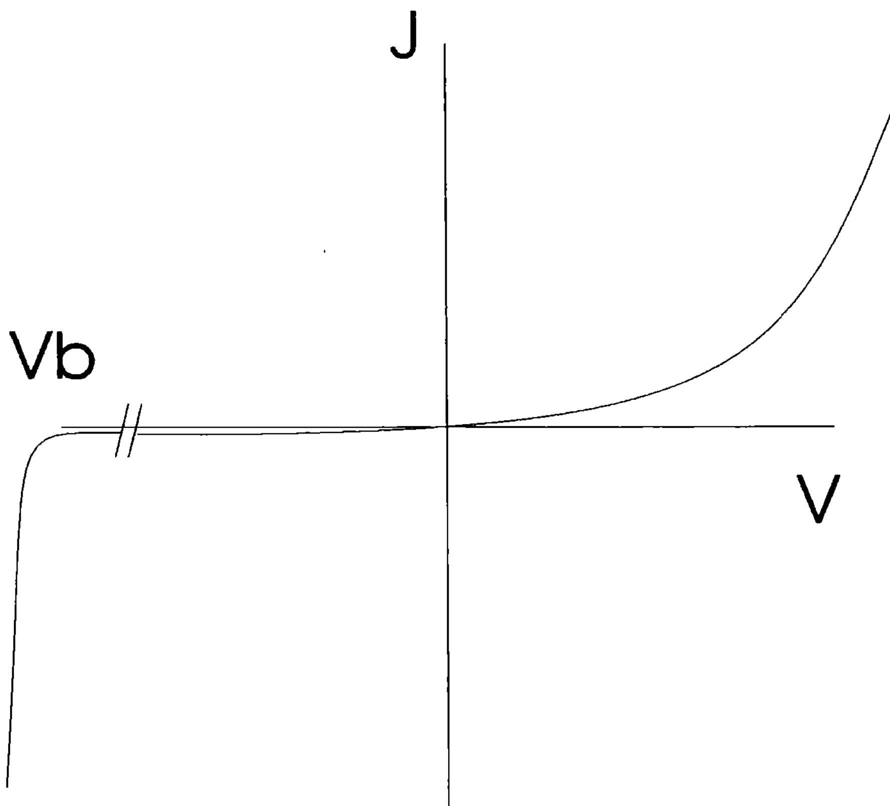


Figure 2.12: Generic J-V characteristics of a p-n junction.

As well as the obvious use of allowing current to flow in only one direction (a diode), p-n junctions can also be used to detect radiation and generate electrical power by allowing incoming photons to excite electrons across the junction. n-p-n junctions can be used to form transistors by only allowing current flow when charge carriers are injected into the central semiconductor layer.

### 2.8 Of Photoluminescence Spectroscopy

Photoluminescence spectroscopy is the primary tool used in this thesis for characterisation of semiconductor devices. In principle this involves exciting electrons into the conduction band of the semiconductor being studied by use of light of photon energy $h\upsilon > E_g$. Thermal processes rapidly move electrons towards the bottom of the conduction band, at which point they can form excitons and recombine with valence band holes, emitting a photon of energy $h\upsilon = E_g - E_{ex}$. Neutral or ionised donor and acceptor states in the semiconductor can trap excitons at their spatially localised sites, causing recombination that gives photons of characteristically lower energy dependant upon the position of the donor or acceptor band within the bandgap (known as $D^oX$, $A^oX$, $D^+X$ and $A^-X$ transitions). Non-excitonic versions of the above transitions can also occur, for example the recombination of a free electron with a hole bound to an acceptor. If the density of impurity states is high enough recombinations between an electron bound at a donor and a hole bound at an acceptor can occur directly, known as Donor-Acceptor Pair (DAP) transitions, having characteristically lower energy than the $D^oX/A^oX$ etc. transitions.

Transitions responsible for the above PL peaks can also create phonon replicas. These are emission peaks created when an electron and hole recombine and also interact with one or more lattice phonons, causing the peak positions to shift by an integer number times the characteristic phonon energy for zero wavevector. In direct bandgap materials the recombination process involves much less change of wavevector than the phonon wavevector, so the process will only couple to optical branch phonons which have non-zero energies as their wavevector approaches zero. In most semiconductor optical processes coupling is preferentially with longitudinal optical (LO) phonons and causes phonon replicas of lower energy than the original peak.

The parameter for coupling between photons and phonons is known as the Huang-Rees parameter, S, which can be defined as the average number of phonons emitted by an excited state in order to return to its ground state. In the low temperature regime $kT \ll E_0$ [2] this parameter can be determined from the phonon replica spectrum of a specific PL peak by fitting to an appropriate formula[3].

$$I_{(h\nu)} = A\sum_{k=0}^{k=\infty} e^{-S}\frac{S^k}{k!}\frac{1}{1+(h\nu - E_0 + kE_{LO})^2/\Gamma^2} \qquad (2.27)$$

Where $E_0$ is the energy of the zero phonon line, $E_{LO}$ is the lattice LO phonon energy and $\Gamma$ is the lineshape broadening parameter.

The lineshapes of PL emissions are determined by two main factors. The first is the probabilistic nature of spontaneous emission. For a system obeying Fermi-Dirac statistics this gives a Lorentzian (homogeneous) profile for the emission peak, of generic form:

$$I_{(\varpi)} = \frac{A}{(\varpi - \varpi_c)^2 + A} \tag{2.28}$$

Where $\omega_c$ depends on the energy levels of the centre causing the peak and A is a constant dependant upon the recombination lifetime of the centre. This type of emission peak is then modified by a gaussian function due to perturbations in the crystal lattice caused by impurities and defects. This broadens the lorentzian emission profile according to:

$$I_{(\varpi)} = e^{-\alpha(\varpi - \varpi_c)^2} \tag{2.29}$$

In all but the most pure semiconductors the gaussian (inhomogeneous) broadening is the dominant mechanism for the majority of observed PL peaks.

The dependence of near band edge PL emission on exciting intensity has been known for some time to vary empirically according to

$$I_{PL} \propto I^{k}_{excitation} \tag{2.30}$$

The value of k is dependent upon the type of recombination process responsible for the PL emission peak. Donor-acceptor pair transitions have the lowest k values (~0.2), followed by the non-excitonic free-bound transitions (k~0.7). Free exciton recombination has a k value of unity. Excitons bound at donors or acceptors have the highest k values (~1.5). Thus intensity dependant analysis can help identify the mechanisms behind PL emission peaks. A more rigorous analysis of intensity dependence is possible by considering the detailed balance of the system as done in[4]. However, such a study will not be entered into here.

The temperature dependence of excitonic PL emissions can also provide information about the centres responsible for specific features in PL spectra. If we assume that an electron-hole pair (exciton) is

bound at some unknown centre with a ground state $E_0$ and several excited states $E_1$, $E_2$ ... at which the pair become dissociated, following the model of Bimberg et al[5] , Maxwell-Boltzman statistics give us:

$$\frac{N_x}{N_0} = \left(\frac{\alpha_x}{\alpha_0}\right) e^{-\frac{(E_x - E_0)}{kT}} \tag{2.31}$$

Where $N_x$ and $N_0$ are the populations of the excited states and the ground state respectively. $\alpha_x$ and $\alpha_0$ are the degeneracy factors of the states. Solving for the total number of excitons within all the levels ($N_g$) we obtain:

$$N_g = N_0\left[1 + \left(\frac{\alpha_1}{\alpha_0}\right) e^{-\frac{(E_1 - E_0)}{kT}} + \left(\frac{\alpha_2}{\alpha_0}\right) e^{-\frac{(E_2 - E_0)}{kT}} + .....\right] \tag{2.32}$$

Re-arranging and replacing $\alpha_x/\alpha_0$ with constants $C_x$ and substituting $E_{Tx}=E_x-E_0$ we obtain:

$$\frac{N_0}{N_g} = \left[1 + C_1 e^{-\frac{E_{T1}}{kT}} + C_2 e^{-\frac{E_{T2}}{kT}} + .....\right]^{-1} \tag{2.33}$$

If we make the assumption that the total number of excitons in the set of states described above does not change significantly with temperature then we can say that, since the fraction $N_0/N_g$ is the fraction of the excitons available to recombine radiatively, and since at T=0, $N_0=N_g$:

$$\frac{I}{I_0} = \left[1 + C_1 e^{-\frac{E_{T1}}{kT}} + C_2 e^{-\frac{E_{T2}}{kT}} + .....\right]^{-1} \tag{2.34}$$

Where $I_0$ is the intensity of the PL emission peak at absolute zero. Bimbergs finding was that a system with two excited states gave predictions for temperature dependence which closely matched his experimental results. Thus by algorithmic fitting of this equation to an Arrhenius plot (a plot of 1/T against log(intensity)) the activation energies $E_{Tx}$ of the centre responsible for the recombination can be determined. A more rigorous analysis of the detailed balance equation, as done by Zimmerman *et al*[6], yields an additional temperature dependence of $T^{3/2}$ in the $C_n$ pre-factors due to the effective density of states of free excitons.

### 2.9 Bibliography

{1} *Introduction to Solid State Physics,* C. Kittel, © 1953-1996 John Wiley & Sons Ltd.

{2} *II-VI Compounds,* B. Ray, © 1969 Pergamon Press Ltd.

{3} *Polycrystalline and Amorphous Thin Films and Devices,* Ed. L. L. Kazowski, © 1980 Academic Press inc.

{4} *Photoelectric Properties of Semiconductors,* R. H. Bube, © 1992 Cambridge University Press.

{5} *Optical Characterisation of Semiconductors,* S. Perkowitz, © 1993 Academic Press Ltd.

{6} *Semiconductor Physics, An Introduction,* K. Seeger, © 1985 Springer-Verlag Berlin.

{7} *Semiconductor Optics*, C. F. Klingshirn, © 1995 Springer-Verlag Berlin Heidelberg.

### 2.10 References

[1] "Nonlocal pseudopotential calculations for the electronic structure of eleven diamond and zinc-blende semiconductors". J.R. Chelikowsky and M.L. Cohen, Phys. Rev. B, 1976. Vol.14(2): pp. 556-582.

[2] Photoluminescence as a diagnostic of semiconductors, P. J. Dean, 1982, Prog. Crystal Growth Charact. Vol. 5, pp.89-174.

[3] Localisation of Y luminescence at glide dislocations in cadmium telluride, S. Hildebrandt, H. Uniewski, J. Schreiber, H. S. Leipner, 1997, J. Phys. III vol. 7, pp. 1505-1514.

[4] The excitation power dependence of the near band edge photoluminescence of II-VI semiconductors, T. Schmidt, G. Daniel and K. Lischka, 1992, J. Crys. Growth, vol.117 (1-4), pp. 748-752.

[5] Thermal dissociation of excitons bound to neutral acceptors in high purity GaAs, D. Bimberg, M. Sondergeld, E. Grobe, 1971, Physical Review B, vol. 4 (10), pp. 3451-3455.

[6] Thermal quenching of bound exciton emission due to phonon-induced non-radiative transitions: experimental data for CdTe and InP, H Zimmerman, R Boyn, K Piel, 1992, J. Phys: Condensed Matter vol. 4 pp. 859-868.

# 3 Experimental

## 3.1 Apparatus Setup - Photoluminescence

The apparatus used for the majority of the measurements is fairly standard fare for most up to date low temperature PL labs. Photoluminescence excitation was achieved using a Coherent Innova 400 continuous wave (CW) argon ion laser. This emits laser radiation at several visible wavelengths in the blue/green end of the spectrum. Initially using stacked dielectric filters three useful wavelengths of light could be selected: 514.5nm green, 488nm blue and 457.9nm deep blue. For the later sections of this thesis, however, the single-line filters were replaced by a single tuneable prism based wavelength selector. The laser used is capable of power output of up to 30W. A 50:1 beamsplitter was used as the first mirror to give practical beam power range of 0-600mW for photoluminescence. After wavelength selection, the beam passed through a series of interchangeable neutral density filters, allowing the power of the beam to be more conveniently controlled. Net optical density of the filters could be varied from 0.08 to 2.54, causing attenuation of the laser beam between 17% and 99.7%. After being redirected for convenience by a couple of further mirrors, the laser beam was then trimmed using an adjustable aperture and focussed onto the sample mounted inside the cryostat. The laser spot size when focussed was typically 0.5mm diameter. Excited luminescence emitted through the same window that the laser beam entered was then focussed onto the monochromator as will be discussed later. Long wavelength pass filters were used to remove the reflected and scattered laser beam from the spectrum to avoid swamping. Luminescence spectra were taken using a Bentham TM300 monochromator coupled to a Peltier cooled EG&G silicon photodiode array. These were operated by a PC using control software developed at Durham.

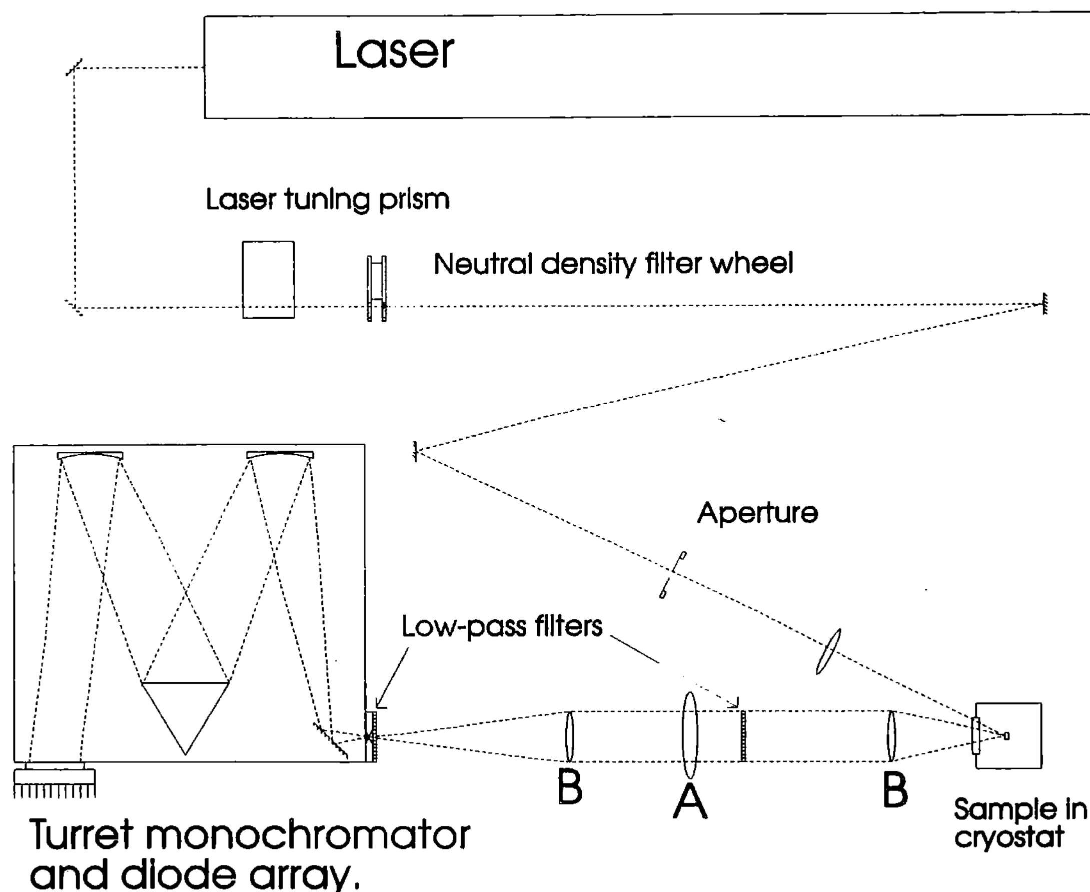


Figure 3.1: Optical Layout for Photoluminescence

Initially light was collected from the sample and focused on the monochromator entrance slit by a single lens labeled A in figure 3.1. In order to maximise the light collection efficiency it was later decided to replace this with a pair of lenses (labeled B in figure 3.1). This allows the primary lens to be placed much closer to the sample (its focal length, 10cm away) as it produces a parallel beam of light from a point source, which is then focussed back to a point on the monochromator slits by the secondary lens (focal length 20cm). This minimizes the light wasted from the sample by making arcs A and B of figure 3.2 of similar subtension. As can be seen in figure 3.2, the difference in subtension between these two arcs need only be large enough for the laser beam to come in to hit the sample. However if the cryostat is to be moved in order to play the beam across the surface of the sample as was necessary for many of my readings then the difference between arcs A and B must be large enough to accommodate the motion. Arrangement B also allowed f-number matching of the luminescence incident on the monochromator for maximum throughput.

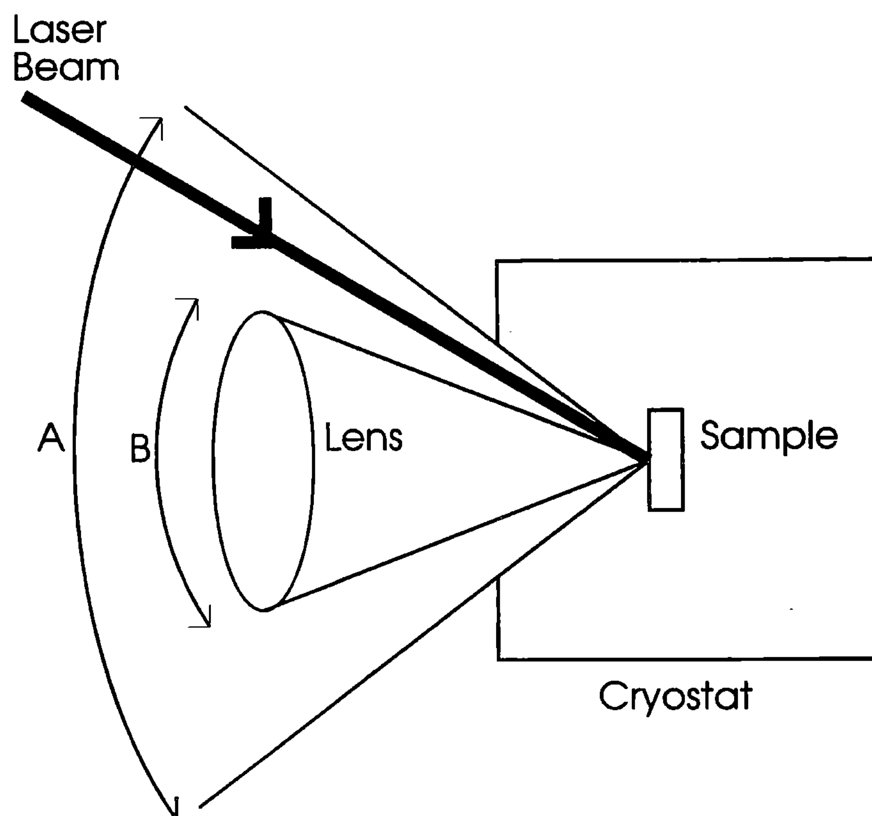


Figure 3.2: Optimising light collection

The positioning of a second low pass filter midway between the cryostat and the monochromator was to eliminate the possibility of room temperature luminescence from the low pass filters influencing the spectra in the case of very faintly luminescent samples where the slit width and exposure times for the monochromator are set very high. Regardless of lens configuration, the luminescence from the sample (including diffused laser light) is at its most diffuse mid way between the cryostat and the monochromator. Any luminescence thus emitted from the filter will then for the most part not be focussed onto the entrance slits of the monochromator.

### 3.2 Electroluminescence

In order to attempt to obtain electroluminescence (EL) from functional CdTe/CdS solar cells, the cells were placed in the cryostat as for photoluminescence measurements with the sample in a front surface configuration (glass side facing the monochromator). Fine (0.1mm) copper wires were used with silver paint to provide electrical connection to the back surface of the cells (which had in this case already had a

gold back contact evaporated on) and to the transparent $SnO_2$ front contact which was exposed by manually scraping away some of the CdTe (though not in the contacted region in order to avoid causing a short circuit). A Keithley 2400 digital source meter was programmed to generate forward bias 10 volt pulses of 10ms duration with a 1/10 duty cycle. This was the high speed limit of the equipment used. Large monochromator slit widths (typically several mm) and long exposure times (up to 5 minutes) were used to enhance the EL signal as much as possible. Even so, the EL response was very faint in all of the samples studied by this method.

### 3.3 Sample Mounting

For all low temperature work including photoluminescence, electroluminescence and far infrared absorption measurements the samples being studied were mounted in a Leybold closed cycle helium cryostat. This uses a helium pump to cool a cold finger on which the sample is mounted, encased in a vacuum. It is capable of achieving temperatures of 10K, which was the standard temperature used for low temperature measurements. The samples were mounted on the cold finger using the flexible rubberoid mounting technique. In this case the rubberoid adhesive used was Cow gum, which maintains a reasonable degree of flexibility at 10 kelvin, minimising stress on the sample. The cold finger contained a hole through which absorption measurements could be taken. Four optical windows were fitted to the cryostat vacuum jacket in two opposing pairs: a pair of sapphire windows (transmission range 150 nm-6000 nm) for visible and near infra red spectroscopy, and a pair of thallium bromo-iodide windows for far infra red measurements. The head could be rotated so that either pair of windows was in line with the cold finger. See figure 3.3.

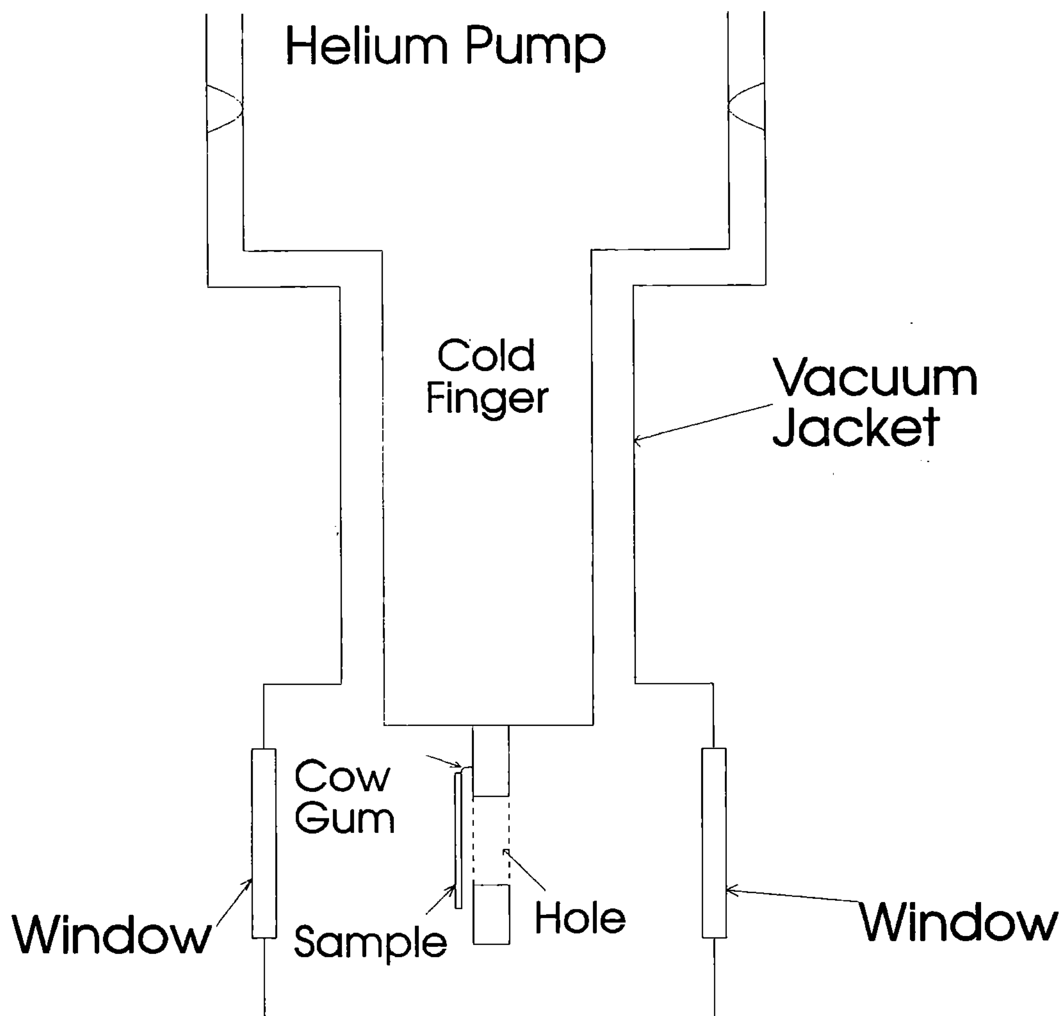


Figure 3.3: The Cryostat head

### 3.4 Equipment Calibration

As has been mentioned previously, a turreted monochromator coupled to a diode array was used to record all PL and EL spectra obtained. This principally operates using concave mirrors to cause a focussed point of light on the entrance slits to fall as a parallel beam onto a reflective diffraction grating mounted on a central turret. The diffracted beam is then directed on to the Si diode array, so that different individual diodes are illuminated by different wavelengths of diffracted light (see figure 3.1). The triangular nature of the central turret allows it to hold three different diffraction grating, any of which can be rotated into

position by a high-accuracy computer controlled stepper motor. For the experiments described in this thesis, two gratings were used. For low-detail spectra a grating of density 150 lines/mm was used, giving a spectral range of ~400nm per scan at optical wavelengths, and a resolution of ~1nm. For high resolution spectra, a grating of 1200 lines/mm was used, giving ~60nm coverage per scan with a resolution of 0.25nm. These gratings were calibrated by comparison to known laser lines (both from the argon ion laser and a 632.8nm HeNe laser) and spectral lines of Na, Xe, Hg and Cd lamps. In the case of the 150 line grating, it was assumed that the dispersion (that is, the relationship between pixel number illuminated and wavelength of illuminating light) was constant across the diode array for a given position of the diffraction grating (given by the "centre wavelength" of the diffraction grating) and varied linearly with centre wavelength. Thus we have a formula:

$$\lambda = c - \frac{(512-n)(ac+b)}{1024} \qquad (3.1)$$

Where c is the centre wavelength of the grating (c was calibrated separately as a function of the number of steps on the stepper motor), n is the nth pixel of the 1024 pixel array and a and b are constants which determine the variation of dispersion with centre wavelength. This approach was found to give calibration to within an acceptable accuracy (1nm) compared to the resolution of the grating.

For the 1200 line grating however a more accurate approach was needed. The dispersion was assumed to vary as a function of wavelength and was not assumed to be constant across the diode array. This variation was most accurately modeled by a second order polynomial (see figure 3.4). Integrating up and applying error functions to account for differences between this formula and actual measurements we obtain a third order polynomial relating wavelength to the pixel number and the centre wavelength. These calibrations were periodically checked to ensure that drifting had not occurred.

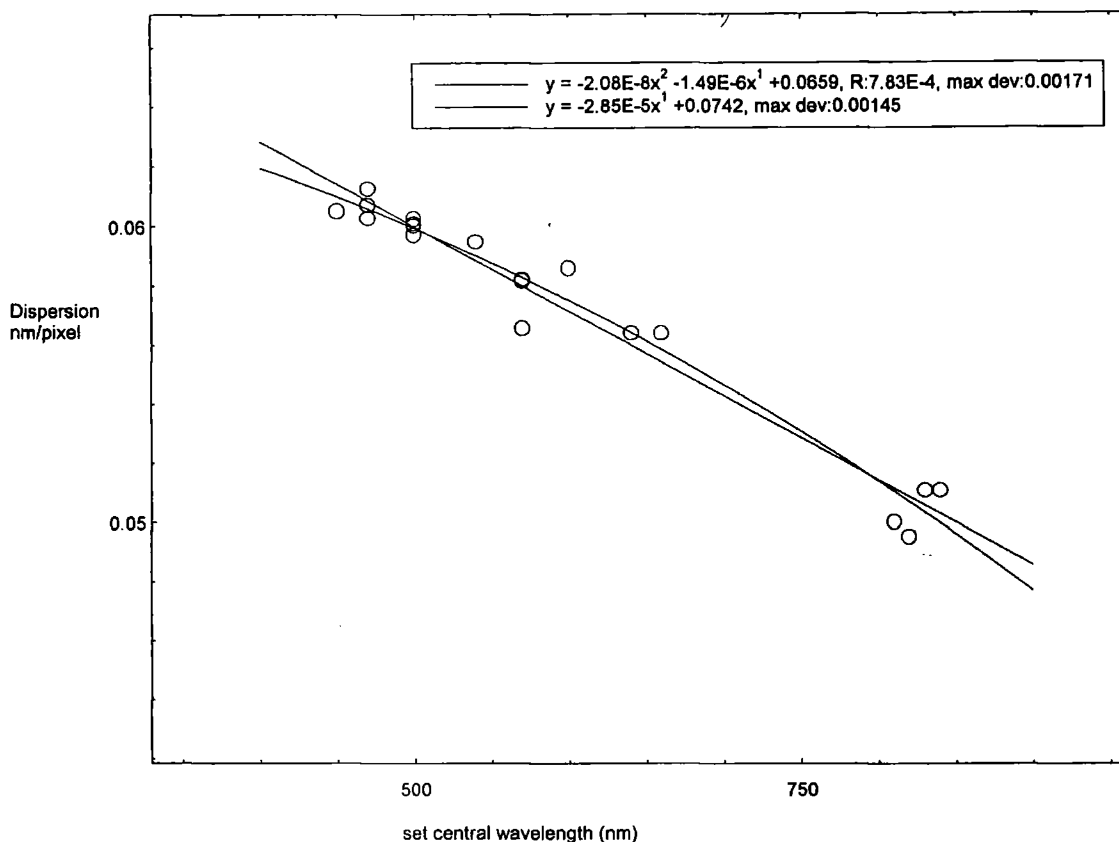


Figure 3.4:Dispersion on 1200 line grating as a function of wavelength

Laser power was measured using a Molectron powermax 500D laser power meter, connected to a PM10 thermal probe positioned after the aperture in figure 3.1 in order to give the net power incident on the sample. The laser spot diameter was manually measured to be ~0.5mm on the sample by replacing the cryostat with a ruler.

# 4 Studies of a Single Crystal Boule of CdTe

## 4.1 Introduction

II-VI semiconductors have an extensive range of applications, especially in the field of radiation detection. Combined with mercury and zinc, CdTe films can be used to form infra-red and X-ray detectors respectively. CdTe single crystals, due to their relatively high bandgap and high atomic numbers (meaning high stopping power) can be used to make gamma ray detectors [1]. CdTe based gamma ray and high energy X-ray detectors have found extensive applications in the field of medicine. When a gamma ray strikes the CdTe crystal lattice, it causes the generation of free carriers via several effects including photoelectric absorption, Compton scattering and pair production. It has been found experimentally [1] that approximately 4.5eV(~3Eg) of gamma ray energy are used creating each free electron/hole pair. These free carriers can then be detected either by an external amplifier circuit with an applied bias coupled to a multi-channel analyser, or by forming an effective p-n junction within the CdTe in order to create a photovoltaic cell and measuring the current produced. This method is simpler and cheaper than using an amplifier and does not suffer problems with high count rates, however, it does not produce an energy spectrum as the output current is a product of both count rate and gamma ray energy.

In both of the above cases, one of the major limiting factors on device performance is the carrier lifetime. Recombination centres induced by impurities or defects in the crystal lattice reduce the number of excited carriers that reach the detection system. Also, defect levels can trap and release the carriers, causing a broadening out of the detected pulses due to gamma ray incidence. Thirdly, impurities can decrease the resistance of the CdTe crystal, reducing the bias voltage that can be applied to it without causing an avalanche current. Thus a process able to produce bulk CdTe crystals of high purity and resistivity would allow fabrication of detectors with higher resolution and sensitivity than are currently available.

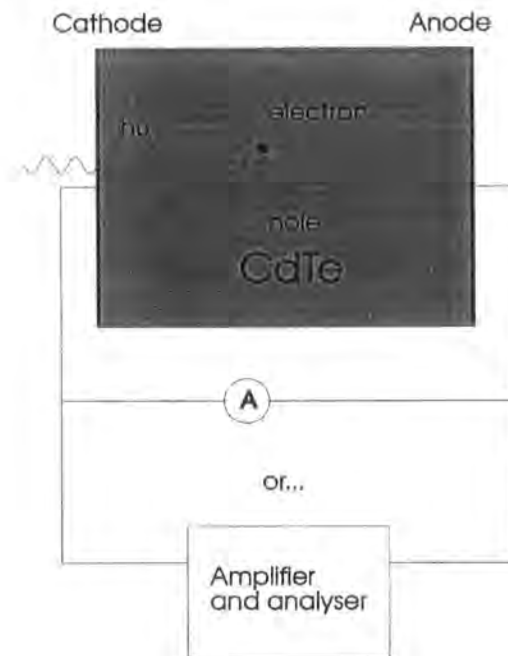


Figure 4.1: A CdTe crystal gamma ray detector

The growth of high purity CdTe crystals using a new "Multi-Tube seeded vapour growth technique" has produced single crystals of unprecedented size. Mullins *et al* [2] working at Durham have produced a crystal of 49mm diameter grown on a [111] oriented CdZnTe substrate. The electronic band structure of this crystal can be partially characterised by use of photoluminescence (PL) measurements [3, 4]. This provides information about the purity of the sample and the dominant electronic transitions [5].

**4.2 Experimental**

The Photoluminescence equipment was set up in the normal configuration (as in figure 3.1) for all readings on the CdTe crystal.

In order to study the variation of PL spectra with position in the crystal boule, and taking into account the need to minimise required data readings (as taking readings from every spatial point in a three dimensional structure is absurdly time consuming), the crystal boule was initially cleaved in half using a high RPM diamond saw. From one half of the crystal wafers were cut, running from the center of the boule to the edge. One side of the wafers was then polished down to remove damage caused by the saw. It is on one of these wafers that PL was performed. Therefore, if the composition of the crystal is assumed to have rotational

symmetry about a vertical axis through its center all relevant data can be obtained from the one representative wafer used. PL measurements were taken at a regular array of points on the surface of the wafer as shown:

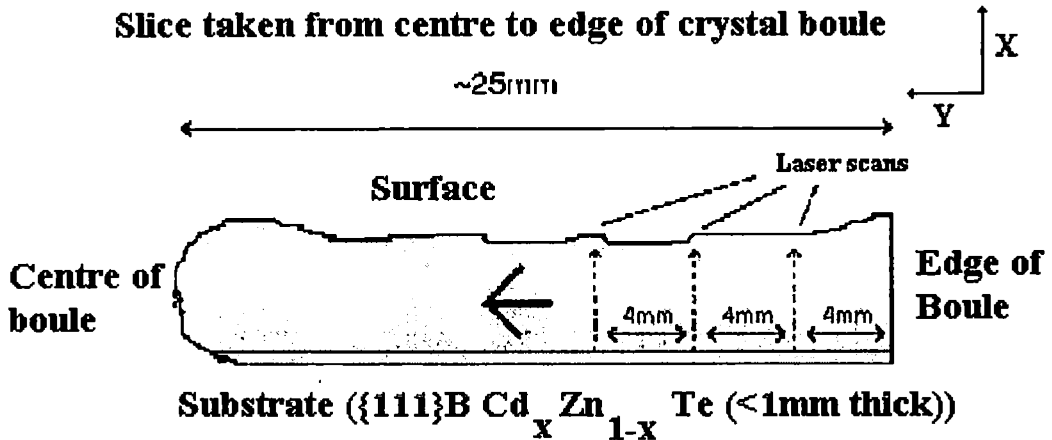


Figure 4.2: PL points on wafer cut from the CdTe crystal boule.

Photoluminescence measurements were taken using the 457.9nm emission line of the laser at a standard power density of 5.6mWmm$^{-2}$. Due to the exceptionally high quality of the sample a diffraction grating of density 1200 lines/mm was used, giving a spectral resolution of 0.2nm with a single scan width of approximately 60nm. This required three overlapping scans to be taken to cover the 780-900nm range over which PL features were observed. PL measurements were taken every 4mm along the long axis of the slice (from edge to center of the boule), and every 0.5mm from substrate to surface. Once a set of spatially resolved readings on the crystal boule had been obtained and the major emission peaks identified (see results section), temperature and intensity dependent analysis were used at locations where specific peaks were most intense in order to further characterize them. Temperature dependence was achieved by using a heating circuit and temperature sensor mounted on the cold finger of the cryostat linked to a Eurotherm controller. This allowed the temperature of the cold finger to be varied between 10K and 350K. About 5 minutes were allowed between readings for the temperature of the sample to stabilize. Intensity dependence was achieved by using a

daisywheel set of neutral density optical filters, allowing optical densities from 0.08 to 3.04 in steps of 0.2, giving a practical range of illumination power densities of 4.7 - 0.0051 $mWmm^{-2}$.

### 4.3 Results and Discussion

Photoluminescence was obtained from all regions of the sample. A typical spectrum identifying most of the significant peaks observed is shown below:

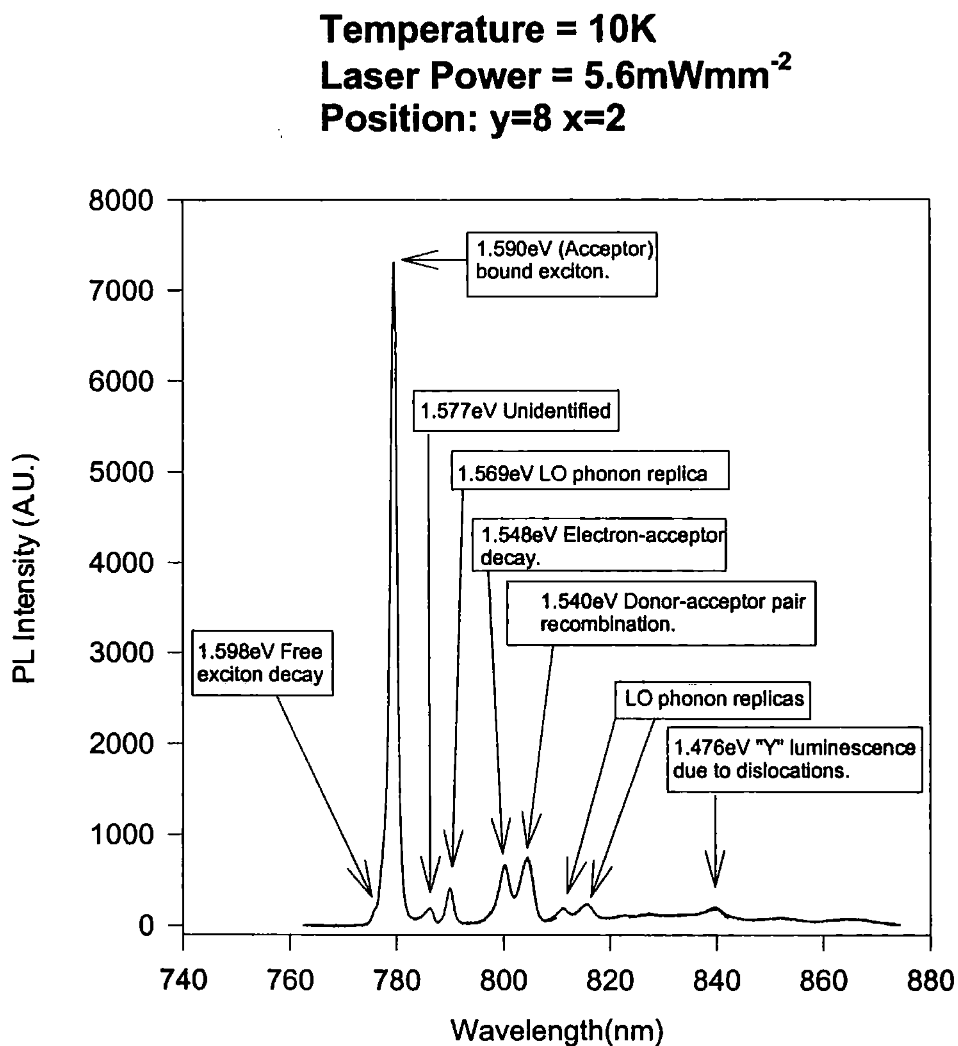


Figure 4.3: Typical PL spectrum from the crystal boule

As can be seen, the PL spectrum is rich in near band edge (NBE) features, which indicates a high overall quality of material and relative freedom from defects. The free exciton peak (1.598eV) is small compared to the acceptor bound exciton decay [6, 7] peak at 1.59eV. The 1.59eV peak exhibits a small full-width half-maximum (FWHM) of typically 3 meV throughout the sample. A shoulder on the high energy side of this peak at 1.5946eV is to be expected due to donor bound exciton decay [6, 8], but is not clearly observed in this sample, suggesting that the material is p type [8]. The 1.548eV electron-acceptor peak and the 1.54eV donor-acceptor pair (DAP) peak are well known in the literature and sometimes attributed to the presence of chlorine [8, 9]. Longitudinal optical (LO) phonon replicas of these peaks as well as of the acceptor bound exciton peak are clearly visible at energies 21.21meV lower than the original peaks, which corresponds to the known q=0 energy of the LO phonons of CdTe [10]. The peak at 1.577eV remains largely unidentified, but it is of the correct energy (although not the expected size) to be the LO phonon replica of the free exciton peak. Giles-Taylor *et al* [4] observe a similar peak in bulk CdTe, but do not offer an explanation for it. The 1.476eV peak (and its faint series of phonon replicas) correspond to the expected energy for "Y" luminescence [11]. This is thought to be caused by recombination of excitons trapped at glide dislocations in the CdTe.

In addition to the peaks shown on figure 3, a further low energy broad peak was observed at 1.51eV in certain regions of the sample. The origin of this peak is as yet unknown but it is associated with the region of the sample near the CdZnTe substrate that showed the lowest NBE PL yield and thus the highest defect/impurity concentrations. The absence of the broad "A" center peak centered around 1.48eV observed in the samples studied in chapters 5 and 6 suggests (by comparison with the studies of Shin [8]) that the sample contains less than 25ppm chlorine contamination.

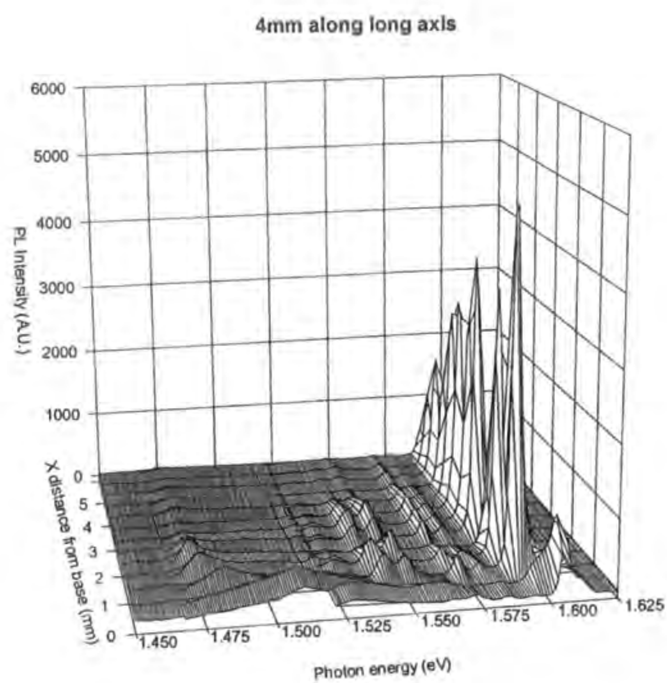


Figure 4.4: PL spectra as a function of position Y=4mm from edge of boule

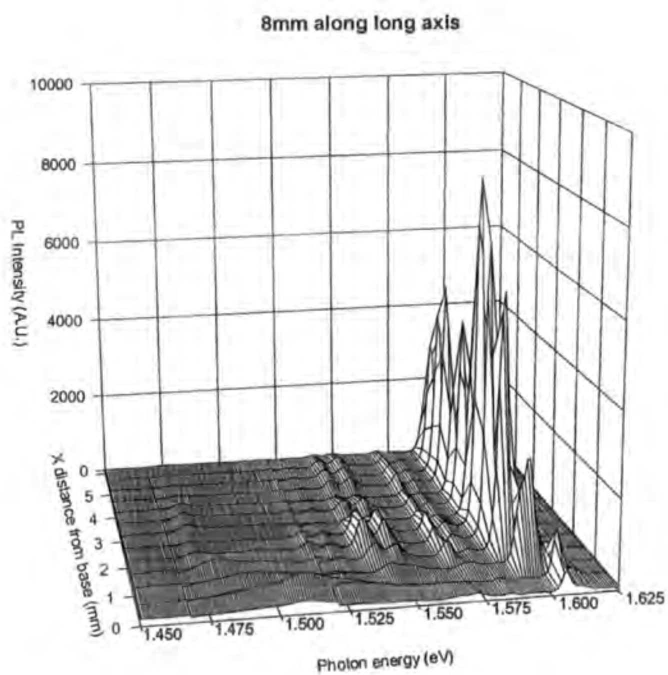


Figure 4.5: PL spectra as a function of position Y=8mm from edge of boule

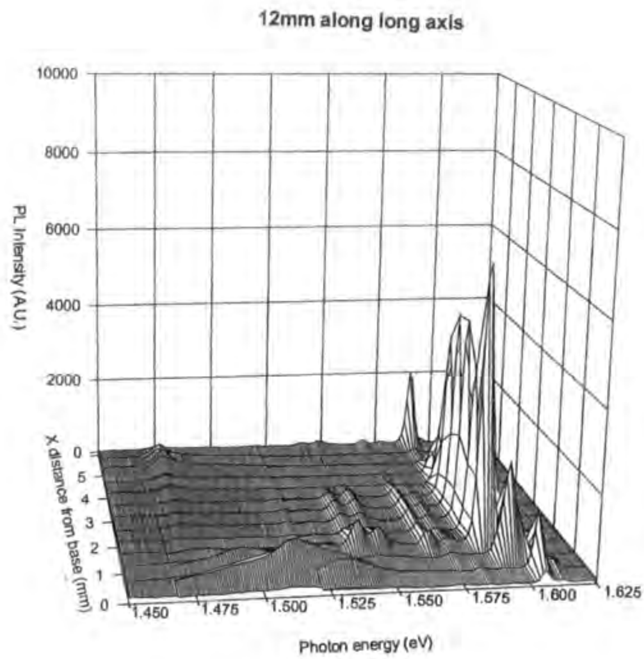


Figure 4.6: PL spectra as a function of position Y=12mm from edge of boule

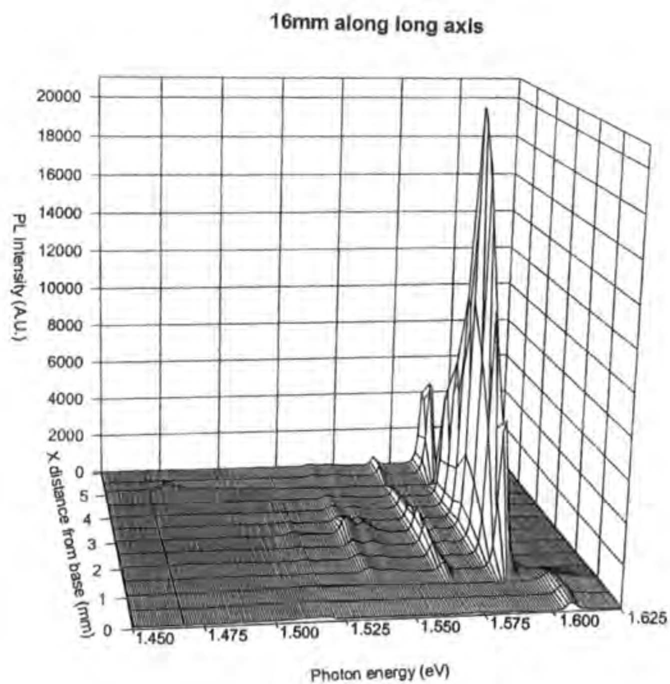


Figure 4.7: PL spectra as a function of position Y=16mm from edge of boule

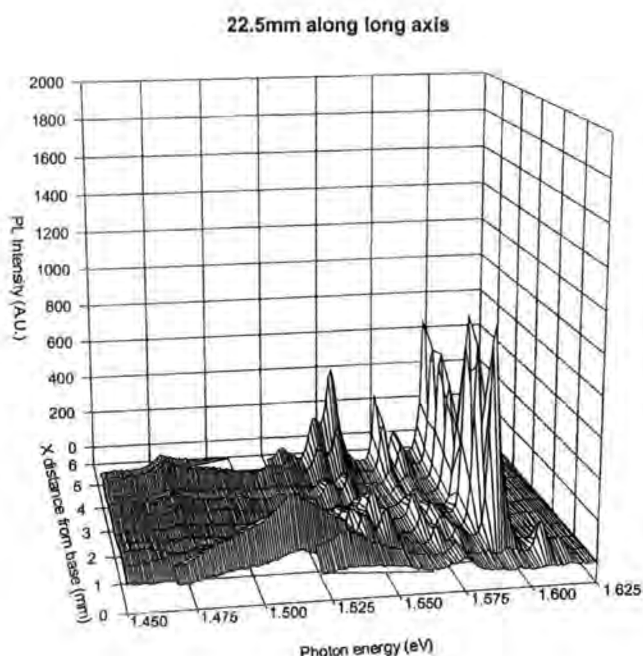


Figure 4.8: PL spectra as a function of position Y=22.5mm from edge of boule

Figures 4.4-4.8 summarize the spatially resolved PL data across the surface of the boule. It can clearly be seen that in the bottom millimeter of the sample (corresponding to the CdZnTe substrate region) there is a distinct shift to higher energies of all spectral features. This shift, of approximately 100meV, can be attributed to the presence of Zinc from the substrate causing an increase of the bandgap [12, 13]. The 1.51eV broadband peak can also be seen to a greater or lesser extent near the interface in all sets of spectra (faintest in figure 4.7, which has the most intense near band edge peaks).

The relative PL intensity of the near band edge (NBE) luminescence (compared to net PL intensity) can be plotted as a function of position on the surface of the wafer. This gives an indication of the quality of the crystal in terms of defects and nonradiative recombination centers [5, 14]. In this case we have defined NBE luminescence as that with photon energies of greater than 1.583eV. PL observed at lower energies can be accounted for by Free-bound recombination, DAP recombination and recombination at defects.

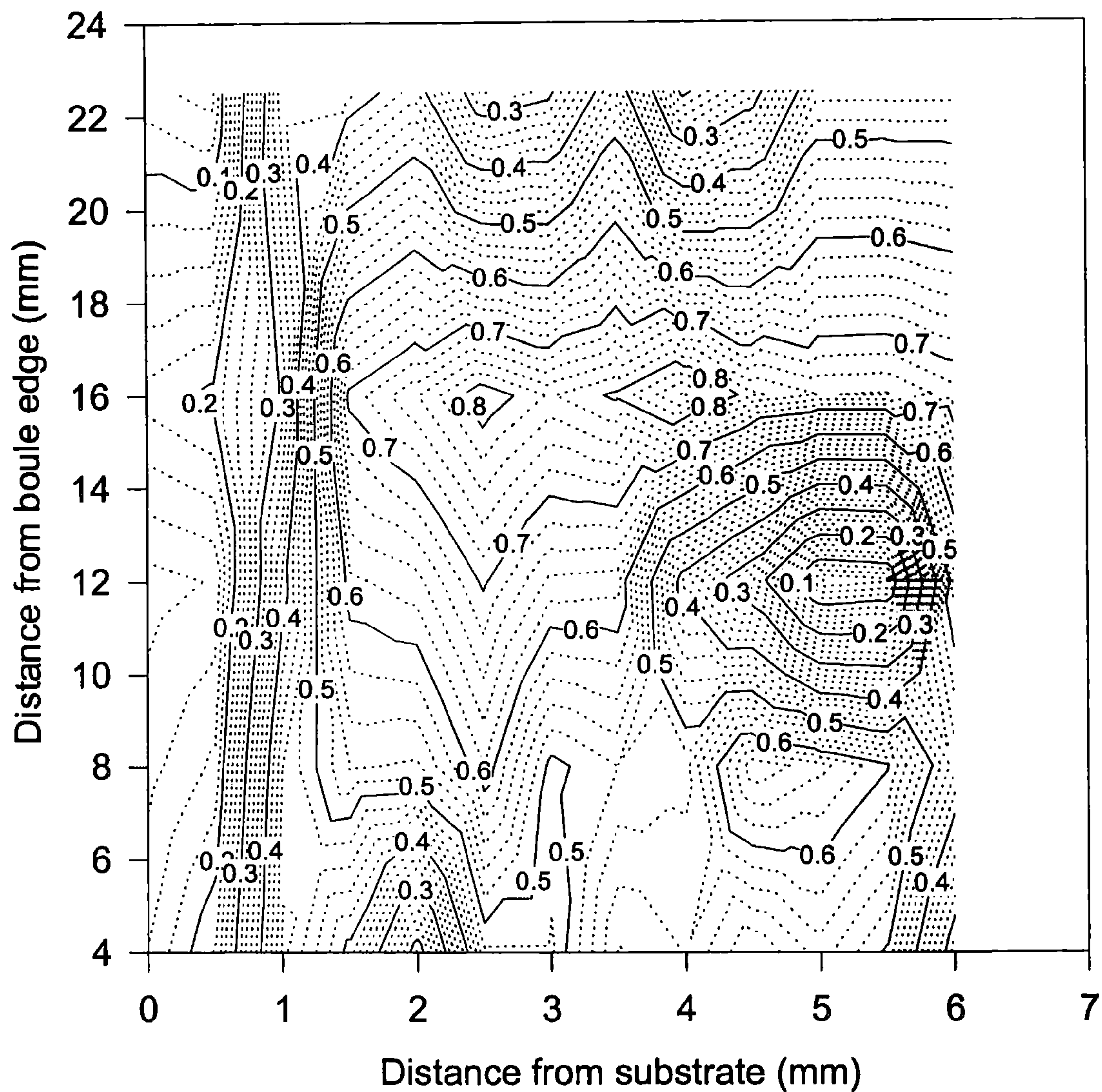


Figure 4.9: Fraction of PL intensity of photon energy E>1.583eV

As can be seen from figure 4.9, the quality of the material is poorest near the substrate, where surface impurities, strain related defects and recombination sites due to the presence of Zinc can all propagate from the substrate to the grown crystal. The region of highest observed crystal quality is in the region 2.5-4 mm above the substrate (approximately in the vertical center of the crystal) and 16mm from the center of the boule (slightly closer to the outer edge). A region of extremely poor crystal quality is also observed 12mm from the center of the boule and near the top surface of the crystal. Figure 4.10 shows net PL intensities as a function of position across the surface of the wafer. It can clearly be seen that regions of poor crystal quality correspond to low overall PL intensities and vice versa, meaning that the presence of PL peaks with energies of less than 1.583eV indicate the existence of other non-radiative recombination routes.

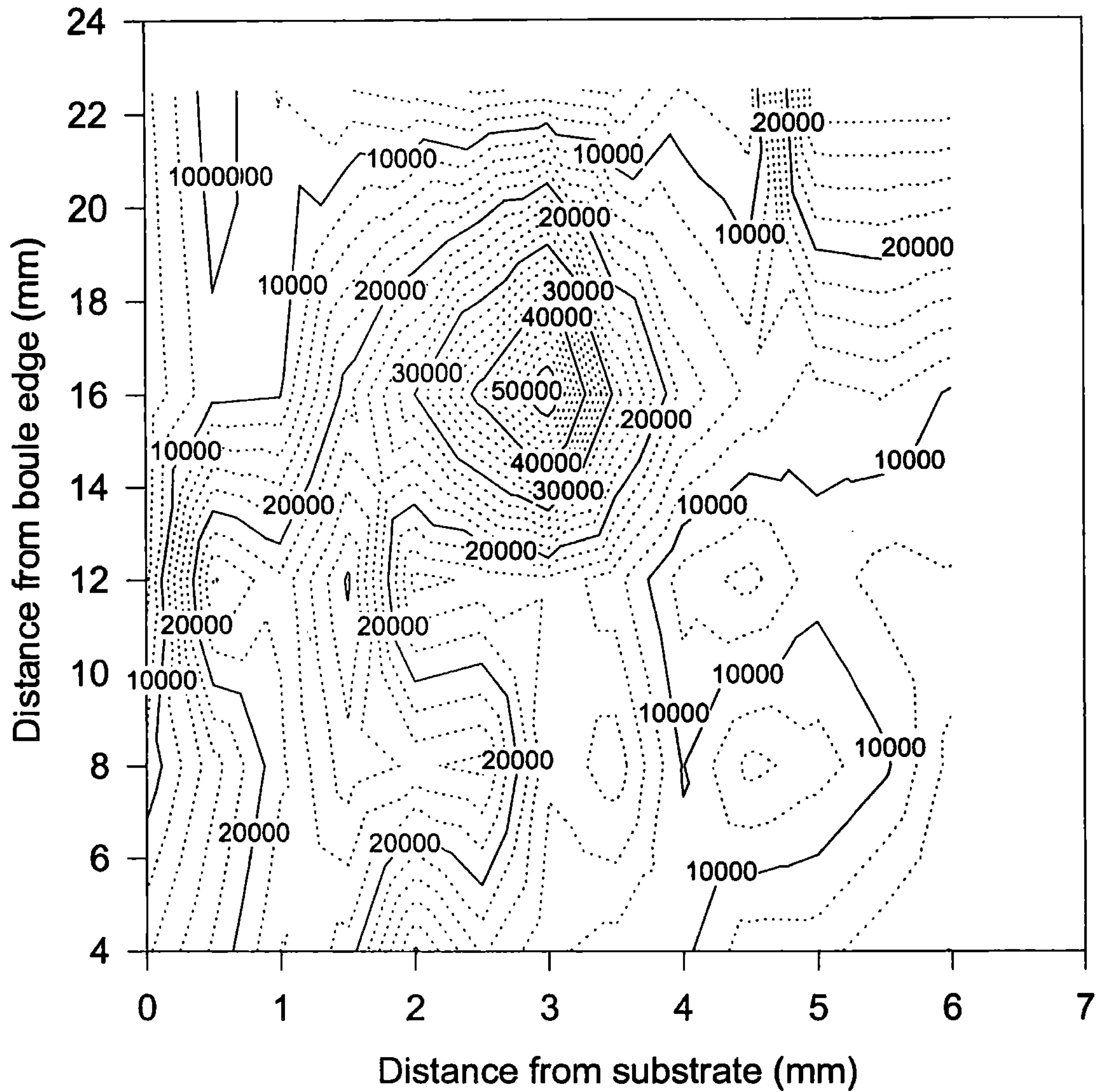


Figure 4.10: Total PL intensity across the wafer

Figure 4.11 shows the variation of intensity of the observed PL peaks as a function of the applied laser excitation intensity. Using the relationship

$$I_{PL} \propto I^{k}_{excitation} \tag{4.1}$$

(see theory section p 33) the k value associated with each PL peak can be found, and thus the nature of the recombination mechanism responsible can be determined. Although a more detailed analysis of excitation

power dependence by Schmidt et al [15] points towards deviation from this rule when the intensity is varied by many orders of magnitude, our results are limited to variation over only a few orders of magnitude so the above relationship can be expected to hold true. A plot of Log(PL peak intensity) versus total optical density of the filters deployed to control illumination intensity will have a gradient of $-k$. The intensity of each individual peak was found using a computer peak fitting algorithm which deduced the total area under each peak. Due to the relatively low intensities of some of the peaks, relatively few data points could be obtained in most cases.

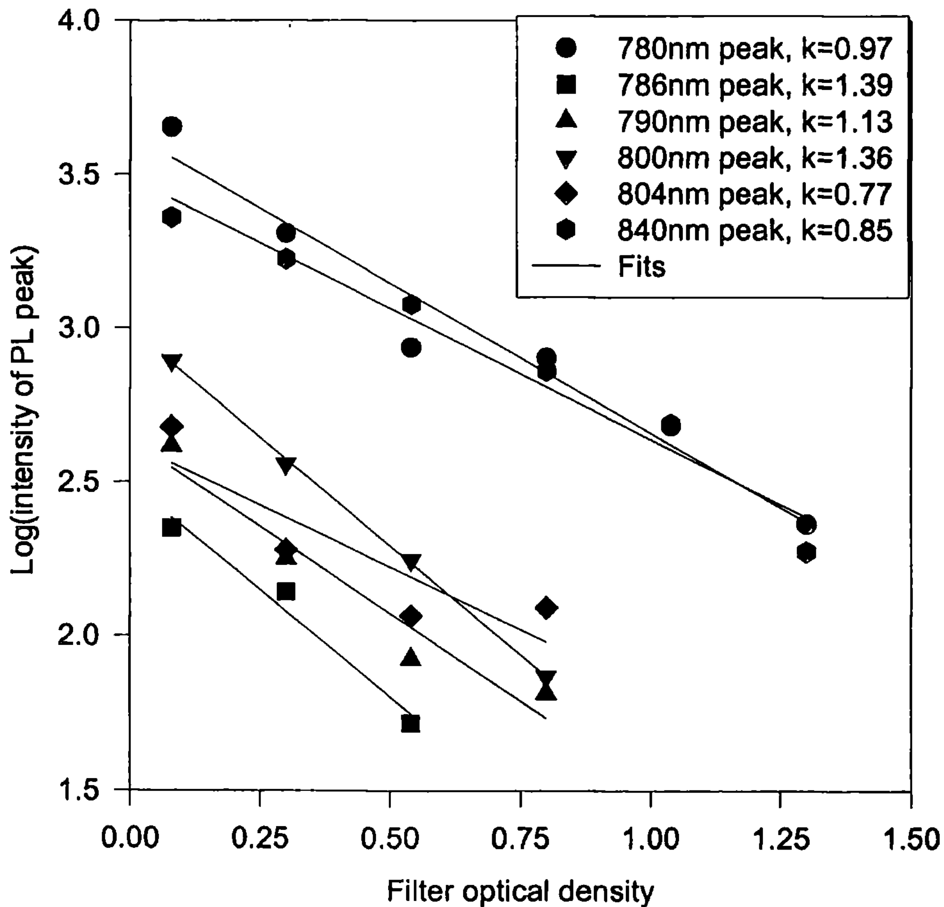


Figure 4.11: PL peak intensity as a function of illumination intensity.

The 1.59eV near band edge peak has a k value approaching unity. A k value of 1 [15-17] is normally observed in the case of free exciton decay or in the case where the exciting photon energy exactly matches the binding energy of the impurity responsible for a bound exciton decay. Since the exciting photon energy is substantially greater than the CdTe bandgap the latter is unlikely to be the case. Since the above value was obtained without attempting to separate out the effect of the free exciton peak (and possibly the donor bound exciton peak if present) it is possible that the effect of these peaks is non-trivial. Using a computer fitting program (Peak-Fit) to separate out the 1.598eV peak from the 1.59eV peak, we obtain k values of 1.53 and 1.44 respectively. 1.44 is what is expected for a bound exciton decay. The fact that the 1.598eV peak now has a k value greater than 1 can be attributed to the inherent difficulties in separating out the two peaks, with the smaller one suffering more greatly from any inaccuracy, and also the possible influence of the donor bound exciton peak which cannot be independently resolved.

The 1.577eV peak has a k value of 1.13, which suggests its nature to be excitonic, as does the LO phonon replica of the 1.59eV peak at 1.5689eV. The 1.548eV peak has a surprisingly high k value considering its assignment as an electron-neutral acceptor decay, whereas the 1.54eV DAP peak has a k value less than 1, which is what is expected for a donor-acceptor pair recombination although it is still substantially greater than the k values for DAP recombinations reported by Schmidt [15]. The apparent increase in intensity of this peak on the last reading exemplifies the difficulties of separating out two overlapping peaks over a range of intensities. The 1.476eV peak (measured at a region of the sample where it is much more intense than in the example spectrum shown) also has a low k value, which is expected of a deep defect level although it is not strictly valid to analyze deep levels in this way.

Figure 4.12 shows the variation of the intensity of the main excitonic emission line with temperature. Due to the inaccuracies involved in separating out the donor and acceptor bound exciton peaks from the free exciton peak, the net intensity of all three was plotted as a function of temperature (though the acceptor bound exciton peak is assumed to be dominant). No distinguishable spectra were observed above a temperature of 40K. By plotting ln(I) against 1/T, the relationship [18]

$$\frac{I}{I_0} = \left[ 1 + C_1 e^{-\frac{E_{T1}}{kT}} + C_2 e^{-\frac{E_{T2}}{kT}} + \ldots.. \right]^{-1}$$

(4.2)

(see theory section) should give us a series of gradients corresponding to the activation energies $E_{Tn}$ of the dissociation routes of the exciton.

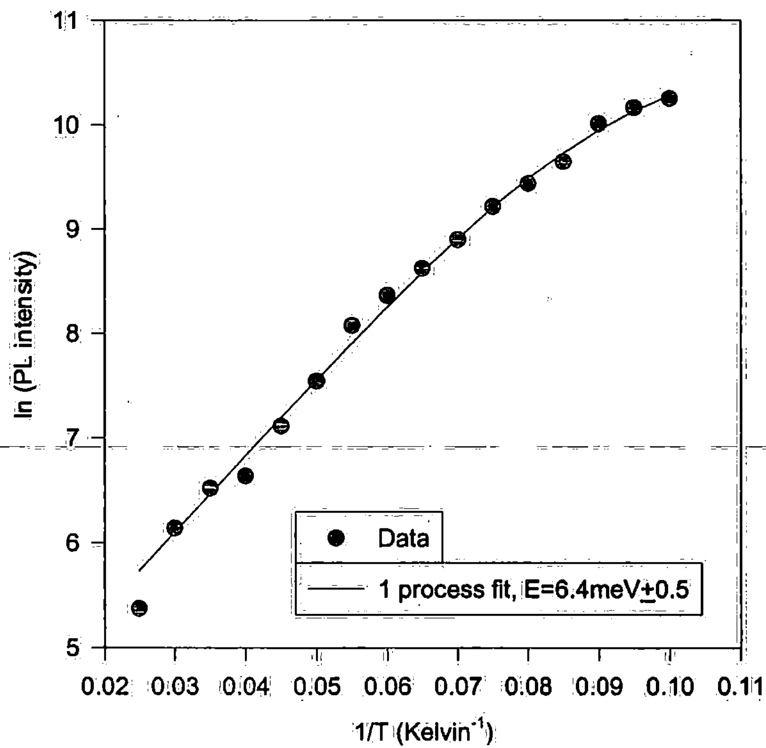


Figure 4.12: Variation of near band edge peak intensity with temperature.

Over the range of temperatures used, the graph has only a single clear gradient, suggesting that the bound exciton has only one main route of dissociation. This is concurrent with the findings of Eggleston [19] who found two dissociation energies for bound excitons in polycrystalline CdTe, but the more energetic process was only dominant at temperatures above 40K and so cannot be observed in the results here. The value of 6.4meV is below the known CdTe exciton binding energy of 10meV [20]. The first mechanism of dissociation likely to be encountered as the temperature is increased from 10K is, according to Zimmerman et al[21] the thermal release of an exciton,

$$(A^0X) \rightarrow A^0 + X \tag{4.3}$$

as this will (in most circumstances) have the lowest activation energy. The result obtained falls within the bounds of the known exciton binding energies [21] of several acceptors in CdTe, such as $Cu_{Cd}$ ($E_b$=6.54meV), $Li_{Cd}$ ($E_b$=6.87meV) and $Na_{Cd}$ ($E_b$=6.94meV). This model cannot be applied to the non-excitonic recombinations observed at energies less than 1.59eV. However, the behavior of the1.548eV and 1.54eV ($eA^0$ and DAP respectively) peaks as the temperature increases can be seen to follow the pattern observed by Dean [22] for the case of a free-bound recombination and a DAP recombination sharing a common acceptor. As can be seen in figure 4.13, the $eA^0$ peak becomes dominant as the temperature is increased.

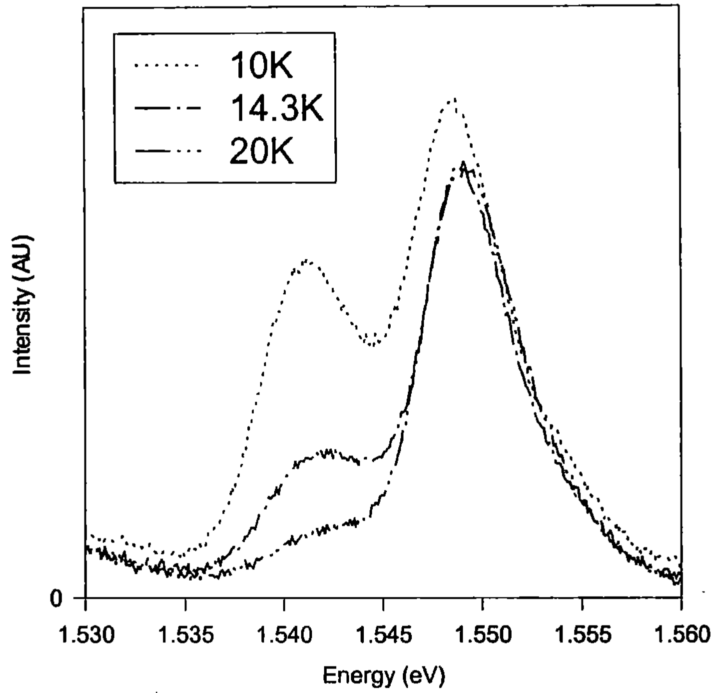


Figure 4.13: Variation in the 1.548 and 1.540eV peaks with temperature.

Following the ideas of Dean [23], the 1.476eV "Y" luminescence emission is excitonic in nature, and thus a similar temperature dependent model can be applied as was applied to the near band edge peaks. Work done by Hildebrandt et al [11] suggests a relationship of the form

$$V(T) = \frac{V_0}{1 + CT^{\frac{3}{2}} e^{\frac{-E}{kT}}} \tag{4.4}$$

Where V(T) is the ratio of the Y luminescence peak to the excitonic near band edge peaks. Unfortunately in the sample studied the Y luminescence peak was significant only in regions where the near band edge peak was negligible, and vice versa, so an accurate ratio could not be obtained.

Some of the observed peaks, most notably the 1.476eV "Y" luminescence peak and the 1.59eV acceptor bound exciton peak have clearly observable LO phonon replicas. By fitting the phonon replica spectrum to the formula

$$I_{(h\nu)} = A\sum_{k=0}^{k=\infty} e^{-S}\frac{S^k}{k!}\frac{1}{1+(h\nu - E_0 + kE_{LO})^2/\Gamma^2} \tag{4.5}$$

(see theory section) the Huang-Rhys phonon coupling parameter S can be determined, which gives a measure of the strength of the interaction between the electrons and the crystal lattice. Figure 4.14 shows the case of the 1.476eV peak and replica spectrum which gives a Huang-Rhys parameter of 0.15±0.01 (after the subtraction of a straight baseline to provide a reasonable fit), somewhat smaller than the value of 0.2 observed by Dean et al [24].

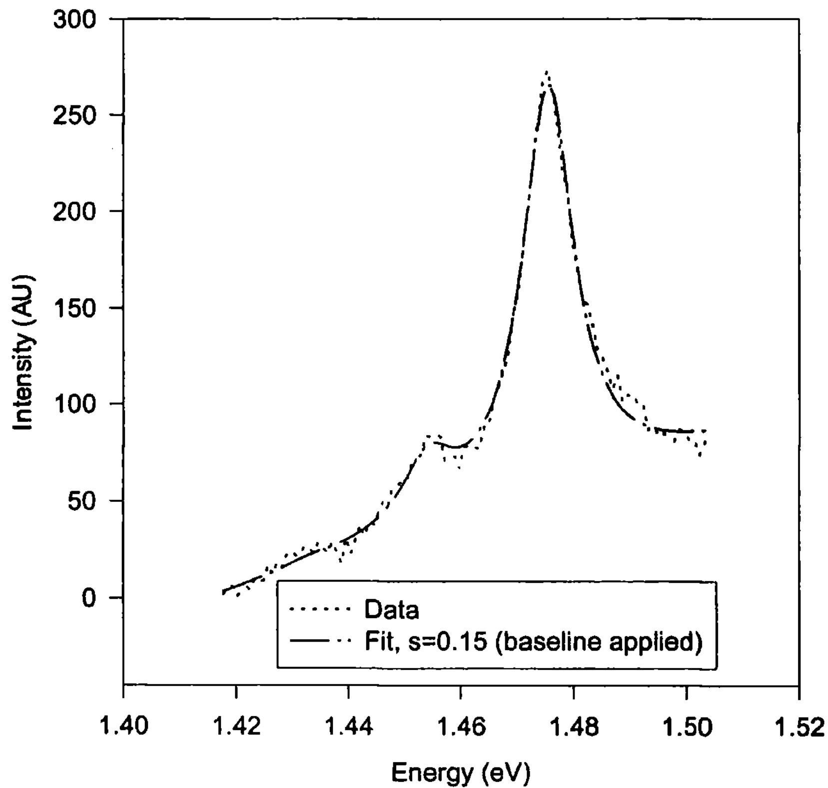


Figure 4.14: The 1.476eV "Y" luminescence peak and LO phonon replica spectrum

The same analysis was applied to the 1.59eV peak and its phonon replica at 1.569eV, giving a Huang-Rhys parameter of 0.04±0.003. The fact that the 1.476eV peak has much stronger lattice coupling than the near band edge excitonic feature suggests that it is related to a lattice defect. However, it is still relatively weak compared to k values for DAP and free-bound transitions (typically s=2-3), suggesting that the transition may still involve an exciton.

### 4.4 Conclusions

Photoluminescence characterization of the representative section of the CdTe crystal boule reveals a relatively pure, defect free crystal, dominated by near band edge excitonic recombination routes. The low FWHM of the main excitonic feature and the high ratio of excitonic to deep level luminescent emission confirm that the boule is of high material quality. Temperature dependent PL confirms that the main excitonic recombination route is an acceptor bound exciton recombination ($A_0X$), suggesting that the material may be p type. Further PL emission peaks such as the $eA^0$, DAP and "Y" luminescence have been identified by comparison to the literature and verified by temperature and intensity dependent measurments. The "best" quality region of the crystal, based on net PL intensity and the ratio of near band edge to deep level luminescence (which were found to correlate) is midway between the substrate and the top surface, and midway between the center and the outer edge of the boule. A shift of all PL peaks to higher energies is observed near the substrate, suggesting the diffusion of Zn from the $Cd_xZn_{1-x}Te$ substrate. This effect is limited to the first millimeter of the sample. Determining the Huang-Rhys parameter from the phonon replica spectrum of the near band edge and "Y" luminescence features gives S=0.04 and S=0.15 respectively, suggesting that the "Y" luminescence is much more strongly coupled to the lattice than the near band edge emission.

### 4.5 References

Ref


1. Capper, E.P., *Narrow-gap II-VI Compounds for Optoelectronic and Electromagnetic Applications*, . 1997, Chapman & Hall. p. 507-560.

2. Mullins, J.T., *et al.*, *A novel "multi-tube" vapour growth system and its application to the growth of bulk crystals of cadmium telluride.* Journal of Crystal Growth, 1999. **208**: p. 211-218.

3. Aitken, N.M., *et al.*, *Characterisation of cadmium telluride bulk crystals grown by a novel "multi-tube" vapour growth technique.* Journal of Crystal Growth, 1999. **199**(Pt2): p. 984-987.

4. Gilestaylor, N.C., *et al.*, *Photoluminescence of CdTe - a comparison of bulk and epitaxial material.* Journal Of Vacuum Science & Technology a-Vacuum Surfaces and Films, 1985. **3**(1): p. 76-82.

5. Cooper, D.E., J. Bajaj, and P.R. Newman, *Photoluminescence spectroscopy of excitons for evaluation of high- quality CdTe crystals.* Journal Of Crystal Growth, 1988. **86**(1-4): p. 544-551.

6. Zimmermann, H., *et al.*, *Mechanism of the temperature-dependence of bound-exciton photoluminescence of CdTe crystals.* Journal Of Crystal Growth, 1990. **101**(1-4): p. 691-694.

7. Kim, Y.H., *et al.*, *Photoluminescence study on the effects of the surface of CdTe by surface passivation.* Journal of Applied Physics, 1999. **85**(10): p. 7370-7373.

8. Shin, H.Y. and C.Y. Sun, *Photoluminescence spectra of Cl-doped CdTe crystals.* Journal Of Crystal Growth, 1998. **186**(3): p. 354-361.

9. Figueroa, J.M., *et al.*, *Photoluminescence spectra and carrier mobilities in polycrystalline films of CdTe.* Journal Of Crystal Growth, 1990. **106**(4): p. 651-656.

10. Madelung, O., *Physics of II-VI and II-VII Compounds and Semimagnetic Semiconductors.* Landolt-Bornstein. Numerical Data and Functional Relationships, ed. K.-H. Hellwege. Vol. 17b. 1982, Berlin: Springer Verlag.

11. Hildebrandt, S., *et al.*, *Localization of Y luminescence at glide dislocations in cadmium telluride.* Journal De Physique III, 1997. **7**(7): p. 1505-1514.

12. Stadler, W., *et al.*, *Optical investigations of defects in Cd1-xZnxTe.* Physical Review B-Condensed Matter, 1995. **51**(16): p. 10619-10630.

13. Davis, C.B., *et al.*, *Photoluminescence and absorption studies of defects in CdTe and ZnxCd1-xTe crystals.* Physical Review B-Condensed Matter, 1993. **47**(20): p. 13363-13369.

14. Lischka, K., *et al.*, *Low-temperature photoluminescence from CdTe grown by hot-wall epitaxy on GaAs.* Applied Physics Letters, 1989. **55**(12): p. 1220-1222.

15. Schmidt, T., K. Lischka, and W. Zulehner, *Excitation-power dependence of the near-band-edge photoluminescence of semiconductors.* Physical Review B-Condensed Matter, 1992. **45**(16): p. 8989-8994.

16. Lee, J.S., *et al.*, *Room-temperature band-edge photoluminescence from cadmium telluride.* Physical Review B-Condensed Matter, 1994. **49**(3): p. 1668-1676.

17. Aguilarhernandez, J., *et al.*, *Photoluminescence studies of semiconducting polycrystalline CdTe-films.* Japanese Journal Of Applied Physics Part 1-Regular Papers Short Notes & Review Papers, 1994. **33**(1A): p. 37-41.

18. Bimberg, D., M. Sondergeld, and E. Grobe, *Thermal dissociation of excitons bound to neutral acceptors in high purity GaAs.* Physical Review B, 1971. **4**(10): p. 3451-3455.

19. Eggleston, J.M., *Optical Spectroscopy of Thin Film Semiconductor Structures*, in *Physics.* 1997, Durham: Durham. p. 188.

20. M. Aven, J.S.P., ed. *Physics and Chemistry of II-VI Compounds.* . 1967, North Holland Publising Company.

21. Zimmermann, H., R. Boyn, and K. Piel, *Thermal quenching of bound exciton emission due to phonon-induced nonradiative-transitions - experimental-data for CdTe and InP.* Journal Of Physics-Condensed Matter, 1992. 4(3): p. 859-868.

22. Dean, P.J., *Photoluminescence as a diagnostic of semiconductors.* Progress in Crystal Growth and Characterization of Materials, 1982. **5**(1-2): p. 89-174.

23. Dean, P.J., *Comparison of MOCVD-grown with conventional II-VI materials parameters for EL thin-films.* Physica Status Solidi a-Applied Research, 1984. **81**(2): p. 625-646.

24. Dean, P.J., G.M. Williams, and G. Blackmore, *Novel type of optical-transition observed in MBE grown CdTe.* Journal Of Physics D-Applied Physics, 1984. **17**(11): p. 2291-2300.

# 5 Studies of Bevelled CdTe/CdS Solar Cells

## 5.1 Introduction

Currently the majority of the worlds electrical power is generated by the burning of fossil fuels. While in principle this is a renewable source of energy generated by the gradual decomposition of bio-matter beneath the planets surface, the immense timescales involved (65-2 million years [1]) mean that in practice these fuels are not renewable, at least not at the rates of current consumption. A further problem with such power sources is the atmospheric pollution generated by any large-scale combustive process (greenhouse gasses, acid rain due to sulphur emission). Nuclear (fission) power has its own safety, pollution and fuel limit issues as well. Although fusion power offers principally a source of virtually inexhaustible "clean" power, the technology is at best several decades away [2]. In order to maintain a readily available source of electrical power to the expanding world population over the next millenium mankind will be forced to turn to more directly renewable sources of electrical power generation such as wind, tidal, biogas and solar power generation. One of the leading contenders for a source of readily available electrical power is the (photovoltaic) solar cell. Based on the principle of a p-n semiconductor junction exposed to sunlight causing the excitation of electrons which are separated from the holes by the junction field and thus forced round an external electrical circuit to maintain charge balance, the phototovoltaic effect was discovered by Bequerel in 1839 [3]. By 1877 [4] the effect was being exploited for light sensing purposes. The earliest practical power generating photovoltaics however were not invented until much later (1954, by Chapin et al [5] and Reynolds et al [6] ). For a more detailed history of photovoltaics see Boyle [7] .

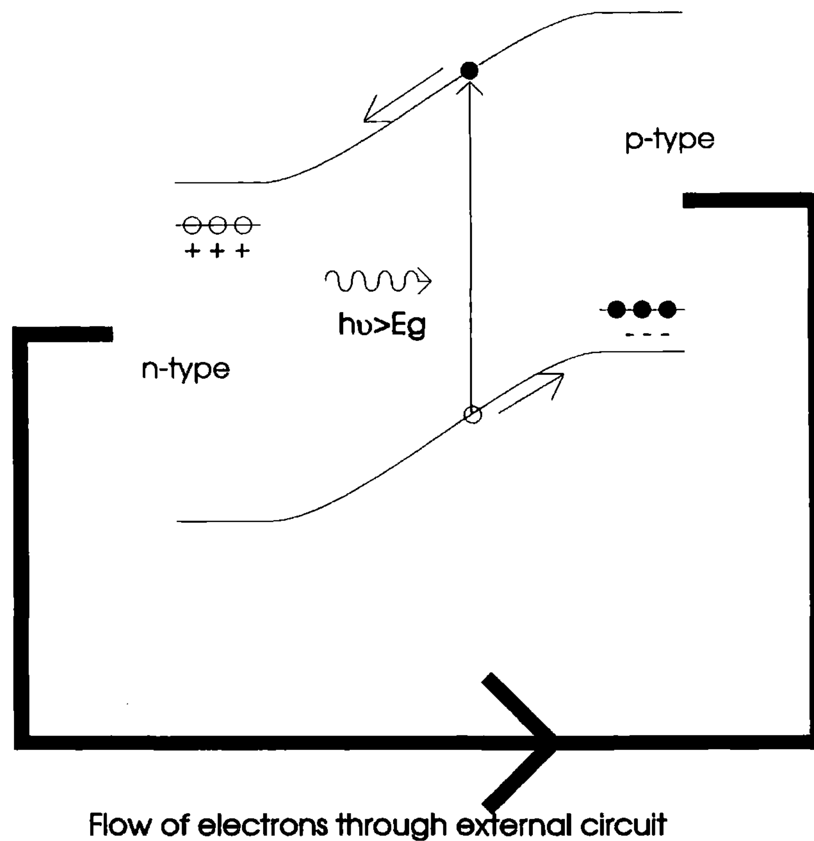


Figure 5.1: Principle of a p-n junction solar cell.

Over the past decades, Silicon has been the leading material for solar cells. Silicon is an indirect bandgap semiconductor and thus has a poor absorption of light, but due to the highly developed state of silicon technology (principally driven by its use in integrated circuits), silicon cells can be manufactured relatively cheaply and to high levels of efficiency (16-24% [8]). However, the fundamental problem of the indirect bandgap means that a large volume of silicon must be used in such devices to compensate for its poor absorption. Silicon is the second most abundant element on the planet next to oxygen, but refining it to electrical grade purities is an expensive process. Further, Silicons bandgap of 1.12eV is not ideally suited to the solar spectrum and while absorbing a large part of the available solar radiation it generates a relatively low voltage compared to the average energy of the incident photons, leading to a large energy pay back time.

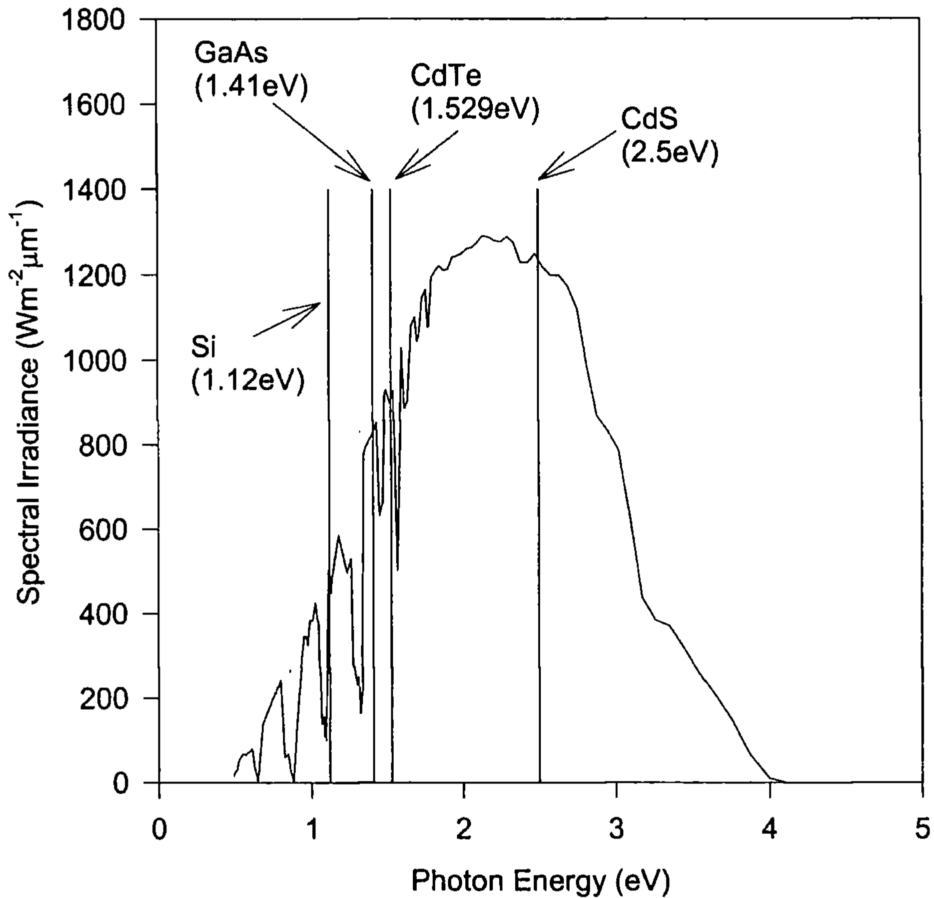


Figure 5.2: The AM1.5 solar spectrum with some semiconductor bandgaps shown (spectrum from NASA data as quoted by Farenbruch and Bube [9] and Edwards [8] ).

### 5.1.1 Thin film cells

Principally a cheaper alternative to silicon cells is the use of direct bandgap semiconductors. With much higher absorption coefficients (>$10^5$ $cm^{-1}$ in the case of CdTe [10] ), the devices need only be microns thick in order to absorb all radiation that enters the device. Of the direct bandgap semiconductors, the III-V material GaAs has produced the most impressive results. GaAs based cells have achieved efficiencies as high as 24%[11] in single junction devices and 35% [12] in a multijunction cell with GaSb. However, while such high efficiencies make GaAs cells ideal for utilities such as powering satellites, where the power to weight ratio is important, high manufacturing costs (generally GaAs cells are grown by single crystal epitaxy [13] ) make them a less appealing prospect for terrestrial applications. This problem can be partially solved by the

use of concentrator cells: arrays of mirrors focussing a light intensity of 100-1000 suns onto a single high efficiency solar panel. However, the geometry involved adds its own cost as well as being unsuitable for such applications as PVs on buildings. The attention of industry is now focussed on cells which, while less efficient on a watt per photon basis, are tolerant of relatively simple and cheap large area manufacturing processes. Two current leading direct gap semiconductor cells being researched for this purpose are copper indium di-selenide cells and cadmium telluride/cadmium sulphide heterojunction solar cells. The solar cell research performed in this thesis is upon the latter type of solar cell.

Cadmium telluride based solar cells have been around since the 1960s when CdTe homojunctions were used to create cells of efficiencies of up to 6% [14] . With the development of heterojunction technology and the CdS heterojunction in the early 1970s [15] efficiencies have gradually increased to 16% [16] in the lab, with best commercial large area efficiencies of around 10% [17], although theoretically the efficiency could be as high as 29% [18]. Currently the most efficient device configuration is that of a 5-10 um thick polycrystalline CdTe absorber layer grown on a ~100nm thick polycrystalline CdS window layer grown on a transparent conducting oxide (TCO) front contact grown on a glass "superstrate" which forms the front of the device. A metalised back contact and rear encapsulation can then be applied to the back of the device. The bandgap of CdTe (1.5eV at room temperature) is well placed for absorbing most of the solar spectrum received at the surface of the earth while the CdS ($E_g$=2.5eV) lets through all light except deep blue/violet (due to the extreme thinness of the CdS layer, some light of $h\upsilon$>2.5eV can penetrate as far as the CdTe).

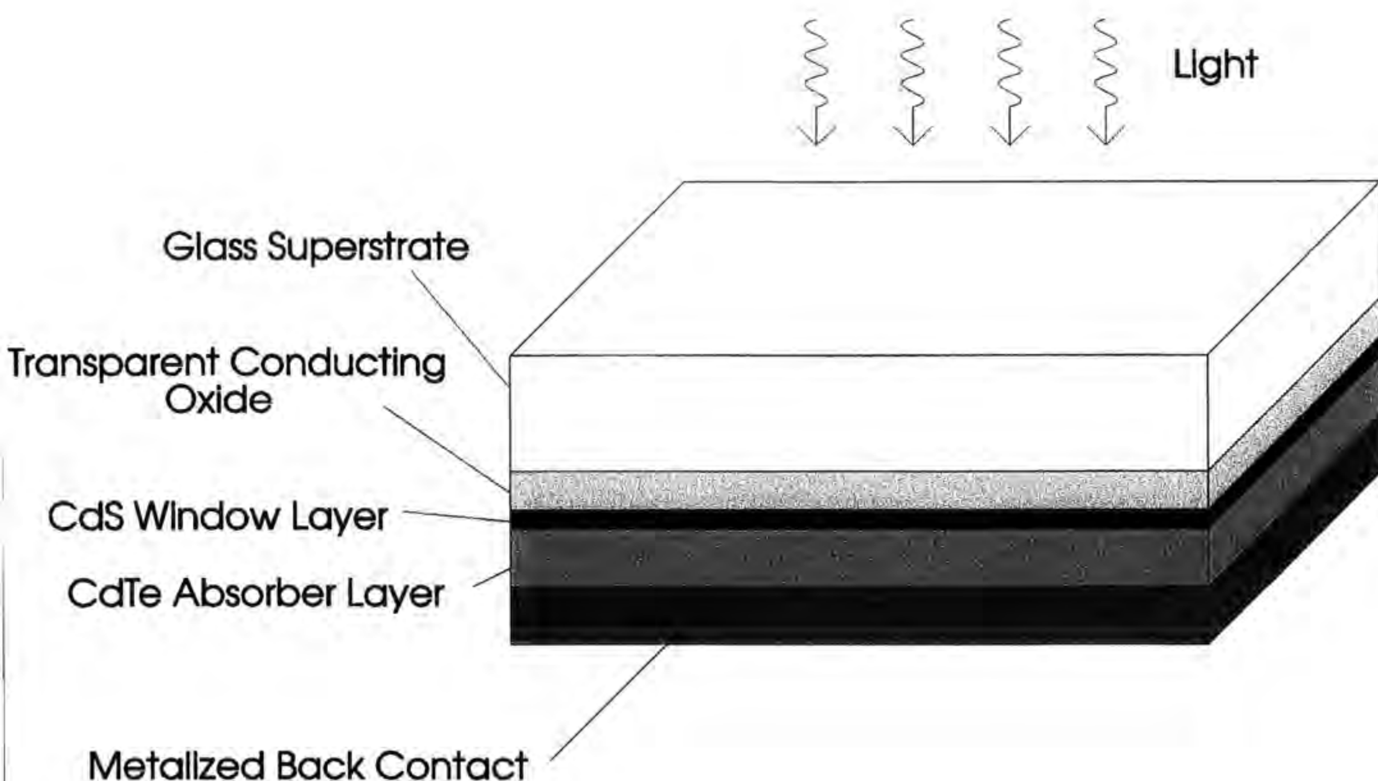


Figure 5.3: A CdTe/CdS solar cell (not to scale)

This cell configuration has the advantage that a metallic front contact is not required, so the entire area of CdTe is useable (although there must be regular breaks in the CdTe layer to make an electrical connection to the TCO front contact). The cells are tolerant of a variety of deposition techniques for deploying the semiconductor layers, including chemical bath deposition (CBD), closed space sublimation (CSS), metallo-organic chemical vapor deposition (MOCVD), physical vapor deposition (PVD) and radio frequency sputtering [19]. However, there is one common factor required in all types of fabrication process that produce efficient cells. Prior to the application of the back contact the cells must be annealed in a chlorine rich environment [20-22] (debatably the presence of oxygen is also required [23]). This increases device efficiency from a few percent to typically over 10%. The reason for this effect is not fully understood. Many observable effects of the chlorine anneal (normally $CdCl_2$ is used to provide a chlorine rich environment suitable for interaction with the cell materials) have been noted, these include:

Microstructural changes in the CdTe: [24] The $CdCl_2$ annealing process has been known to cause recovery (the moving of defects to form sub-grain boundaries), recrystallization and grain growth in the CdTe. Grain growth is not observed in large grained material [25] although the increase in efficiency is still observed. A roughening of the interface has been observed on $CdCl_2$ annealing [26], causing better light collection due to multiple reflections. A reduction in stress due to lattice mismatch between the CdTe and the CdS has also been observed [27], possibly due to the interdiffusion of S into the CdTe.

Changes to the electrical characteristics: The anneal has been observed to convert the CdTe from n type to p type (thus increasing the definition of the electrical p-n junction) [17, 28], and to passivate the grain boundaries within the CdTe, reducing the density of recombination centers [29]. Both of these effects may contribute to an observed drop in the series resistance of the CdTe after the $CdCl_2$ anneal [30, 31]. Near the interface region the anneal has been observed to reduce the density of defects responsible for recombination losses. In addition the $CdCl_2$ process has been observed to promote the diffusion of sulphur into the CdTe layer [30] and enhance both the open circuit voltage (Voc) and short circuit current (Jsc) of the devices. It also changes the carrier transport mechanism from tunneling to thermally activated transport.

It is certainly worth mentioning here that another critical limiting factor in the performance of CdTe/CdS solar cells is the application of a conducting back contact to the CdTe layer. Due to the high electron affinity of CdTe (4.5eV) any metallic contact will tend to form a diode like junction which will impede current flow. However, a detailed study of this problem will not be entered into in this thesis, and for more information I would suggest consulting Durose [24], Farenbruch [9] or Brinkman [32].

Using photoluminescence (PL) spectroscopy in conjunction with electrical measurements and grain size analysis [33] we will gain further insights into the effects of the $CdCl_2$ anneal and the principal mechanism(s) by which it increases device performance. This will be achieved by performing measurements on cells subjected to $CdCl_2$ anneals of varying duration, as well as studying untreated cells for reference. In addition, spatially resolved PL will be used to study the electronic bandstructure at different positions throughout the cells and time resolved PL will be used to study the carrier lifetimes. The possibility of obtaining low temperature electroluminescence spectra from the samples will also be explored.

## 5.2 Experimental

### 5.2.1 Device Preparation

The cells to be studied arrived from Antec GmbH in identical 25mmX25mm sections. Each section consisted of 2mm thick glass, followed by 100nm transparent conducting oxide, 80nm CSS deposited CdS and 10μm CSS deposited CdTe. The sections had not been subjected to a $CdCl_2$ anneal or the application of any form of back contact, with the exception of one section which had been annealed in $CdCl_2$ in air at Antec at 400°C for 10 minutes. In the case of the sections that were to be $CdCl_2$ annealed, 60nm of $CdCl_2$ was vacuum evaporated onto the CdTe back surface of the sections. The sections were then placed into a furnace at 400°C open to the air for varying lengths of time before being rinsed with de-ionised water to remove remaining $CdCl_2$. Each section was then cleaved into two 25mm x 12.5mm samples using a tungsten scribing wheel. One sample from each section had a gold back contact vacuum evaporated onto it (after a brief etch in nitric/phosphoric acid mixture to remove surface oxides) and a section of CdTe removed to allow connection to the front contact using silver paint. These samples were used for electrical I-V characterization under illumination (AM1.5 solar simulator, ~100mWcm$^{-2}$) and dark conditions. It is worth noting that gold is not an ideal back contact for a CdTe/CdS solar cell. Aside from forming a diode like junction as discussed earlier it is unstable over time as gold atoms migrate into the CdTe, effectively short circuiting the device. However, provided that the readings are taken within a short time of the contact evaporation (ideally the same day or next day) gold contacts are sufficient for a comparison of the samples electrical characteristics relative to each other. The gold contacts were 3mm in diameter and a mask was of the same dimensions was placed directly above the contacts as shown in figure 5.4 to minimize the effect of carriers being excited in uncontacted areas of the device and migrating through the CdTe to the contact, making the effective area of the device unknown. The electrical characterization was performed in collaboration with M.A.Cousins and the majority of the results will be found also in his thesis [33].

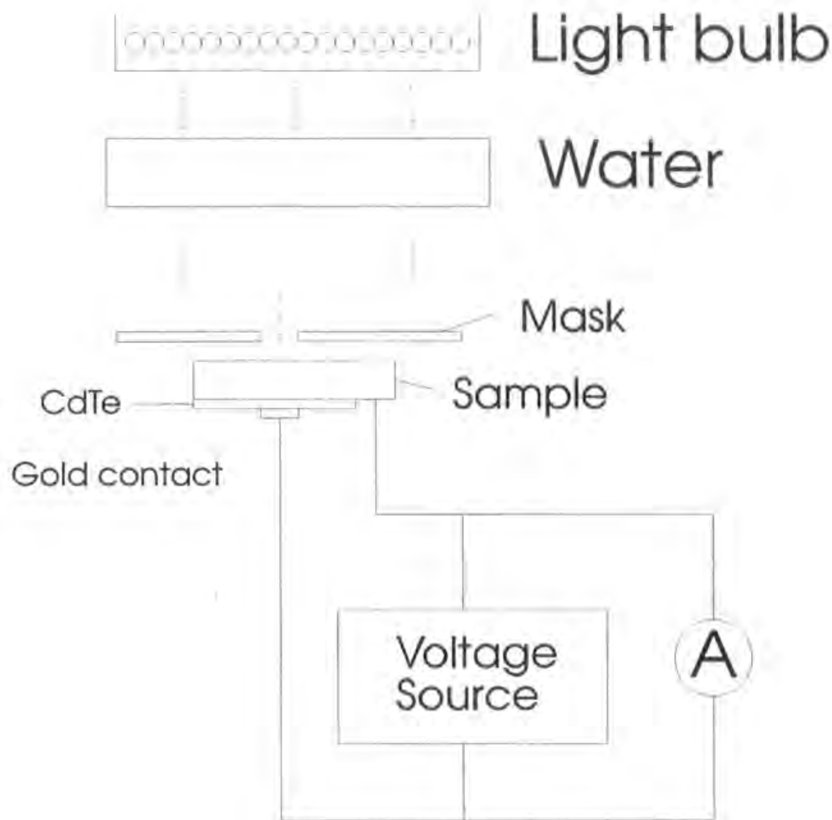


Figure 5.4: The setup used for electrical characterization (not to scale).

The other half of each section was (in the first instance) then polished manually with ¼μm diamond paste until no surface morphology was observed on the CdTe under an optical microscope (the back CdTe surface of the samples as provided was rough, having surface morphology of the order of a micron in depth). At the risk of pre-empting the results, it should be said at this point that the PL from this first batch of samples suggested that the back surface polishing may have influenced the spectra substantially. In order to verify this a second batch of samples was prepared without the back surface polishing. The anneal times for this second series of sample were adjusted to focus around the region of greatest interest as revealed by the first series. The samples were then all bevel etched as described below.

5.2.2 Bevel Etching

In order to study the properties of CdTe/CdS thin film photovoltaic cells by photoluminescence spectroscopy throughout the volume of the cells it is necessary to remove the outer CdTe down to the depth we wish to probe. This was done by means of a chemical bevel. The sample of solar cell material (without back contact) was attached to a glass slide and placed vertically into a cylinder and immersed in methanol. A solution comprising 5% Bromine, 72.5% Ethylene glycol and 22.5% Methanol by volume was the admitted to the bottom of the cylinder by an inlet valve, causing an interface between the bromine mixture and the methanol. The height of this interface could be controlled by varying the height of the cylinder via an electric motor while the bromine mixture reservoir was kept at a constant height (see figure 5.5). The liquid-liquid

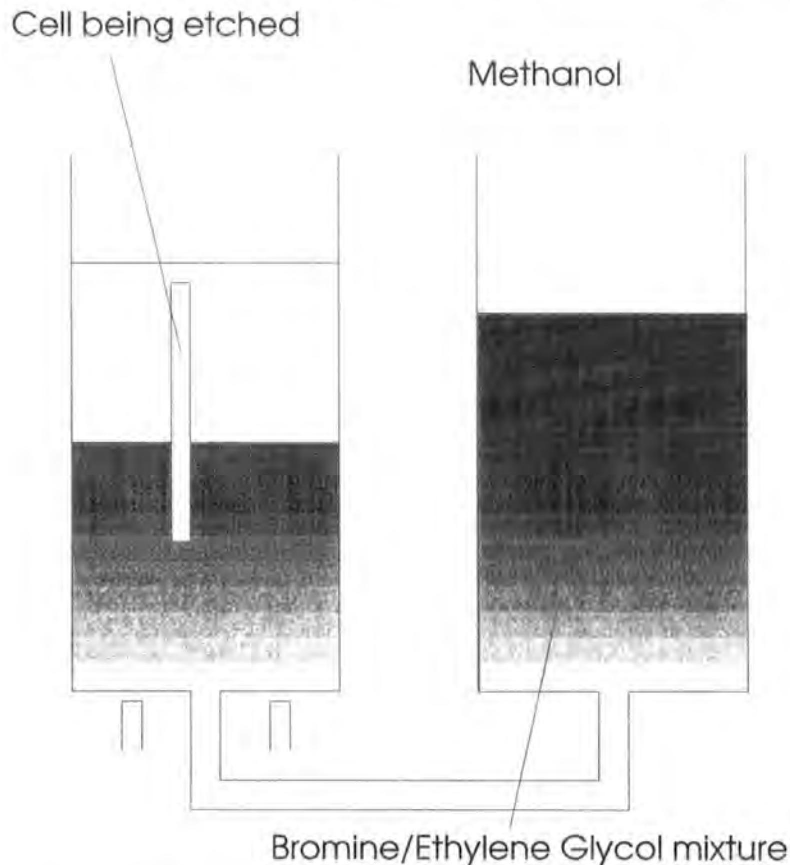


Figure 5.5: The bevel etching arrangement

interface was raised slowly over the solar cell sample until the bottom end of the sample was observed to have been completely dissolved (several test runs were required to determine the correct rate of interface movement so that the top of the sample was still above the interface while the bottom was completely dissolved). The cell was then removed and immediately rinsed in methanol to remove any remaining bromine mixture.

The profile of the resulting bevel was taken using a Tencor instruments Alpha-Step 200 profiler after the photoluminescence characterisation had been done, by manually scraping a line through to the glass substrate using a scalpel along the path that the laser beam had travelled. The surface profiler was then used to measure the thickness of CdTe remaining as a function of position along the bevel. This highly destructive technique was made necessary by the fact that the surface profiler was unable to take single profiles along the entire length of the bevel due to range limitations.

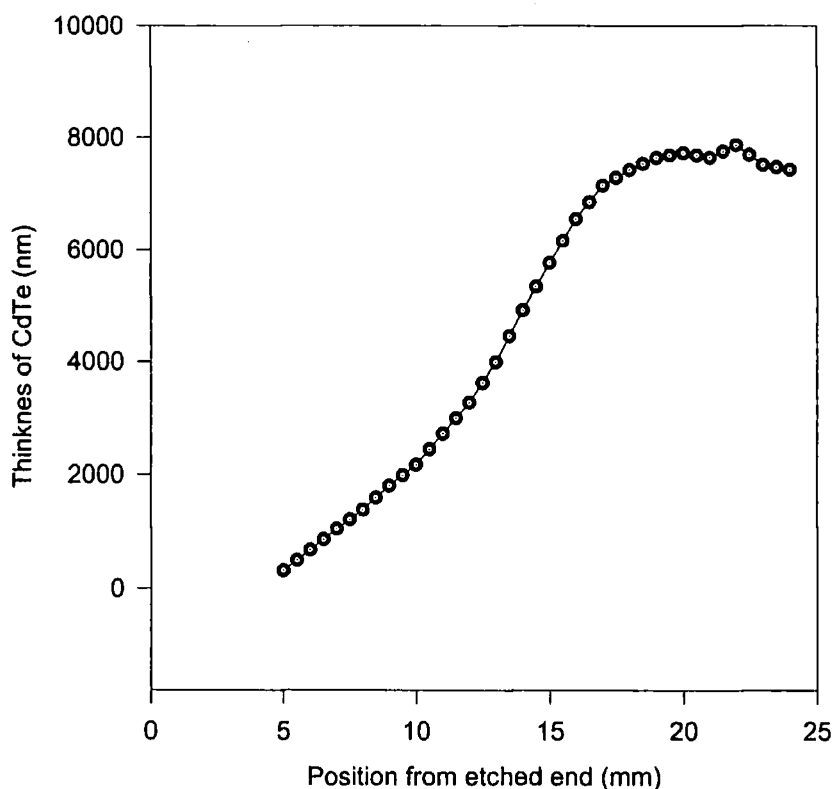


Figure 5.6: Typical profile of a bevelled CdTe/CdS solar cell (untreated sample)

The photoluminescence spectra were taken along the length of the bevel (from fully etched to unetched) using the method described in the experimental techniques section. The PL was taken at 10K using the 150 line/mm diffraction grating and the 457.9nm laser excitation line (in order to excite above the CdS bandgap). The laser power density was $1mWmm^{-2}$ on average over a spot of 0.5mm diameter. Once the spectra had been taken for the whole range of samples, regions of specific interest were returned to and further spectra were taken for a range of illumination intensities.

**5.3 Results and Discussion**

The detailed results of the electron microscopy and grain size analysis are not mentioned here as they were not the work of the author of this thesis. For more detail see the thesis of Mike Cousins [33].

5.3.1 Electrical Characterisation

Figure 5.7 shows the I-V curves (under standard illumination) for all the samples considered. The overall efficiency of a solar cell can be determined by finding its fill factor (FF), open circuit voltage and short circuit current. The fill factor is defined as the maximum area under the negative current/positive bias quadrant of the I-V curve that can be filled by a rectangle drawn from the origin to any point on the I-V curve as a fraction of the area of a rectangle drawn from the origin out to $V_{oc}$ and $J_{sc}$. In other words the maximum possible value of areas A/(A+B) on the upper graph of figure 5.7. The overall efficiency of a cell is defined as:

$$\text{Efficiency} = \frac{V_{oc} J_{sc} FF}{\text{Illu min ationPower}} \tag{5.1}$$

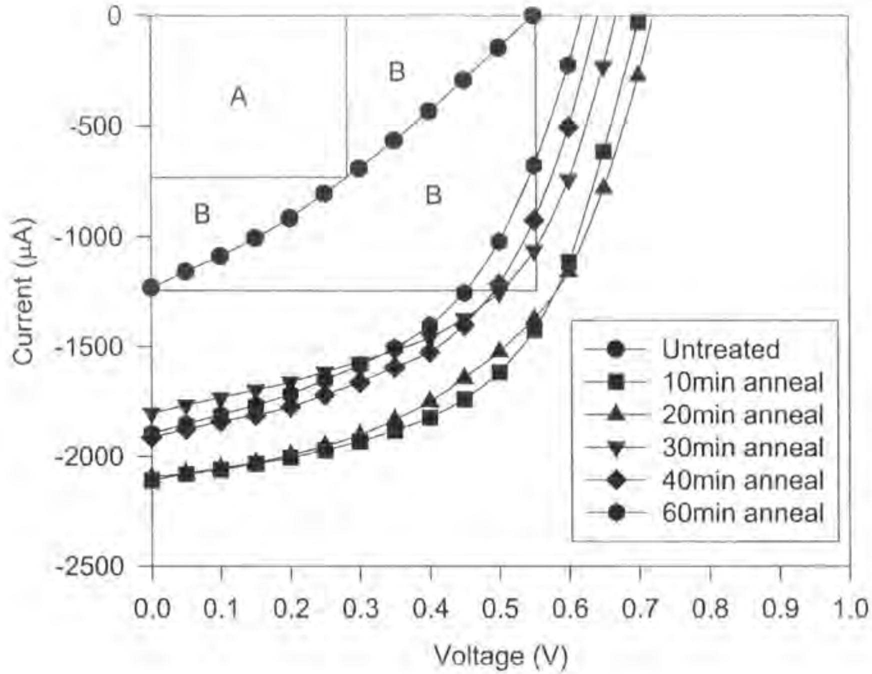


Figure 5.7: I-V curves for samples under standard illumination with example of fill factor shown.

The effects of the $CdCl_2$ anneal can be clearly seen in figure 5.7. The magnitudes of $V_{oc}$ and $J_{sc}$ increase substantially as do the fill factors for all the annealed cells. The 10 and 20 minute annealed samples have significantly higher $V_{oc}$ and $J_{sc}$ values than the samples annealed for longer periods. These results are also summarised below in table 5.1. As can be seen, the 10 minute anneal is the most efficient, with efficiencies generally dropping off with increasing anneal time.

Table 5.1: Electrical characteristics of solar cells

| Anneal Time(Mins): | Untreated | 10 | 20 | 30 | 40 | 60 |
|---|---|---|---|---|---|---|
| Efficiency (%) | 3.121 | 12.326 | 11.545 | 9.576 | 9.745 | 8.745 |
| Fill Factor (%) | 30.801 | 55.657 | 51.156 | 53.179 | 52.956 | 49.748 |
| $V_{oc}$ (V) | 0.550 | 0.702 | 0.720 | 0.668 | 0.643 | 0.620 |
| $I_{sc}$ (mA) | -1.232 | -2.110 | -2.096 | -1.804 | -1.915 | -1.897 |
| $J_{sc}$ (mA cm^-2) | -18.418 | -31.536 | -31.336 | -26.973 | -28.620 | -28.357 |
| $V_{mp}$ (V) | 0.295 | 0.495 | 0.548 | 0.495 | 0.445 | 0.445 |
| $J_{mp}$ (mA cm^-2) | -10.581 | -24.901 | -21.087 | -19.346 | -21.900 | -19.652 |
| $P_{mp}$ (mW cm^-2) | 3.121 | 12.326 | 11.545 | 9.576 | 9.745 | 8.745 |

($V_{mp}$,$J_{mp}$ and $P_{mp}$ are respectively voltage, current density and power output at the position of maximum power output on the I-V curve)

The fractional increase in $J_{sc}$ between the unannealed sample and the samples annealed for a short time (~75%) is greater than the fractional increase of $V_{oc}$(~27%) suggesting a decrease in the series resistance of the sample as noted by Okamoto et al [30]. Both $V_{oc}$ and $J_{sc}$ then decrease by a similar fraction (~10%) towards longer annealing times. The sample annealed for 30 minutes had an anomalously low efficiency due to a low $J_{sc}$ and $J_{mp}$. The reason for this is not known but as we will see later, it does agree with the PL results.

### 5.3.2 Spatially Resolved Photoluminescence

Figure 5.8 shows the variation in PL spectra for a typical $CdCl_2$ treated back surface polished sample. At the back surface a single broad peak is visible between 1.3 and 1.5 eV as well as a sharper peak to higher energies

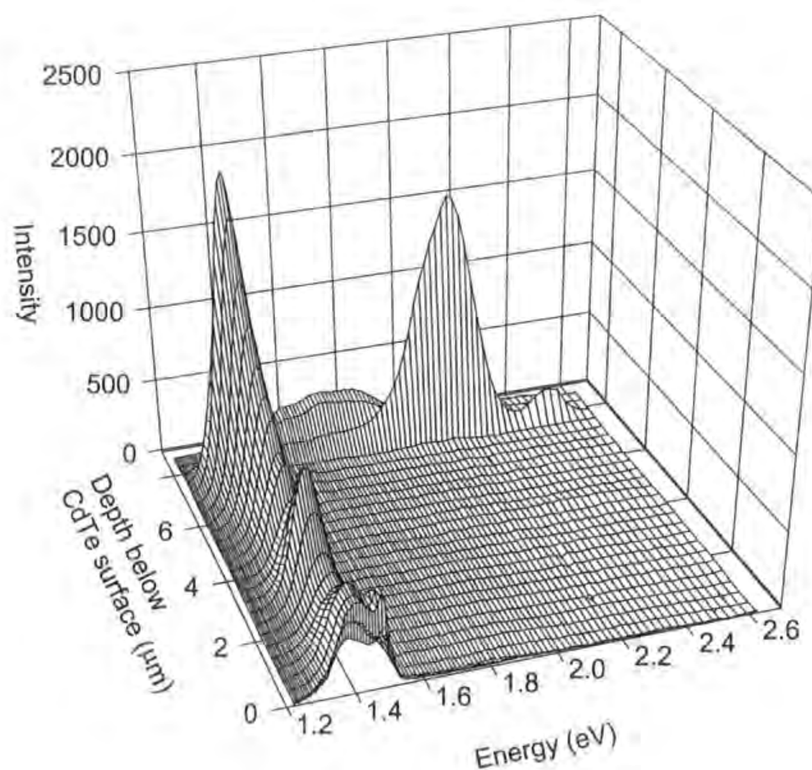


Figure 5.8: PL spectrum as a function of depth into a typical sample

at 1.48eV. Between 400 and 4000nm into the sample the 1.48eV peak disappears. In some cases (to be discussed and shown explicitly later) the broad 1.3-1.5eV peak shifts to lower energies. The intensity of this peak tends to a maximum as the CdS layer is approached. As the CdS layer is reached we observe a spectrum consisting of two peaks of much higher energy (1.9-2.2eV and 2.53eV) due to the CdS. The spectra obtained from below the CdS layer were too broad and inconsistent to interpret meaningfully and are regarded as noise caused by the laser beam passing through the sample and striking the cryostat. Comparing the observed peaks with the observations of other authors, the 1.48eV peak can be assigned to "Y" luminescence caused by recombination of excitons localised at dislocations in the crystal lattice. Usually Te glide dislocations are quoted as the source of the peak [34] but work done by Seto et al [35] reveals the same peak induced by the strain field associated with Frenkel defects. The expected LO phonon replica structure of this peak is subsumed by the broad 1.3-1.5eV peak in most cases. However, in the case of the unannealed polished sample it is visible and can be measured to have a Huang-Rhys constant of $S \sim 0.4$, suggesting a weak coupling to the lattice due to the extended nature of the exciton. The broad 1.3-1.5eV peak is usually attributed to a donor-acceptor pair recombination between a cadmium vacancy complex acting as the acceptor and a shallow chlorine donor [30]. This band is generally found to dominate the PL spectrum in large grained material with a relatively high defect density and low carrier mobilities [36]. When seen in isolation this band has a pronounced phonon replica spectrum with Huang-Rhys parameter of ~2.2. The fact that this spectrum is not observed here suggests the presence of other recombination mechanisms. References on the PL peaks of CdS in a thin film device are more rare, but the 2.53eV CdS peak can be tentatively assigned to a variety of near band-edge transitions shifted to lower energies by the bandgap reduction caused by diffusion of Te into the CdS (although Akimoto et al [37] attribute this peak to an Oxygen related donor-acceptor pair recombination). The lower energy "O" band peak between 1.9 and 2.2 eV has been attributed by various authors to Cd interstitials [38] and Te substitutionals on S lattice sites [39]. At no point on any of the samples studied is there a strong peak observed in the CdTe near band edge (NBE) region of ~1.59eV. Although this implies that the CdTe is not of the highest quality, it cannot be used as direct evidence of poor quality material. Bubulac et al [40] found that near band edge emission in polycrystalline CdTe arose from the sub grain boundaries due to perturbations in the crystal structure. The fact that the exciting laser radiation had an energy substantially greater than the CdTe bandgap in order to excite emission in the CdS also will tend to

cause NBE emissions to be weaker than if a longer wavelength (eg. 488nm or 514.5nm) had been used. Weak near band edge emissions have also been associated with large grains [36] , and short optical lifetimes [41] .

Figures 5.9-5.11 show a representative selection of PL spectra (polished and unpolished samples, unannealed, optimally annealed and annealed for excess time) from the back surface, mid bevel and near-interface regions of the samples.

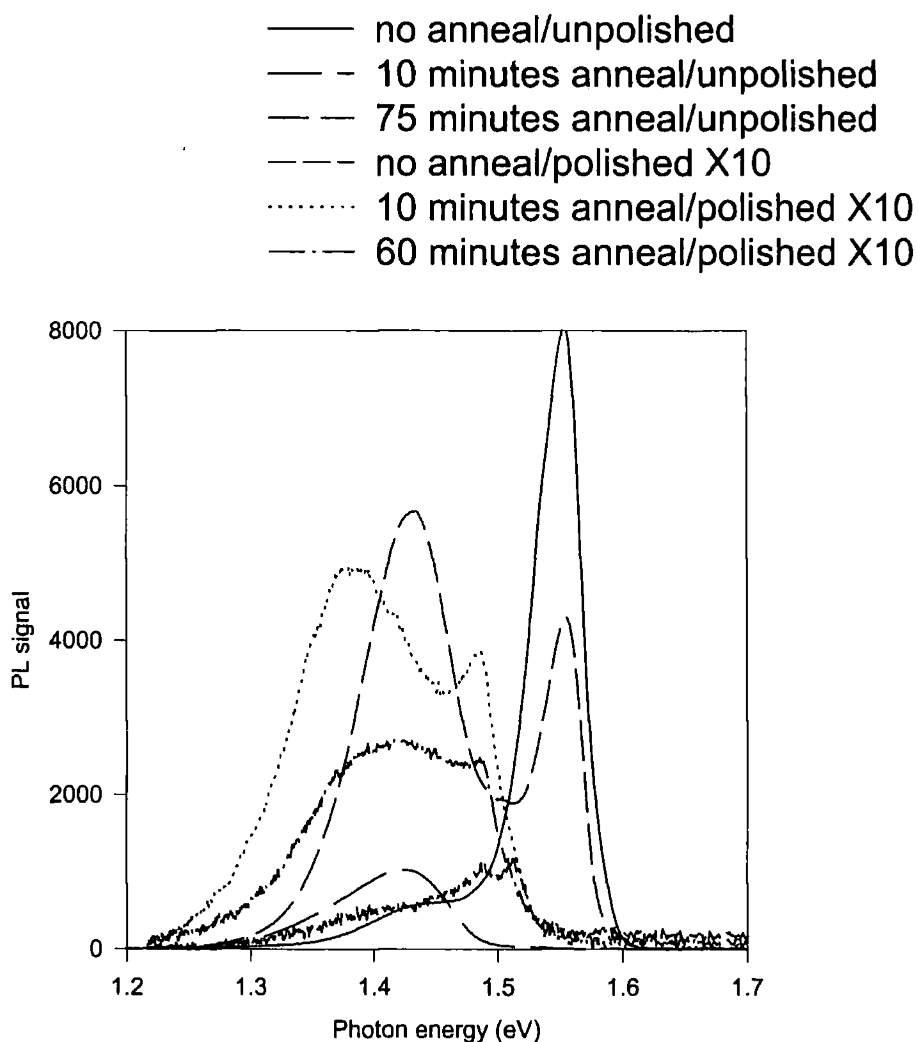


Figure 5.9: A selection of back surface spectra

As can be seen in figure 5.9, the 1.48eV peak is only visible at the back surface of the samples that had been subjected to the 1/4μm diamond paste polishing process prior to PL being performed. This is strong evidence that the 1.48eV peak is due to induced defects. The PL from the polished samples is also noticeably (almost exactly an order of magnitude) fainter than that from the unpolished samples, suggesting that significant nonradiative recombination routes are induced in the back surface of the samples by polishing. The $CdCl_2$ anneal both increases the overall PL intensity and reduces the relative intensity of the 1.48eV peak, suggesting that it at least partially compensates for the damage done by polishing the samples.

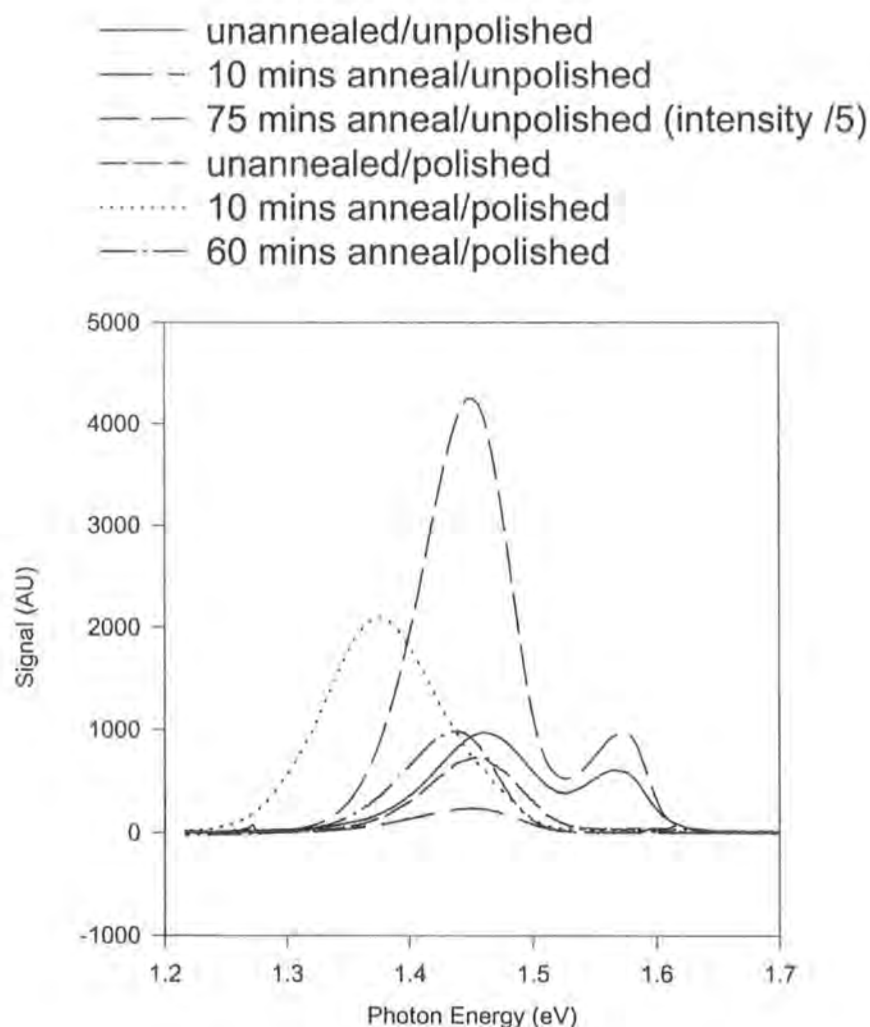


Figure 5.10: A selection of mid bevel spectra

The 1.3-1.5eV peak has the smallest relative intensity at the back surface in the untreated samples. Its relative intensity increases with increasing $CdCl_2$ anneal time. This favours the explanation that the peak is mainly due to a chlorine related DAP transition as described previously. The fact that it is visible at all in the untreated samples suggests either that the PL spectrum is sensitive to traces of Cl intrinsically present in the material [41] or that other mechanisms also contribute to this peak as mentioned previously (for example other shallow donor states causing recombination with the $V_{Cd}$ acceptor complex). The reason that this peak is at lower energies in the 10 minute annealed polished sample is not known. The broadness of this peak and its lack of a fine structure, when compared to the work of Zanio [14] with In doped CdTe, suggests a defect concentration of $>10^{18}cm^{-3}$. This has been verified by Okamoto et al [30] by PL analysis. The peak present at 1.51eV in the untreated, polished sample has been attributed in the past to bulk recombination from the centre of grains of CdTe [40, 42]. The species responsible has not been conclusively identified but the fact that this peak is only visible in the polished, untreated sample suggests that it is related to lattice defects. In the case of the unpolished samples, a strong peak at 1.55eV is observed in the majority of the samples (notably however, not in the most efficient sample). This peak has been attributed (by various authors) to Cadmium vacancies [36, 43, 44], Oxygen related DAP transitions with $O_{Te}$ acting as a shallow acceptor [23, 37, 45] or to chlorine related transitions [46]. The fact that $CdCl_2$ treatment seems to at least temporarily passivate the centre responsible for this peak rejects the latter explanation.

Figure 5.10 shows the PL spectra of the same set of samples at a position along the bevel measured to correspond to approximately the centre of the device in each case. The disappearance of the 1.48eV and 1.51eV peaks is noted, as we are now too far below the back surface for the direct effects of the back surface polishing to be observed. The intensity of the 1.55eV peak in the unpolished samples is falling off. Eggleston et al [41] observe a similar peak in polycrystalline CdTe devices, but in that case the 1.55eV peak was found to increase in intensity as the interface was approached and was ascribed to an $O_{Te}$ acceptor state induced during the anneal. Since the peak is here observed in the untreated sample and not in the 10 minute annealed sample, this cannot be the case. It is possible that the 1.55eV peak is related to substitutional oxygen incorporated during the deposition of the CdTe layer (This layer was deposited by closed space sublimation, but a low vacuum or the presence of oxide impurities could account for the presence of oxygen) or later when the samples were exposed to air during transit from Antec. If this is the case then the $CdCl_2$ treatment initially

passivates the $O_{Te}$ centres responsible, but with excess anneal times either the chlorine migrates further into the device or more oxygen is incorporated from the back surface causing the peak to appear again. Alternatively, the peak could be caused by excess tellurium at the

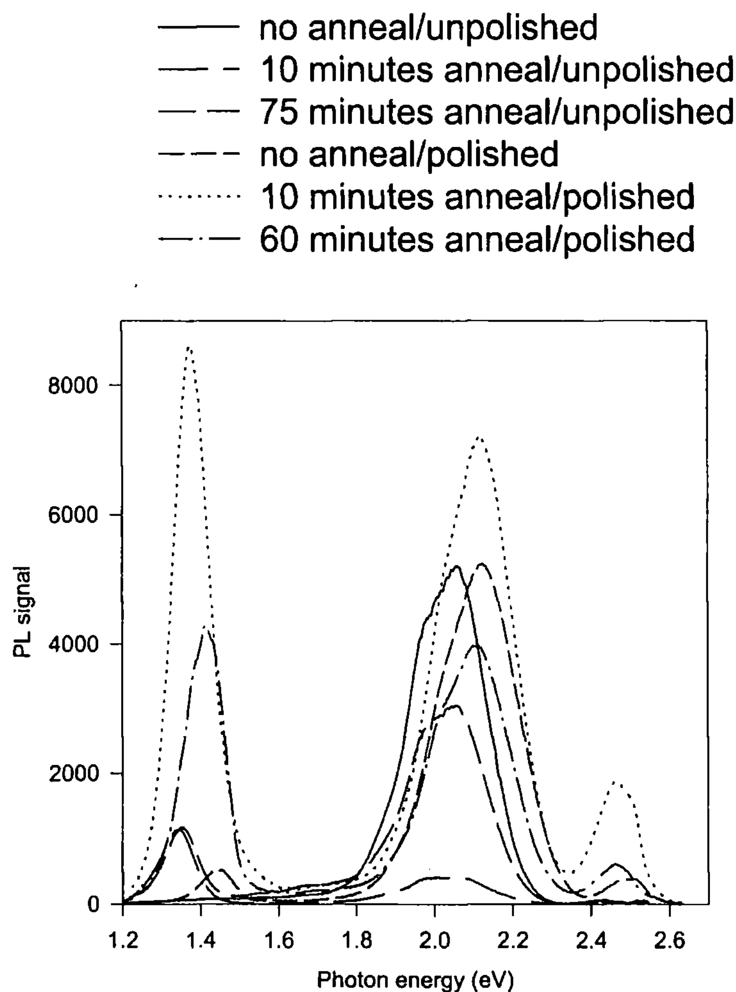


Figure 5.11: A selection of near interface spectra

back surface causing cadmium vacancies from the back surface inwards. In either case the polishing of the samples completely destroys this peak by providing a preferred recombination route (the 1.48eV emission peak plus any non-radiative recombination routes induced). The 1.3-1.5eV peak now dominates the spectrum in all cases. The 10 minute polished sample shows significant redshifting of this peak compared to the others, which could be attributed to the diffusion of sulphur as will be discussed later. With the exception of the 75

minute annealed unpolished sample the intensities of the polished and unpolished samples are more similar than at the back surface.

Figure 5.11 shows the near-interface spectra for the same six representative samples. The 2.53eV peak is present in some samples and absent in others, obeying no clear rule. The 1.3-1.5eV peak can be seen in most samples. For the more efficient samples (most notably the 10 minute annealed samples but also in some of the samples annealed for longer times) this peak is shifted to lower energies. This is attributed to the diffusion of sulphur into the CdTe [26] causing a shift in the bandgap, and will be quantitatively analysed later. In all cases the spectra from the polished samples can be seen to be shifted to higher energy than the spectra from the equivalent unpolished samples by at least 10meV. The reason for this is unknown though it may be associated with stress induced in the sample by polishing. The ratio of the 1.9eV-2.2eV CdS band to the 1.3eV-1.5eV CdTe band is smallest in the case of the untreated samples (regardless of polishing), which suggests there is less intermixing of the CdTe and CdS layers without the $CdCl_2$ treatment. Notable by its absence in all spectra is the 1.75eV "R" band observed by other authors [47] due to the diffusion of Te into the CdS layer. The presence of oxygen has been known to reduce the intensity of this peak in RF sputtered material [47]. The study by Kazlauskas et al [48] on single crystal CdS suggests that the 1.9eV-2.2eV peak intensity increases relative to the 1.75eV peak intensity for increasingly Cd rich (ie. S deficient) crystals.

A more detailed summary of the variation in peak positions with depth through the samples is shown in figures 5.12 and 5.13. For clarity peaks of energy above 1.5eV (e.g. CdS related peaks) are not shown. The broad 1.3-1.5eV emission peak mentioned earlier can be seen to be centred around 1.425eV, with a considerably broader spread of positions in the polished sample, possibly due to the strain induced in the crystal lattice by polishing causing local shifts in the bandgap [49]. Most notable in the polished samples is a shift to lower energies near to the back surface, particularly in the 10, 20 and 40 minute annealed samples (although the effect is also visible in the 30 and 60 minute annealed samples. As this shift is not observed in the unpolished samples it can again be attributed to strain causing bandgap reduction. In both the polished and unpolished samples the 1.3-1.5eV broadband is not visible in the untreated samples several microns from the back surface, again suggesting that at least one component of this peak is not chlorine related.

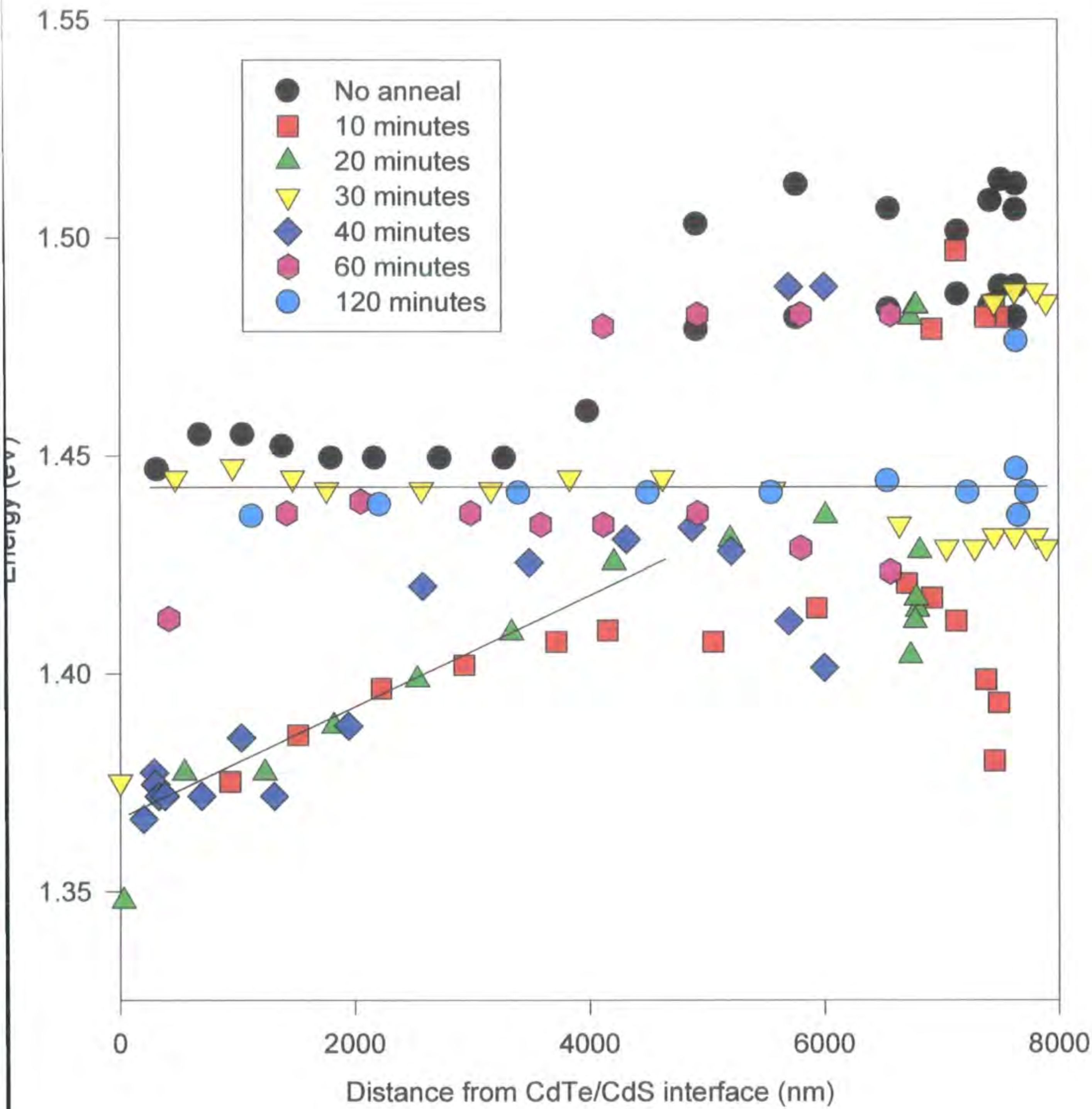


Figure 5.12: Variation of peak positions with depth in polished samples

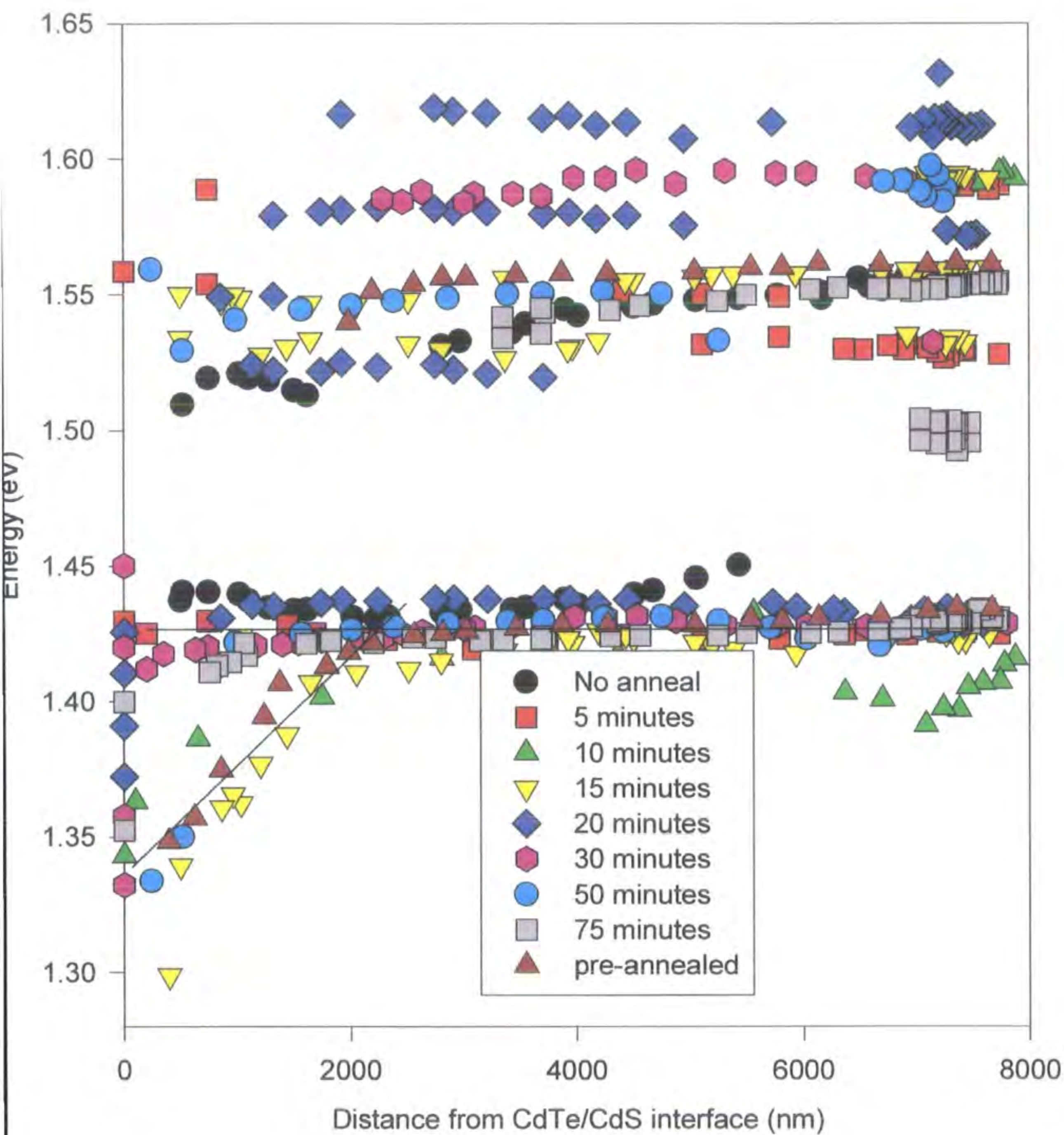


Figure 5.13: Variation of peak positions with depth in unpolished samples

Notable in all the samples that have been treated with $CdCl_2$ (with the exception of the sample annealed for 120 minutes) is a tendency for the position of the broad 1.3-1.5eV peak to shift to lower energies as the interface with the CdS is approached. In the case of the most efficient samples (10, 20 and 40 minute anneals in the case of the unpolished samples) this shift is gradual over several microns as the interface is approached. It is known that diffusion of Sulphur into CdTe causes the formation of a mixed layer $CdS_xTe_{1-x}$ with a bandgap which can for certain values of x be lower than the CdTe bandgap. Ohata [50] and Pal [51] find that the bandgap varies as:

$$E_{g(mixture)} = kx^2 + (E_{g(CdS)} - E_{g(CdTe)} - k)x + E_{g(CdTe)} \tag{5.2}$$

Using k=1.7eV from [51] gives the variation in bandgap with composition shown in figure 5.14.

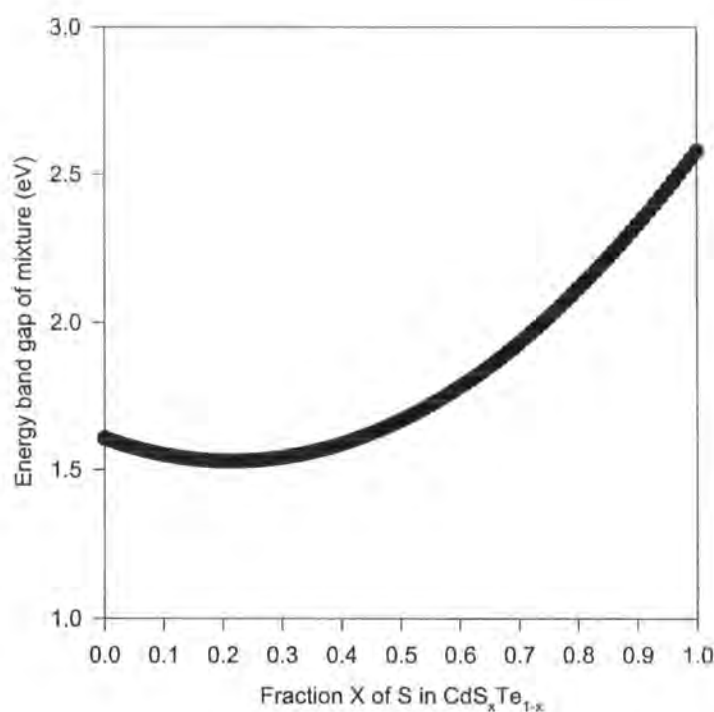


Figure 5.14: Variation of the $CdS_xTe_{1-x}$ bandgap with composition

Applying this to the shift in position of the 1.3-1.5eV peak from its highest energy value in each sample, the sulphur diffusion profile can be estimated in each case. This is shown in figures 5.15 and 5.16. As can be seen, the more efficient samples have a large amount of sulphur present near the interface, with the amount

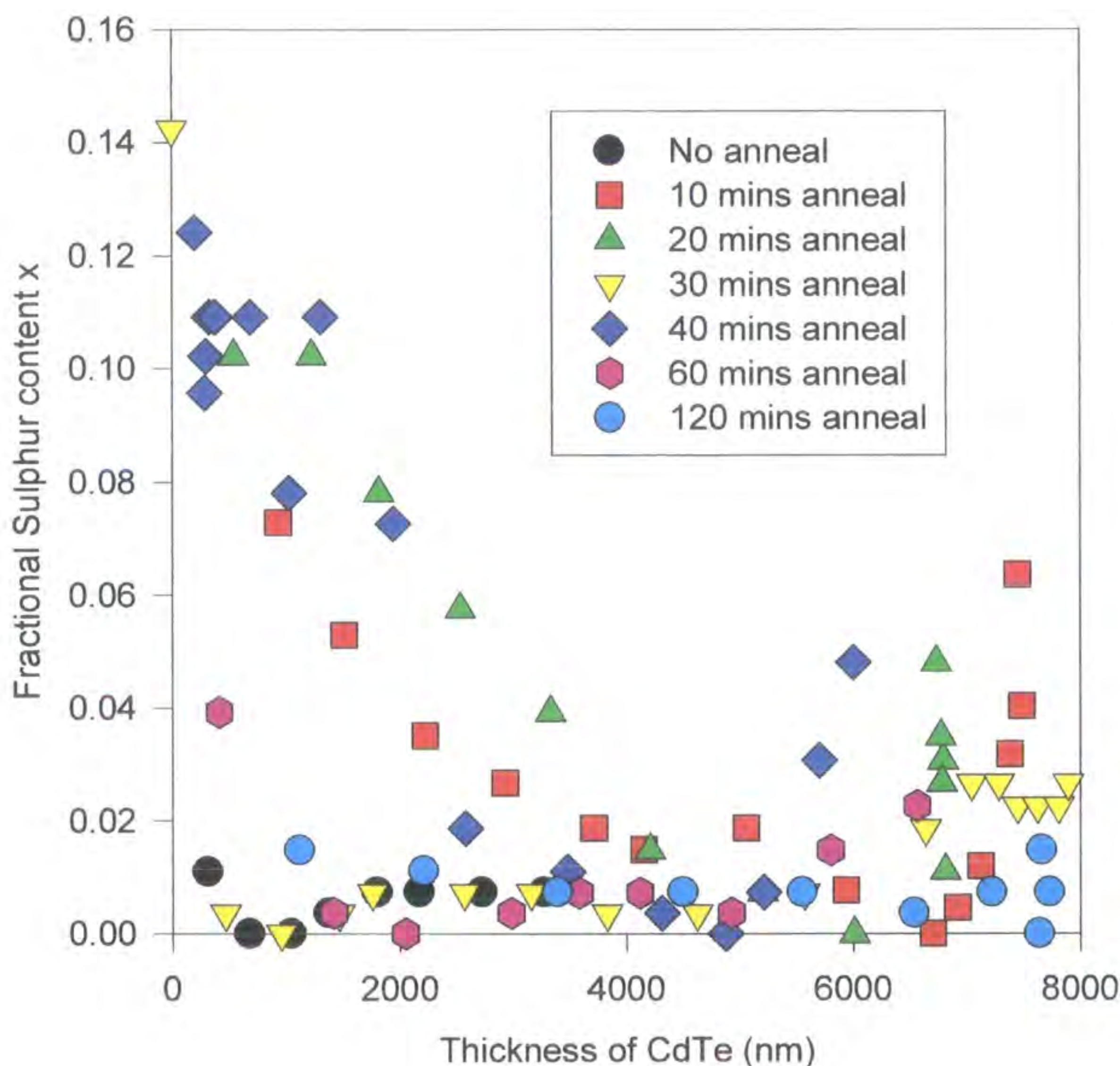


Figure 5.15: Estimated sulphur diffusion in polished samples

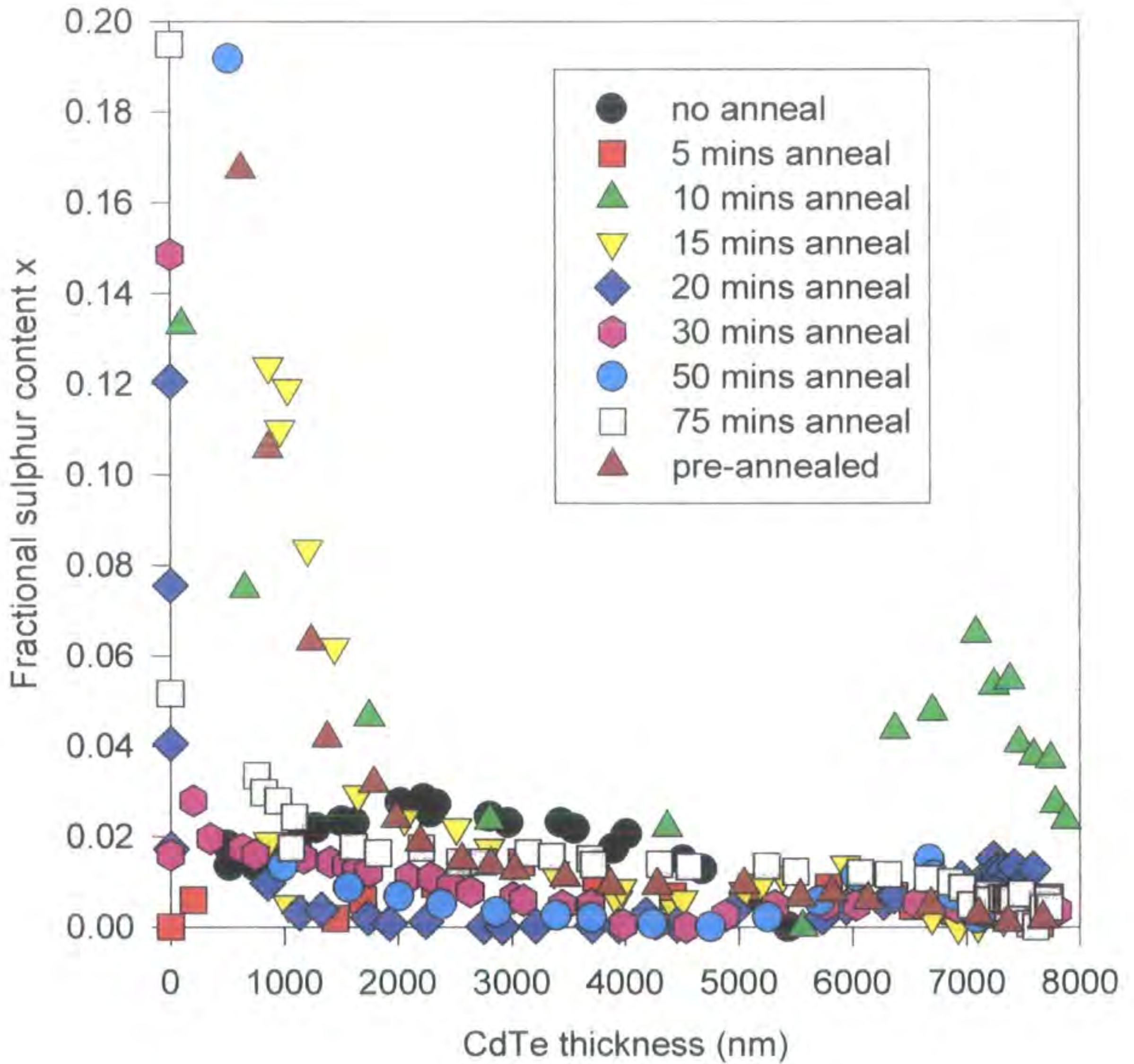


Figure 5.16: Estimated sulphur diffusion in unpolished samples

smoothly decreasing over several microns as the interface is moved away from. Work done by McCandless et al [52] implies that sulphur diffusion is not essential for high efficiency cells, but it is clearly linked to the mechanism that does increase the efficiency. The sulphur diffusion profile is sharper in the unpolished samples, suggesting that strain related defects may assist the propagation of sulphur throughout the device.

Generally for longer anneal times the sulphur diffusion profile becomes increasingly sharp, the exception being the 30 minute annealed polished sample, which as has already been observed exhibited an anomalous low efficiency. However, there are several pieces of evidence which contradict this interpretation of the reason for the peak shift:

1) In the case of the 15 minute annealed unpolished sample there is a higher energy peak present as the interface is approached which does not shift to lower energies at the same rate as the 1.3-1.5eV peak.
2) Work done by Edwards et al [53] observes a similar (though smaller,~50meV) shift to lower energies which remains present (albeit to a lesser degree) in a sample which contained no CdS layer. This was attributed to the presence of a different acceptor species or screening effects.
3) The miscibility limit of the $CdS_xTe_{1-x}$ mixture at 400°C is known to be 6% [54], which is substantially lower than the near-interface CdS content implied by this interpretation.

This suggests that segregation may be occurring in the CdTe layer as has been observed by Jensen et al [54]. Discrete regions of higher sulphur concentration may form either in the bulk or at the grain boundaries of the CdTe. Chlorine certainly must be assumed to diffuse through the CdTe preferentially along the grain boundaries as Jones et al [55] found it to diffuse only a few μm in the bulk crystal even after 24 hours anneal at 400°C. Charge carriers will preferentially recombine where the bandgap is lowest (highest sulphur concentration), causing an overestimation of the true sulphur content by PL. Also since the size of the laser spot is large compared to the CdTe grain size regions of high and low sulphur concentration will be probed simultaneously, which could explain the effect found in the 15 minute annealed unpolished sample. Altosaar et al [56]find that Na diffusion into CdTe causes a similar effect (shift of a PL band from 1.4eV to 1.34eV). However, this also caused a drop in PL intensity by at least an order of magnitude, which is not observed here. Rogers et al [21] report the formation of layers of $CdS_xTe_{1-x}$ with discrete values of x in CBD CdS/ vacuum evaporated CdTe material. Our findings do not agree with this as the extent of the sulphur gradient in the samples studied here is 2-4μm, which is several times the estimated penetration depth of 457.9nm light into CdTe(~90% absorption within 500nm for 457.9nm light [57]).

5.3.3 Temperature and Intensity dependent Photoluminescence

The variation of PL intensity with illumination intensity for a selection of the peaks observed is shown in figure 5.17. Following the empirical relationship:

$$I_{peak} \propto I^{k}_{illu\,min\,tion} \tag{5.3}$$

we obtain k values of 0.87 and 1.54 for the 1.43eV and 1.54eV peaks respectively. Comparing this with the work of Schmidt et al [58] suggests that the 1.54eV peak is a donor or acceptor bound exciton recombination

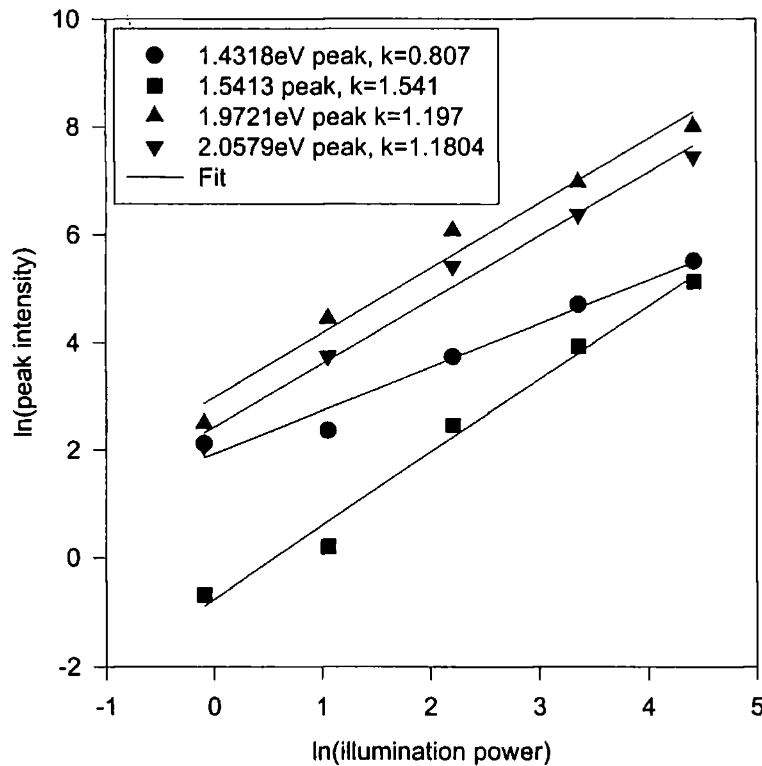


Figure 5.17: Intensity dependence of some PL peaks.

(although the peak energy is somewhat lower than would normally be expected for such a transition), whereas the 1.432eV peak is a free-bound recombination. At first glance, the 1.9eV-2.2eV peak (here deconvoluted into two separate components each with a k value of 1.2), may be assumed to be non-excitonic, since they are

well below the band edge of CdS. However, some authors [59] attribute this emission to excitons bound at Te substitutionals at S lattice sites. The observed k value (>1) supports this hypothesis.

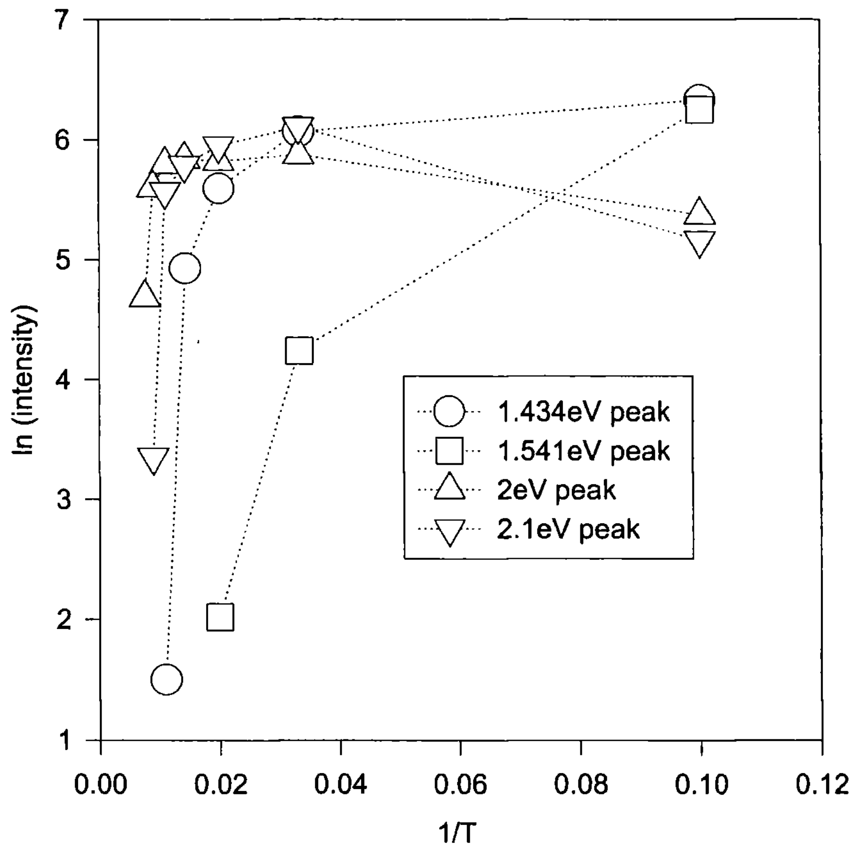


Figure 5.18: Temperature dependence of PL peak intensities.

Figure 5.18 shows the arrhenius plots for some of the more prominent PL peaks on the untreated sample. Employing the appropriate formula after the work of Bimberg et al [60], we can fit the peak intensity

I to the illumination intensity $I_0$ by:

$$I = \frac{I_0}{\left(1 + Ae^{\frac{-Ea}{kT}}\right)} \qquad (5.4)$$

Where Ea is the activation energy associated with the recombination route. This yields activation energies of 15, 152 and 146 meV for the 1.434, 2.0 and 2.1eV emission lines. The 1.54eV emission line could not be analysed as the intensity decayed too rapidly with temperature to provide a valid set of points, however this suggests a thermal activation energy <<15meV. The high activation energies of the CdS like peaks suggests that they are relatively deep level emissions.

Figure 5.19 shows the net integrated PL intensity for the polished samples as a function of remaining CdTe thickness. The regions of highest PL intensity occur as the interface is being approached. This is most notable in the case of the more efficient samples (10, 20, 40 minute anneals). Increased PL intensity implies a reduction in nonradiative recombination mechanisms and thus better device efficiency. A correlation between the PL intensity and the estimated sulphur diffusion (figure 5.15) can clearly be observed, suggesting that sulphur has an important role in passivating defects in the region of the CdTe/CdS interface. In the sample annealed for an excess time the region of maximum intensity shifts towards the rear of the device. Figure 5.20 shows the variations in PL intensity with depth for the unpolished samples. In this case the intensity is generally higher for longer anneal times and spread more through the bulk of the CdTe. One possible explanation for this is that because the back surface morphology was not removed from these samples, the change in crystal size throughout the CdTe layer had a greater effect on the PL response than in the case of the polished samples.

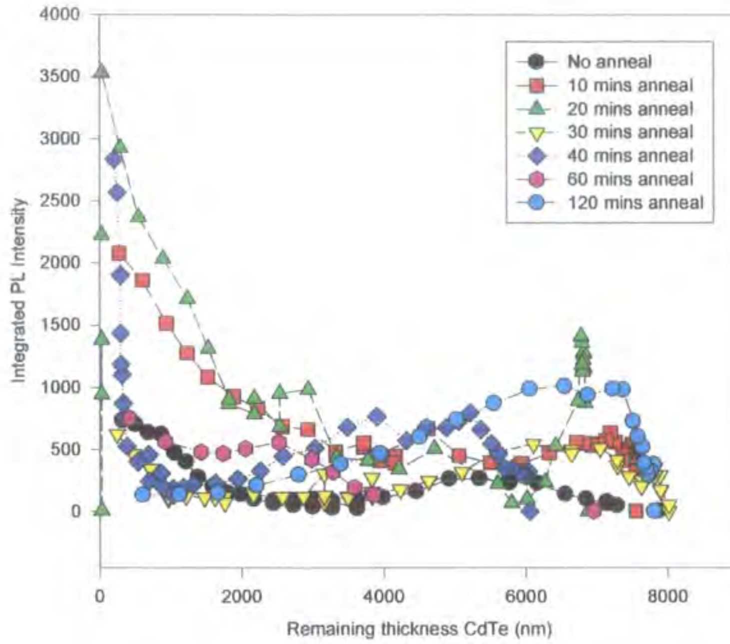


Figure 5.19: Variation of net PL intensity with CdTe thickness in polished samples

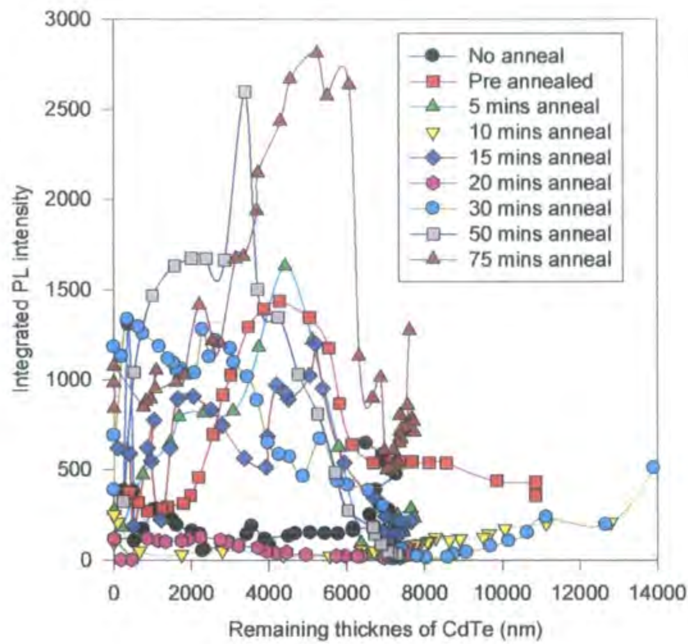


Figure 5.20: Variation of net PL intensity with CdTe thickness in unpolished samples

### 5.3.4 Time Resolved Photoluminescence

Time resolved PL was performed on a selection of the bevelled samples with the assistance of C. J. Bridge, P. D. Buckle and P. Dawson at UMIST. Luminescence was excited at room temperature using a cavity dumped mode-locked dye laser. The subsequent PL emissions were monitored as a function of time at a fixed wavelength using a cooled S1 micro-channel plate photomultiplier. Both the bevelled back surfaces and the front surfaces of the samples were probed in this manner. The results for the front surface (through the glass) time resolved PL are shown below in figure 5.21. The more efficient (10, 20 minute annealed) samples show an increased PL lifetime in the region of the CdTe/CdS interface compared to the unannealed and excess annealed samples. This has been attributed by Bridge [13] to sulphur diffusion causing passivation of nonradiative recombination routes at the interface or grain boundaries. Edwards et al have confirmed that

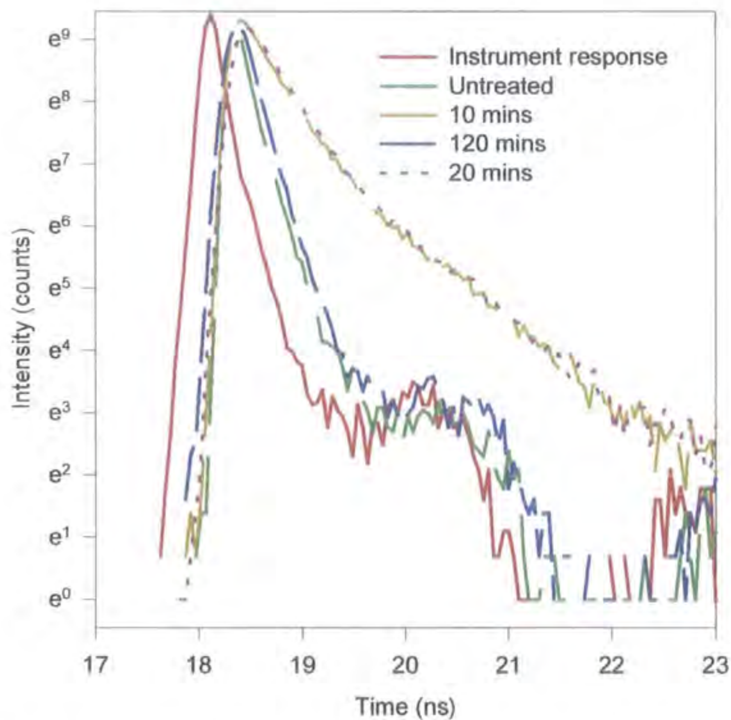


Figure 5.21: Front surface room temperature time resolved PL at 820nm for a variety of cells.

CdTe grain boundaries can be passivated by potential barriers which repel the minority carriers [61]. Sulphur diffusion would also reduce stress at the interface, again reducing the nonradiative recombination rate [62].

This increase in PL decay time is indicative of longer minority carrier lifetimes which are essential to the efficient operation of the device. The entire set of lifetimes for the 10 minute annealed sample are summarised in figure 5.22. The front surface lifetimes are consistently longer. When the back surface bevel is probed the lifetimes are longest about 1μm away from

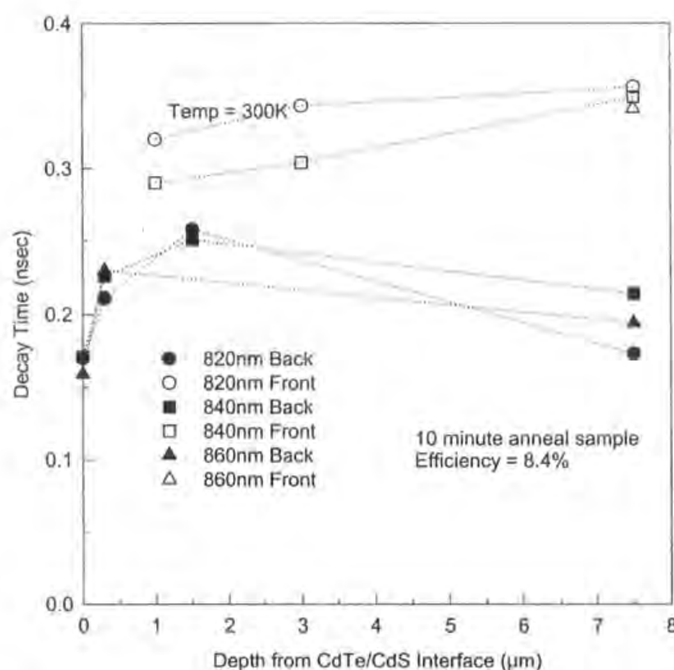


Figure 5.22: Summary of time resolved PL data for 10 minute annealed sample

the interface but rapidly decrease as the interface is approached, possibly due to surface recombination effects in the $CdS_xTe_{1-x}$ (CdTe is known to have a high surface recombination velocity ). The works of both Bridge [63] and Ahrenkiel et al [64] point to the existence of a longer lived component to the decay(decay time 3-8ns) which is not observed here, which suggests that the relatively fast nonradiative minority carrier recombination at grain boundaries (due to the high surface recombination velocity) dominates the PL lifetimes even in the most efficient samples. The PL decay was exponential in all cases, suggesting that we are operating in the low injection regime [65], and that the effect of minority carrier diffusion out of the active region of the device is small [66].

### 5.3.5 Electroluminescence

After electrical characterisation had been performed on the contacted sections of the samples, electroluminescence (EL) analysis was attempted at 10K using a 10V pulsed source as described in the experimental techniques section. Of the samples tried, four produced detectable EL spectra as shown in figure 5.23. The untreated sample produced a distinct two peak EL spectrum with peaks at 1.37eV and 1.5eV. The $CdCl_2$ annealed samples however exhibited a single broad peak centred at 1.45eV with the 20 minute annealed sample giving maximum intensity. The untreated sample EL bears some similarity to results obtained by Ferrer and Salvador for polycrystalline CdS electrodes [67], who observed a peak at 1.35eV. (room temperature) due to sulphur vacancy-cadmium vacancy DAP recombination in polycrystalline CdS. The fact that after annealing we observe a single peak at 1.45eV, an energy associated previously with a DAP level in CdTe, suggests that the annealing process causes a shift in the position of the electrical junction from the CdS layer to the CdTe layer. No direct comparison to references can be made as to the best of my knowledge this technique has not been applied to thin film CdTe/CdS heterojunctions previously. The fact that EL was not obtained for samples with anneal times longer than 30 minutes suggests that the centres responsible are passivated by excess $CdCl_2$ annealing. EL intensity does not correlate with cell efficiency, the most efficient device (10 minutes anneal) having the weakest EL signal.

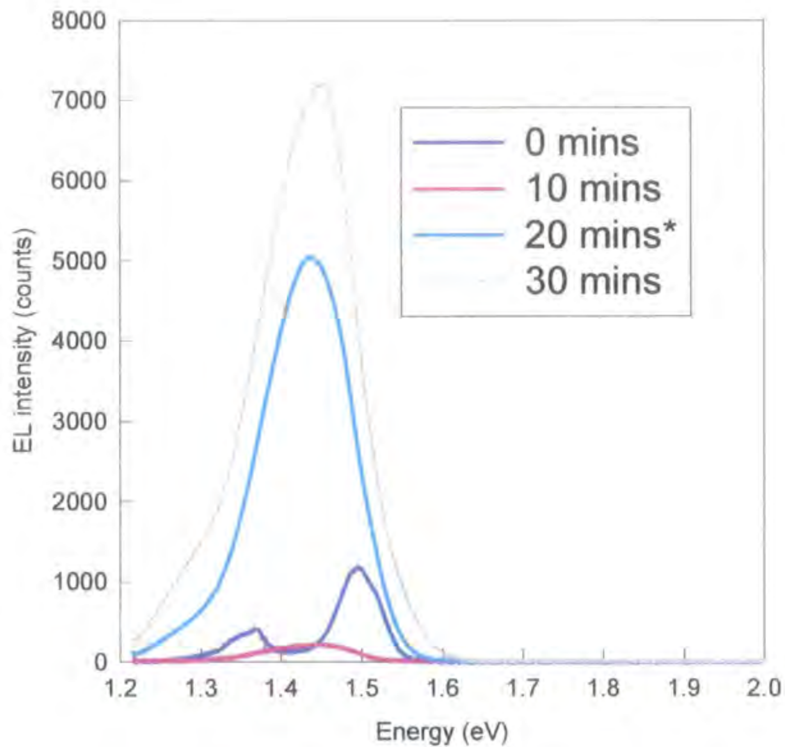


Figure 5.23: EL spectra for samples annealed for different lengths of time.

*20 minute sample shown at 1/12 intensity.

### 5.4 Conclusions

Photoluminescence spectroscopy has been successfully used to characterise the changes that occur throughout the CdTe/CdS solar cell during the $CdCl_2$ annealing process. Negligible near band edge emission was observed in all samples, suggesting that they were large grained both before and after annealing and contain high defect densities. Back surface polishing (a common technique prior to bevel etched PL) was found to induce structural defects in the CdTe which gave rise to a "Y" luminescence emission at 1.48eV. In the unpolished samples a peak was observed at 1.55eV, most likely due to cadmium vacancy related transitions. In all samples a broad peak was observed between 1.3eV and 1.5eV (typical maxima position=1.43eV throughout the bulk of the CdTe) attributed to a donor acceptor pair recombination between a cadmium

vacancy acceptor complex and a shallow chlorine donor. Evidence has been found for the promotion of sulphur diffusion into the CdTe from the CdS layer by the anneal. A distinct gradient of sulphur content has been found to correlate with optimum cell efficiency for an annealing time of 10 minutes. This also correlates with enhanced minority carrier lifetimes at the CdTe/CdS interface. The size of these lifetimes suggests that they are dominated by recombination at CdTe grain boundaries, which are passivated during the $CdCl_2$ anneal, possibly by S diffusion. It has been demonstrated that electroluminescence spectroscopy is a valid method for analysing CdTe/CdS solar cells; the change in EL spectrum after annealing suggests a shift in the position of the electrical junction.

### 5.5 References


1. Hower, J.C., *et al.*, *Coal: Availability, mining and preparation*, in *The Wiley Encyclopedia of Energy and the Environment*, S.B. Attilio Biso, Editor. 1997, John Wiley & Sons. p. 378-405.
2. Ellis, W.R., *Fusion Energy*, in *The Wiley Encyclopedia of Energy and the Environment*, S.B. Attilio Biso, Editor. 1997, John Wiley & Sons. p. 911-920.
3. Bequerel, E., *On electric effects under the influence of solar radiation.* Comptes Rendus Hebdomaires des Seances de l'Academie des Sciences, 1839. **9**: p. 561.
4. Adams, W.G. and R.E. Day, *The action of light on selenium.* Proceedings of the Royal Society of London, Series A, 1877. **25**: p. 113.
5. Chapin, D.M., C.S. Fuller, and G.L. Pearson, *A new silicon p-n junction photocell for converting solar radiation into electrical power.* Journal of Applied Physics, 1954. **25**: p. 676-677.
6. Reynolds, D.C., *et al.*, *Photovoltaic effect in Cadmium Sulfide.* Physics Review, 1954. **96**: p. 533-534.
7. Boyle, G., *Renewable Energy Power for a Sustainable Future.* 1996, Oxford: Oxford university press. 89-97.
8. Edwards, P.R., *Beam induced studies of CdTe/CdS solar cells*, in *Physics.* 1998, Durham: Durham. p. 176.
9. Fahrenbruch, A.L. and R.H. Bube, *Fundamentals of Solar Cells.* 1983, New York: Academic Press.

10. Durose, K., P.R. Edwards, and D.P. Halliday. *Materials aspects of CdTe/CdS solar cells*. in *Journal of Crystal Growth*. 1999. Symposium on Growth, Characterisation and Applications of Bulk II- VIs, at the E-MRS Spring Conference, STRASBOURG, FRANCE, 16-18 Jun 1998.

11. Bertness, K.C., M.L. Ristow, and H.C. Hamaker. . in *20th IEEE Photovoltaic Specialists Conference*. New York.

12. Fraas, L.M. and J.E. Avery, Optoelectronics Devices Technology, 1990. **5**: p. 297-310.

13. Bridge, C., *Optical Electrical and Microstructural Characterisation of Polycrystalline Thin Film CdTe/CdS Heterojunction Solar Cells*, in *Physics*. 1999, UMIST: Manchester.

14. Zanio, K., *Cadmium Telluride*. Semiconductors and Semimetals, ed. A.C. Beer and R.K. Willardson. Vol. 13. 1978: Academic Press.

15. Adirovich, E.I., Y.M. Yuabov, and G.R. Yagudaev, *Photoelectric effects in film diodes with CdS-CdTe heterojunctions*. Fiz. Tech. Poluprovodnikov, 1969. **3 (1)**: p. 81-85.

16. Aramoto, T., *et al.*, *16.0% efficient thin-film CdS/CdTe solar cells*. Japanese Journal Of Applied Physics Part 1-Regular Papers Short Notes & Review Papers, 1997. **36**(10): p. 6304-6305.

17. Woodcock, J.M., *et al. Thin-film solar-cells based on electrodeposited CdTe*. in *Conference Record Of the Twenty Second Iee Photovoltaic Specialists Conference - 1991, Vols 1 and 2*. 1991. 22ND IEEE PHOTOVOLTAIC SPECIALISTS CONF, LAS VEGAS, NV, 7 - 11 Oct 1991: I E E E Service Center, 445 Hoes Lane, Piscataway Nj 08854 5855 Naples Plaza, Suite 301a, Long Beach Ca 90803.

18. DeVos, A., *et al.*, *Bandgap effects in thin film heterojunction solar cells*. Proceedings of the 12th European Solar Energy Conference, 1994: p. 1315 - 1318.

19. Durose, K., *et al.*, *Microstructure and Impurities in Thin Film CdTe/CdS Solar Cells*. Journal of Microscopy, 2000: p. To be published.

20. Roh, J.S. and H.B. Im, *Effects of cdcl2 in CdTe on the properties of sintered CdS/CdTe solar-cells*. Journal Of Materials Science, 1988. **23**(6): p. 2267-2272.

21. Rogers, K.D., *et al.*, *The structural changes in CdS-CdTe thin films due to annealing*. Journal of Electronic Materials, 1999. **28**(2): p. 112-117.

22. Ayesh, A., J. Abushama, and R.N. Ahmadbitar, *Effect of heat and CdCl2 treatment on the structure and photoluminescence of CdTe/CdS thin-films.* Arab Gulf Journal Of Scientific Research, 1996. **14**(2): p. 349-362.

23. Tang, C.W. and F. Vazan, *Effect of oxygen on the photoluminescence of CdS/CdTe thin-films.* Journal Of Applied Physics, 1984. **55**(10): p. 3886-3888.

24. Durose, K., P.R. Edwards, and D.P. Halliday, *Materials aspects of CdTe/CdS solar cells.* Journal of Crystal Growth, 1999. **197**(3): p. 733-742.

25. Moutinho, H.R., *et al.*, *Investigation of polycrystalline CdTe thin-films deposited by physical vapor-deposition, close-spaced sublimation, and sputtering.* Journal Of Vacuum Science & Technology a-Vacuum Surfaces and Films, 1995. **13**(6): p. 2877-2883.

26. Li, K., *et al.*, *A microstructural study on the surface and interface of CdTe/CdS solar cells.* Journal Of Materials Science-Materials In Electronics, 1997. **8**(3): p. 125-132.

27. Romeo, A., *et al.*, *Recrystallization in CdTe/CdS.* Thin Solid Films, 2000. **361**: p. 420-425.

28. Basol, B.M., *High-efficiency electroplated heterojunction solar cell.* Journal of Applied Physics, 1984. **55**: p. 601-603.

29. Galloway, S.A., P.R. Edwards, and K. Durose, *Characterisation of thin film CdS/CdTe solar cells using electron and optical beam induced current.* Solar Energy Materials and Solar Cells, 1999. **57**(1): p. 61-74.

30. Okamoto, T., *et al.*, *Characterization of highly efficient CdTe thin film solar cells by low-temperature photoluminescence.* Japanese Journal of Applied Physics Part 1-Regular Papers Short Notes & Review Papers, 1998. **37**(7): p. 3894-3899.

31. Alallak, H.M., *et al. Dependence of cds/CdTe thin-film solar-cell characteristics on the processing conditions.* in *Journal Of Crystal Growth.* 1996. 7TH INTERNATIONAL CONFERENCE ON II-VI COMPOUNDS AND DEVICES, HERIOT WATT UNIV, EDINBURGH, SCOTLAND, 13 - 18 Aug 1995.

32. Brinkman, A.W., *CdTe-based solar cells*, in *Properties of Narrow Gap Cadmium-based Compounds*, P. Capper, Editor. 1994, INSPEC: London. p. 591-597.

33. Cousins, M., *Microstructure of Absorber Layers in CdTe/CdS Solar Cells*, in *Physics*. 2000, Durham: Durham.

34. Hildebrandt, S., *et al.*, *Localization of Y luminescence at glide dislocations in cadmium telluride.* Journal De Physique III, 1997. **7**(7): p. 1505-1514.

35. Seto, S., *et al.*, *Defect-induced emission band in CdTe.* Journal Of Crystal Growth, 1994. **138**(1-4): p. 346-351.

36. Figueroa, J.M., *et al.*, *Photoluminescence spectra and carrier mobilities in polycrystalline films of CdTe.* Journal Of Crystal Growth, 1990. **106**(4): p. 651-656.

37. Akimoto, K., *et al.*, *Oxygen doping in CdTe, CdS and ZnS.* Journal Of Crystal Growth, 1992. **117**(1-4): p. 420-423.

38. Lozadamorales, R. and O. Zelayaangel, *Photoluminescence analysis of CdS thin-films under phase-transition.* Thin Solid Films, 1996. **282**(1-2): p. 386-389.

39. Hopfield, J.J., D.G. Thomas, and R.T. Linch, *Isoelectronic donors and acceptors.* Physical Review Letters, 1966. **17**: p. 312-315.

40. Bubulac, L.O., *et al.*, *Spatial origin of various PL lines in CdTe at 77K.* Journal Of Crystal Growth, 1988. **86**(1-4): p. 536-543.

41. Halliday, D.P., J.M. Eggleston, and K. Durose, *A study of the depth dependence of photoluminescence from thin film CdS/CdTe solar cells using bevel etched samples.* Thin Solid Films, 1998. **322**(1-2): p. 314-318.

42. Levi, D.H., *et al. Back contact effects on junction photoluminescence in CdTe/CdS solar cells.* in *Conference Record Of the Twenty Sixth Ieee Photovoltaic Specialists Conference - 1997.* 1997. 26th IEEE Photovoltaic Specialists Conference, ANAHEIM, CA, 29 Sep - 3 Oct 1997: I E E E Service Center, 445 Hoes Lane, Po Box 1331, Piscataway, Nj 08855-1331.

43. Aguilarhernandez, J., *et al.*, *Photoluminescence studies of semiconducting polycrystalline CdTe-films.* Japanese Journal Of Applied Physics Part 1-Regular Papers Short Notes & Review Papers, 1994. **33**(1A): p. 37-41.

44. Figueroa, J.M., *et al.*, *Influence of Cd vacancies on the photoluminescence of CdTe.* Journal Of Applied Physics, 1986. **60**(1): p. 452-454.

45. Akimoto, K., *et al.*, *Isoelectronic oxygen in II-VI semiconductors.* Applied Physics Letters, 1992. **60**(1): p. 91-93.

46. Shin, H.Y. and C.Y. Sun, *Photoluminescence spectra of Cl-doped CdTe crystals.* Journal Of Crystal Growth, 1998. **186**(3): p. 354-361.

47. Fischer, A., *et al.*, *Interdiffusion of CdS/CdTe in laser-deposited and RF sputtered alloys, bilayers and solar cells.* Proceedings of the 25th Photovoltaic Specialists Conference, 1996: p. 921-924.

48. Kazlauskas, A., *et al.*, *Stoichiometry of CdS crystals and their optical and lasing properties.* Journal Of Crystal Growth, 1995. **146**(1-4): p. 59-64.

49. Bugajski, M., *et al.*. in *Materials Research Society.* 1988. Pittsburgh: Materials Research Society.

50. Ohata K, S.J., Tanaka T, *Optical Energy Gap of the Mixed Crystal CdSxTe1-x.* Japanese Journal of Applied Physics, 1973. **12**(10): p. 1641 - 1642.

51. Pal, R., *et al.*, *CdSxTe1-x films - preparation and properties.* Journal Of Physics D-Applied Physics, 1993. **26**(4): p. 704-710.

52. McCandless, B.E., I. Youm, and R.W. Birkmire, *Optimization of Vapour Post-deposition Processing for Evaporated CdS/CdTe Solar Cells.* Progress in Photovoltaics Research and Applications, 1999. **7**: p. 21-30.

53. Edwards, P.R., *et al.*, *The influence of CdCl2 treatment and interdiffusion on grain boundary passivation in CdTe/CdS solar cells.* Proceedings of 14th European Conference on Photovoltaics, 1997. **2**: p. 2083-2086.

54. Jensen, D.G., B.E. McCandless, and R.W. Birkmire. *thin film cadmium telluride-cadmium sulfide alloys and devices.* in *25th PVSC.* 1996. Washington, D. C.: IEEE.

55. Jones, E.D., *et al.*, *The diffusion of cl into CdTe.* Journal Of Physics-Condensed Matter, 1994. **6**(37): p. 7499-7504.

56. Altosaar, M. and P.E. Kukk, *Radiative and nonradiative recombination centers in Cl and Na doped CdTe monograin powders.* Journal of Materials Science, 2000. **35**: p. 1135-1138.

57. Eggleston, J.M., *Optical Spectroscopy of Thin Film Semiconductor Structures*, in *Physics.* 1997, Durham: Durham. p. 188.

58. Schmidt, T., K. Lischka, and W. Zulehner, *Excitation-power dependence of the near-band-edge photoluminescence of semiconductors.* Physical Review B-Condensed Matter, 1992. **45**(16): p. 8989-8994.

59. Lovergine, N., *et al., Photoluminescence of cvd grown CdS epilayers on CdTe substrates.* Journal Of Crystal Growth, 1992. **118**(3-4): p. 304-308.

60. Bimberg, D., M. Sondergeld, and E. Grobe, *Thermal dissociation of excitons bound to neutral acceptors in high purity GaAs.* Physical Review B, 1971. **4**(10): p. 3451-3455.

61. Edwards, P.R., S.A. Galloway, and K. Durose, *EBIC and luminescence mapping of CdTe/CdS solar cells.* Thin Solid Films, 2000. **361**: p. 364-370.

62. Feng, Z.C., *et al., Correlations between CdTe/CdS/sno2/glass solar-cell performance and the interface surface-properties.* Journal Of Applied Physics, 1996. **79**(4): p. 2151-2153.

63. Bridge, C.J., *et al., Photoluminescence time decay measurements on polycrystalline thin film CdTe/CdS heterojunction solar cells.* Proceedings of the 24th International Conference on Physics of Semiconductors, 1998.

64. Ahrenkiel, R.K., *et al., Spatial uniformity of minority-carrier lifetime in polycrystalline CdTe solar-cells.* Applied Physics Letters, 1994. **64**(21): p. 2879-2881.

65. Ahrenkiel, R.K., *et al. Minority-carrier lifetime of polycrystalline CdTe in cds/CdTe solar- cells.* in *Conference Record Of the Twenty Second Iee Photovoltaic Specialists Conference - 1991, Vols 1 and 2.* 1991. 22ND IEEE PHOTOVOLTAIC SPECIALISTS CONF, LAS VEGAS, NV, 7 - 11 Oct 1991: I E E E Service Center, 445 Hoes Lane, Piscataway Nj 08854 5855 Naples Plaza, Suite 301a, Long Beach Ca 90803.

66. Ahrenkiel, R.K., *Influence of Junctions On Photoluminescence Decay in Thin-Film Devices.* Journal of Applied Physics, 1987. **62**: p. 2937-2941.

67. Ferrer, I.J. and P. Salvador, *Photoluminescence and electroluminescence mechanisms at polycrystalline CdS in air and in contact with aqueous-electrolytes.* Journal Of Applied Physics, 1989. **66**(6): p. 2568-2577.

# 6 Studies of Ion Beam Implanted CdTe

## 6.1 Introduction

As has been already demonstrated throughout this thesis, photoluminescence (PL) spectroscopy is a useful tool for the characterisation and diagnosis of semiconductors. However, one of the limitations of the technique is that although detailed spectra are often obtained, the specific origins of the centres responsible for the spectral features are often difficult to assign. This is because the position of spectral features is influenced by local structural stresses and defects within the semiconductor, temperature and excitation intensity as well as by the species and concentration of any impurities present. In addition, where there is more than one type of impurity or defect, complexes can be formed producing additional energy levels. Considering that additional optical transitions can occur between different impurity complexes, this makes compiling the PL emissions associated with different types of impurity for even a single type of semiconductor a daunting prospect. In order to assist in this and future characterisation work on CdTe, a set of high quality monocrystalline CdTe samples grown by GEC Marconi using the Bridgemann technique have been doped with known concentrations of sodium, copper, chlorine, sulphur, antimony and oxygen by ion beam implantation. The implantation was performed at the EPSRC Ion Beam Implantation Centre, Surrey. By studying the changes in the PL spectra of these samples compared to an undoped control, the effects of doping with these specific impurities can be quantified. It should be noted that even "pure" CdTe crystals are regarded as containing enough impurities from the source materials or the manufacturing techniques to influence their PL spectra. Unintentional impurities reported by other authors in high quality CdTe include Ga, In, Cl, Al, F [1], Cu, Na [2], Li [3] and Ag [4, 5].

## 6.2 Experimental

PL spectroscopy was performed on a selection of ion beam implanted single crystal CdTe samples. The details of the technique have been covered elsewhere in this thesis. Laser intensity dependent and temperature dependent PL was performed on each sample under the usual conditions. The high resolution 1200 lines/mm spectrometer grating was used to obtain the spectra. The two-lens focussing system was employed, as described in the experimental techniques section. Temperatures used ranged from 10K to 70K, and laser power densities varied from $24mWmm^{-2}$ to $0.083mWmm^{-2}$. Table 6.1 shows the dopant densities and accelerating voltages used to implant the impurities into the CdTe. Accelerating voltages

were chosen to produce a smooth gaussian distribution of impurities in the first few microns of the material.

Table 6.1: The doped single crystal CdTe samples used

| Dopant | Undoped | O | Cl | Cu | S | Na | Sb |
|---|---|---|---|---|---|---|---|
| Accelerating voltage (KeV) | N/A | 80 | 80 | 160 | 160 | 80 | 160 |
| Doping density ($cm^{-3}$) | N/A | $1x10^{15}$ | $1x10^{15}$ | $1x10^{15}$ | $2x10^{14}$ | $1x10^{15}$ | $1x10^{15}$ |

### 6.3 Results and Discussion

Figures 6.1-6.7 show a summary of the PL spectra obtained for all the samples at 10K, illumination intensity 24mWmm$^{-2}$. Several scans were used in each case to cover all observed PL features.

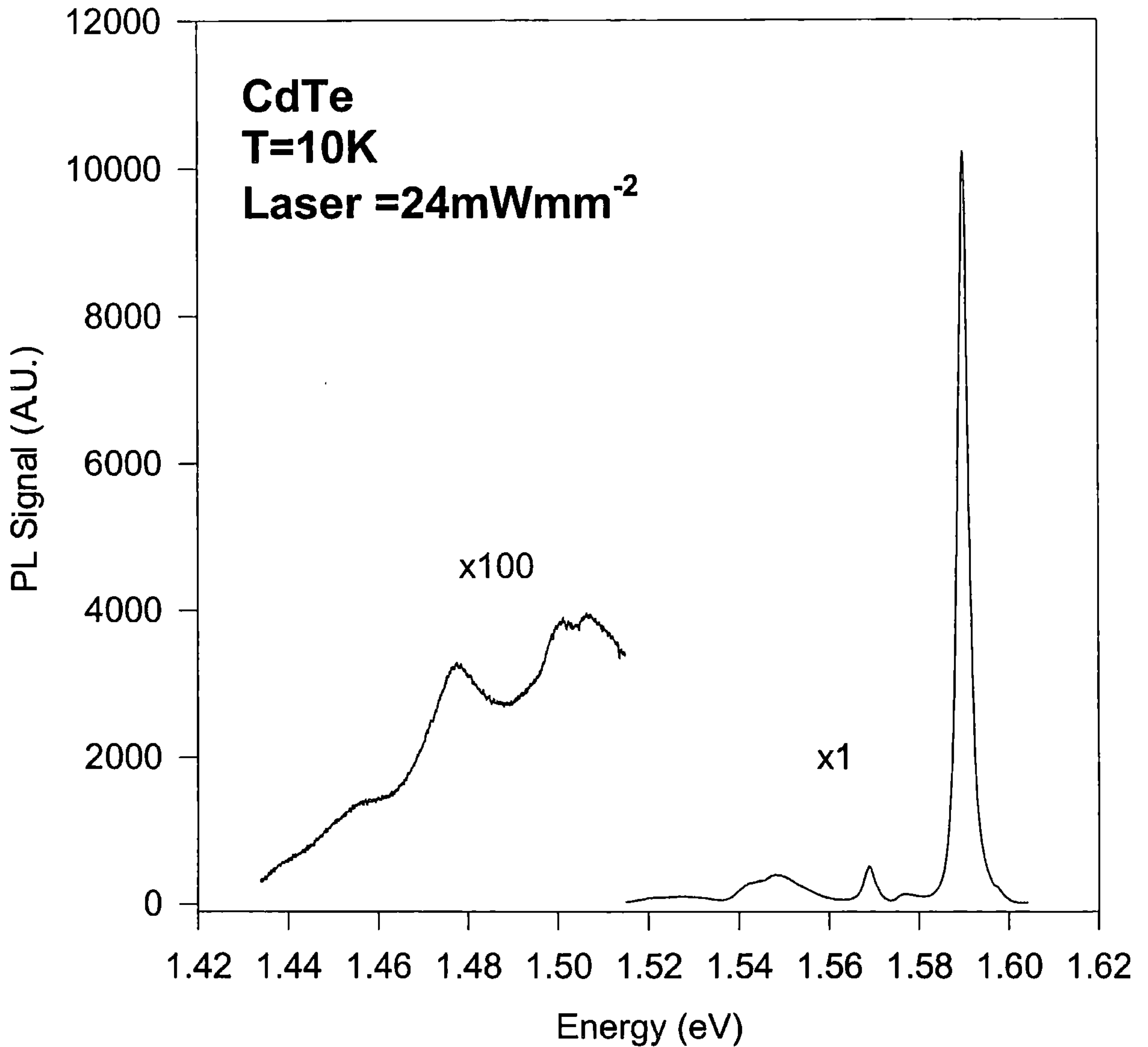


Figure 6.1: PL spectrum for undoped sample

The spectra observed for the (nominally) undoped sample bears much similarity to that obtained for the Bridgemann grown CdTe crystal studied in chapter 4. To summarise, the features observed include a sharp near band edge emission at 1.590eV due to an acceptor bound exciton ($A_0X$), with sidebands to

higher energies due to further (donor or acceptor) bound excitons or free exciton (FE) recombination. An unidentified peak is observed at 1.576eV (possibly a LO phonon replica of the free exciton recombination (~1.6eV), as is a LO phonon replica of the dominant near band edge emission at 1.57eV. A pair of overlapping emissions are observed at 1.55eV and 1.542eV due to an electron bound at a neutral acceptor ($eA_o$) and a donor-acceptor pair (DAP) recombination respectively (see chapter 4 for more details on how these mechanisms were deduced), with LO phonon replicas of both peaks visible to lower energies. The dominance of the 1.59eV exciton peak suggests a high crystalline quality with minimal defects. Excitons have small binding energies and as such are very susceptible to electric fields associated with impurities and defects in the crystal. While the acceptor species responsible for the $A_oX$ line and the $eA_o$ peak can be attributed to a variety of trace dopants even in material which has been grown under the most stringent conditions [6], the limits of temperature and resolution prevent a conclusive analysis of the origin of these lines in the undoped material. Due to its relatively low cohesive strength when compared to other tetrahedral structures, CdTe is particularly prone to the formation of lattice site vacancies and consequent interstitials [2]. This, and the fact that in all of the intentionally doped samples the relative intensity of the 1.59eV peak is lower suggests that a cadmium vacancy double acceptor may be the dominant species in the undoped sample [7]. The undoped sample shows no evidence of a broad 1.3-1.5eV peak which is often observed in low quality CdTe and is associated with a high concentration of impurities or structural defects. A weak band is observed at 1.477eV, which is thought to be the "Y" luminescence band associated with the presence of glide dislocations [8] or frenkel defects [9] in the material. Work performed at Durham [10] has determined that Y luminescence is in fact caused by Cd glide dislocations.

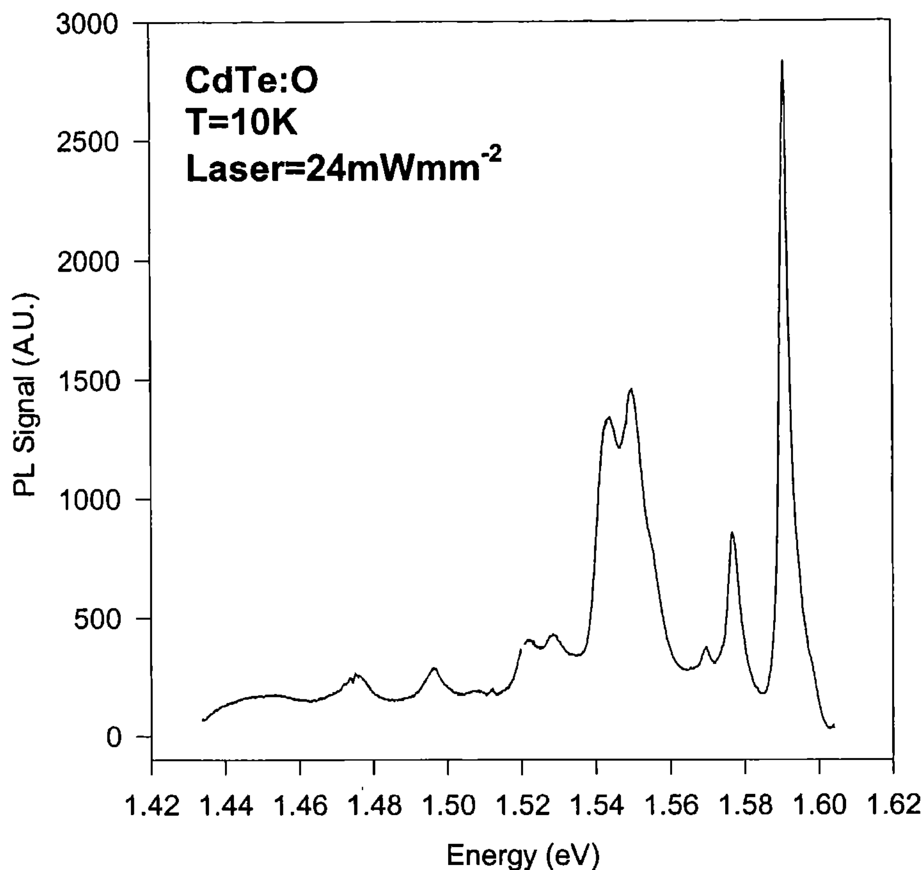


Figure 6.2: PL spectrum for oxygen doped sample

The oxygen doped sample also has a dominant 1.590eV emission peak, but also exhibits relatively brighter PL emission from the $eA_0$/DAP region, with clearly visible LO phonon replicas. Also, a peak is observed at 1.496eVwhich is observed in no other samples, and thus must be related exclusively to the presence of oxygen but has not been observed by other authors [11, 12]. A clear "Y" luminescence peak at 1.475eV suggests the presence of significant structural defects in the material. There is a faint broadband emission centered around 1.45eV. Akimoto et al [12] found oxygen to create a strong DAP peak at 1.55eV in Molecular Beam Epitaxy (MBE) grown CdTe. This coincides with the position of the peak we have assigned to $eA_0$ recombination. Either interpretation implies that oxygen is acting as an acceptor and thus a p-type dopant [13] despite the well known self-compensation effect in CdTe (the tendency of a dopant to form complexes with a doping effect counter to the direct doping effect, neutralising the dopant). Since oxygen is in the same group as Te (group 6), it is most likely to form an acceptor by substitutional incorporation at a Te lattice site [2].

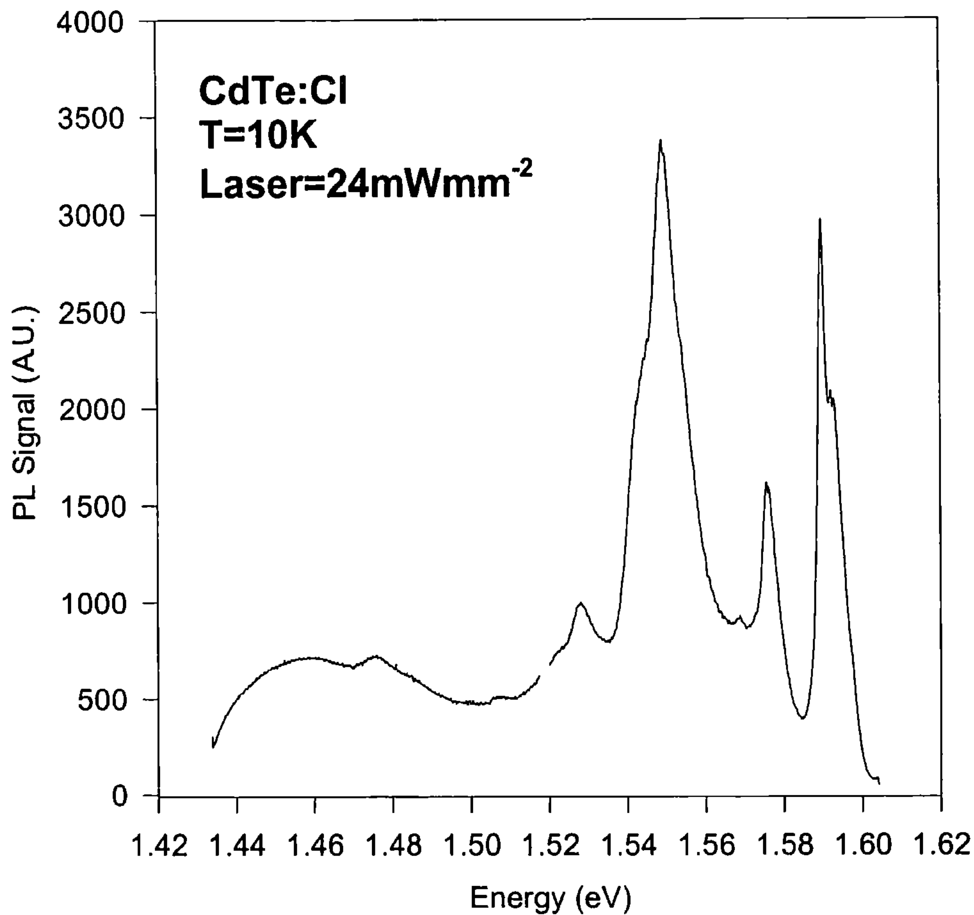


Figure 6.3: PL spectrum for chlorine doped sample

The chlorine doped sample exhibits a strong $eA_o$ emission, as well as an observable "Y" luminescence peak and a broadband emission centered around 1.46eV. The near band edge emission has peaks at1.592eV and 1.593eV clearly visible, and of comparable intensity to the 1.59eV $A_oX$ peak. Chlorine is known to directly form a shallow donor in CdTe, substituting for Te lattice sites, but also can form acceptor complexes with cadmium vacancies [14] such as $V_{Cd}$-$Cl_{Te}$ and $V_{Cd}$-$2Cl_{Te}$. The former has an emission at 1.586eV which is not observed, but the latter has an emission at 1.59eV which coincides with the $V_{Cd}$ $A_oX$ peak. The 1.593eV peak has been attributed by other authors [15] to a donor bound exciton caused by the $Cl_{Te}$ donor, and is also observed in the case of I doping [16] . The emission at 1.47eV has been attributed by Shin et al [14] to a convolution of $eA_o$ and DAP recombination involving a chlorine donor and the "A" centre, a relatively deep acceptor level thought to be caused [17] by a $V_{Cd}$-$Cl_{Te}$ complex. If this is the case the peak would be expected to shift to higher energies with increasing temperature as the $eA_o$ transition becomes increasingly favoured.

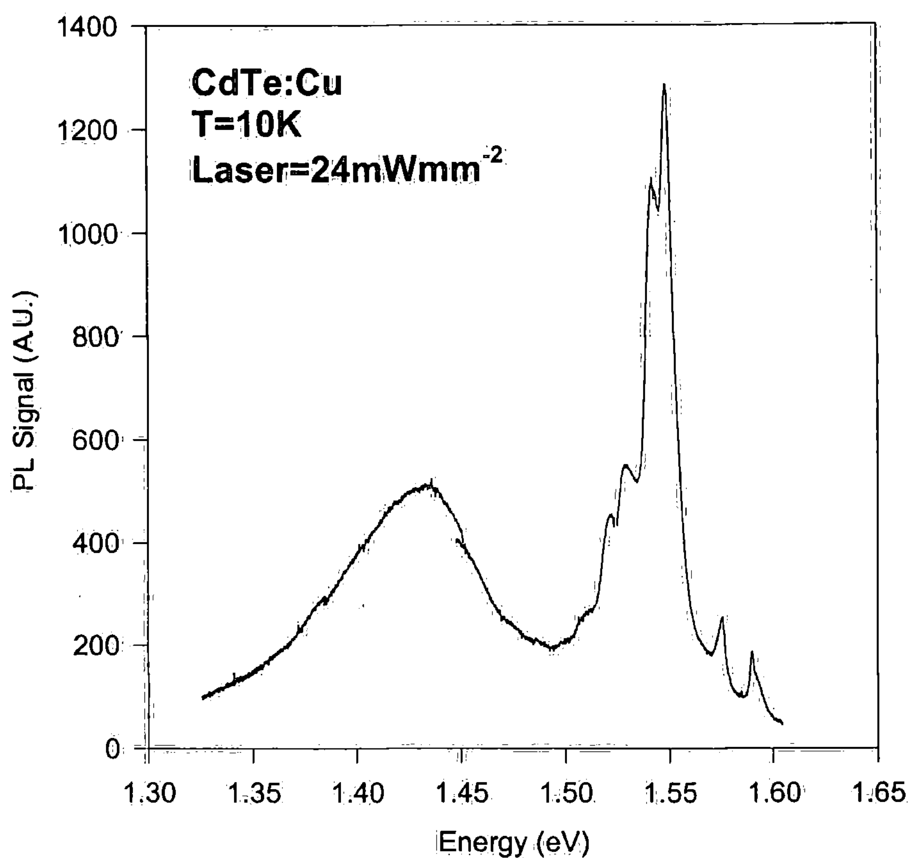


Figure 6.4: PL spectrum for copper doped sample

The 1.59eV $A_0X$ peak is relatively weak in the copper emission spectrum (its LO phonon replica is not observable). The $eA_0$ peak is far brighter than the DAP emission, and there is a large broad feature centred around 1.418eV. This feature may be related directly to the copper, which is known [2] to form a relatively deep level in CdTe. Cu forms acceptors by substituting at Cd sites, and (at higher concentrations), interstitial donors.

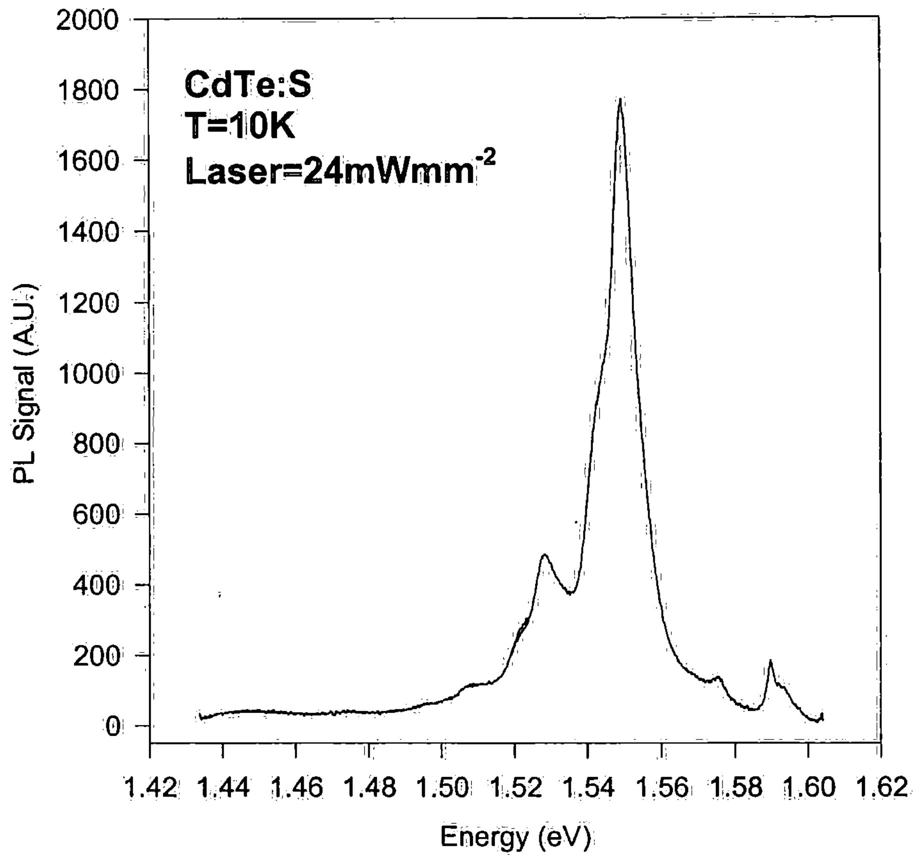


Figure 6.5: PL spectrum for sulphur doped sample

The emission spectrum for sulphur shows a relatively small 1.59eV peak with a well defined shoulder to higher energy, put down to a 1.593eV $D_0X$ recombination. The spectrum is dominated by the $eA_0$ peak at 1.55eV, and any "Y" luminescence or deep level emission is trivial.

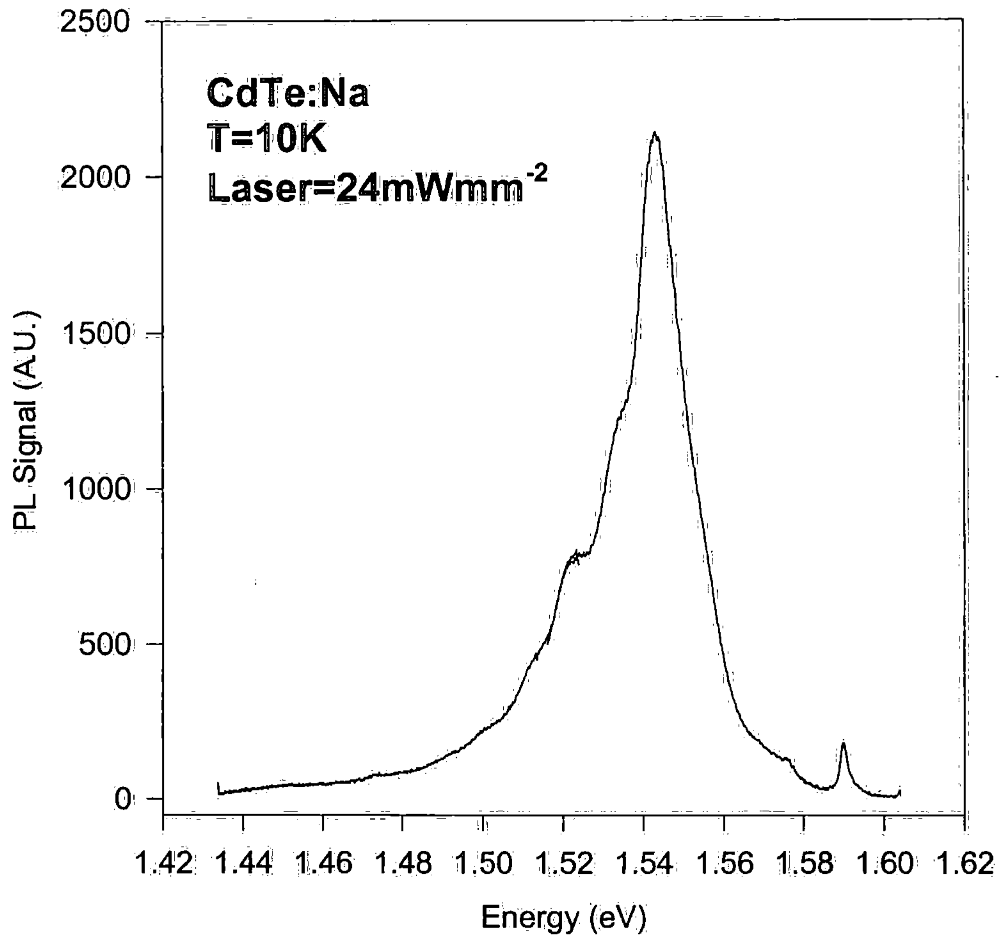


Figure 6.6: PL spectrum for sodium doped sample

The sodium spectra has a weak 1.59eV emission, without a well defined high energy shoulder. The spectrum is entirely dominated by a pair of emission peaks at 1.543eV and 1.533eV and their phonon replicas. Temperature dependent analysis reveals them to behave as an $eA_o$/DAP doublet, with the $eA_o$ emission becoming increasingly dominant with temperature. The position of the $eA_o$ peak also shifts to ~1.5485eV (a similar position to the $eA_o$ peaks observed in the other samples) above 20 Kelvin. The Na spectrum has some similarity to the Cu spectrum, which may be expected as they have the same outer shell configuration.

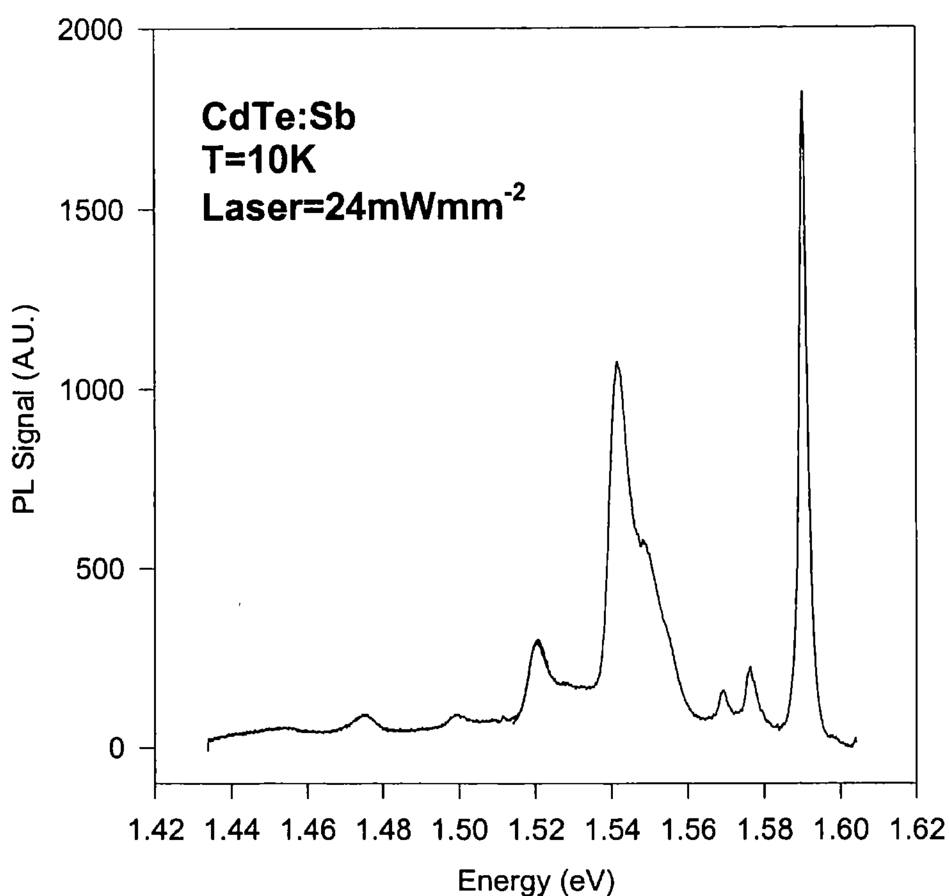


Figure 6.7: PL spectrum for antimony doped sample

The antimony doped sample has a spectrum dominated by the 1.59eV $A_0X$ line with a clear phonon replica. Uniquely among the spectra it has a more intense DAP emission than the $eA_0$ emission. "Y" luminescence is visible at 1.475eV. This has been noted in CdTe implanted with other group V elements (N,P,As) by Molva el al [6] with the acceptors being substitutional group V elements on Te lattice sites, although the donors involved were not identified. It is perhaps worth noting that generally (with the exception of Na, in which the doublet energies are different suggesting a different mechanism), the samples displaying a more prominent $D_0X$ line (Notably S, Cl) compared with the 1.59 $A_0X$ line also tend to favour the $eA_0$ line over the DAP line in the 1.549eV/1.541eV $eA_0$/DAP doublet. This can be taken as further evidence of self compensation in CdTe as impurities tend to give rise to both donors and acceptors.

For convenience, the table below summarises the variation in position of these peaks (if any) between the different samples studied. In the case of convoluted peaks an attempt was made to deconvolute them using PeakFit. The limiting accuracy of the detection equipment was found to be ~0.25nm (0.4-0.5meV at the wavelengths used), though in the case of highly convoluted peaks the uncertainty in determining the underlying peak energies may be higher.

Table 6.2: Peak Positions (eV)

| Sample Doping | None | Cl | S | O | Sb | Na | Cu |
|---|---|---|---|---|---|---|---|
| Near band edge | 1.5899 | 1.5898<br>1.5921<br>1.5929 | 1.5897<br>1.5920<br>1.5923 | 1.5908 | 1.5903 | 1.5900 | 1.5898 |
| F.E.-LO | 1.5772 | 1.5757<br>1.5762 | 1.5755 | 1.5768 | 1.5764 | 1.5756 | 1.5754 |
| NBE-LO | 1.569 | 1.5688 | | 1.5697 | 1.5692 | | |
| $EA_o$ | 1.5483 | 1.5491 | 1.5492 | 1.5495 | 1.5493 | 1.5431 | 1.5486 |
| DAP | 1.5417 | 1.5424 | 1.5419 | 1.5435 | 1.5415 | 1.5330 | 1.5421 |
| "Y" | 1.477 | 1.4752 | | 1.4749 | 1.4752 | | |
| 1.3-1.5eV broadband | | 1.4566 | | 1.4492 | 1.4539 | | 1.4177 |
| OTHER | | | | 1.496 | | | |

The region of the spectra between 1.59eV and the band edge is known from the works of other authors [1, 18, 19] to contain a plethora of fine detail characteristic of the impurities present. Although we are unable to resolve the details of these features to a sufficient resolution to determine the differences between different impurities (for example, Cu has been known to create an $A_oX$ line at 1.5896eV whereas Cl creates an $A_oX$ line at 1.5903eV), by studying the variations in intensity of the near band-edge emissions with illumination intensity and temperature, further details specific to each impurity can be obtained. For further details on the theory of temperature and intensity dependent measurements see chapters 2 and 4.

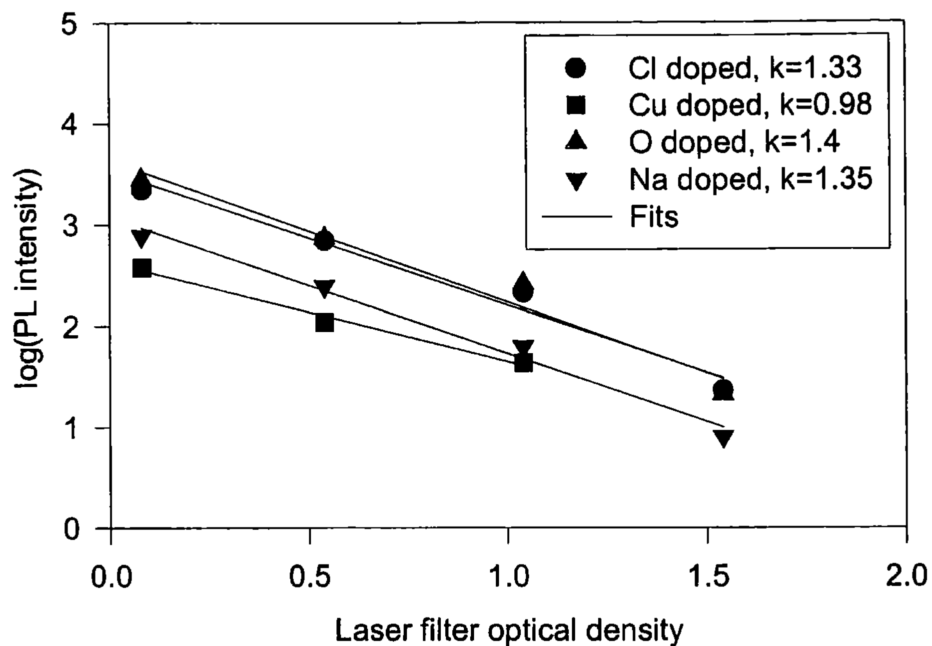


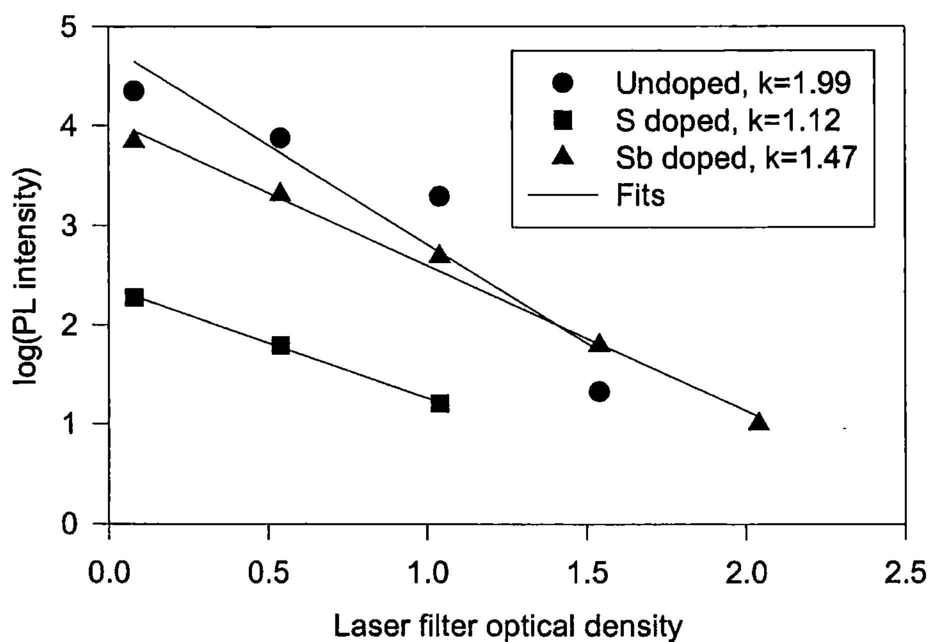


Figure 6.8: Laser intensity dependence of near band edge (NBE) peaks

All samples have k values of approximately equal to or greater than one, implying excitonic emission in all cases. The undoped sample has substantially higher intensity dependence (k=2) than any of the doped samples (although the last point may be spurious, in which case the emission would have a k value of

1.1). Various sources[20] quote K values between 1.1 and 1.5 for the $A_oX$ and $D_oX$ bound exciton lines, which satisfies the majority of the cases observed here. The wide range of excitonic K values observed suggests that there are different acceptor species involved in the different samples NBE emissions.

Temperature dependent analysis reveals a shift in NBE peak position from 1.59eV to 1.593eV in all the samples (though in the case of Cu this shift is difficult to observe as the NBE emission rapidly becomes negligible) implying that $D_oX$ recombination becomes increasingly dominant at higher temperatures. This is contrary to what might be expected, as the $A_0X$ has a higher binding energy and so would theoretically persist at higher temperatures than the $D_0X$ line. This suggests that other effects such as screening may have more effect on the relative intensities of the NBE emission peaks than their binding energies.

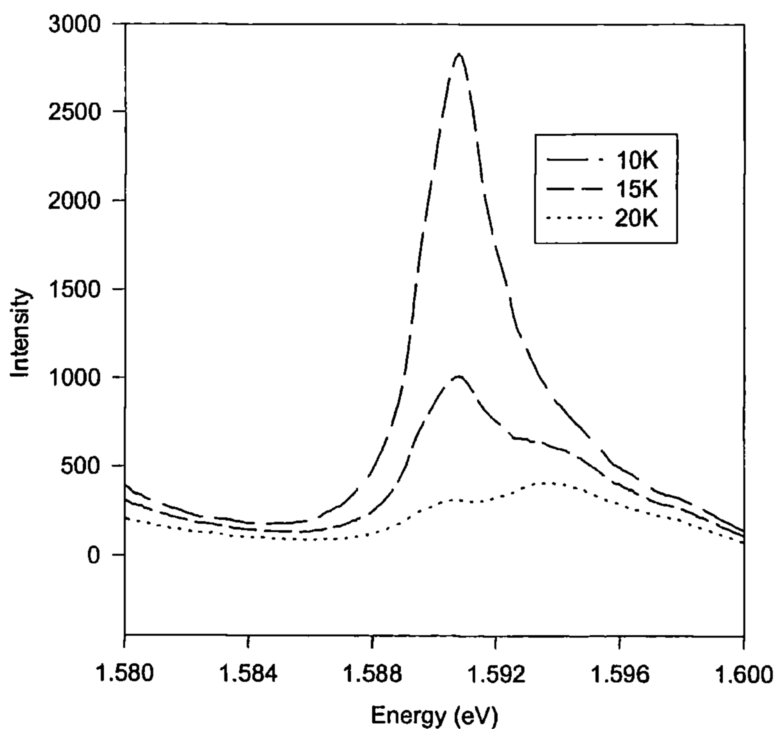


Figure 6.9: Change of dominant NBE emission peak with temperature, example: Oxygen

In some samples (O, Sb, undoped) a third peak was observed at 1.597eV as the temperature increased above 10K. Using Peakfit to de-convolute the emission peaks leaves only a small number of good data points to work with for some of the peaks. A summary of the temperature dependent NBE peaks is shown below. Following the methods detailed in the theory section and in chapter 4, the activation energies of the impurities can be determined from the curves in figure 6.10 for regions where they assume an approximately constant gradient. The table below shows activation energies obtained from the above graphs, along with energies obtained by other authors.

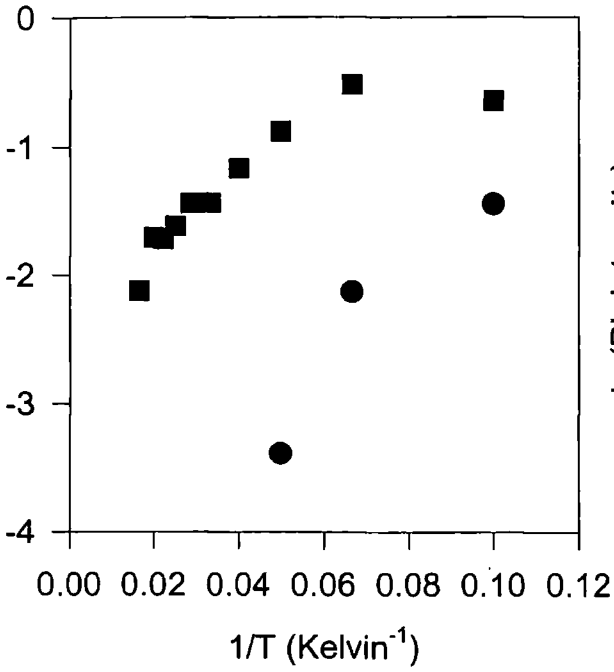
Sulphur 1.59eV
Sulphur 1.593eV
ln (PL intensity)
1/T (Kelvin$^{-1}$)

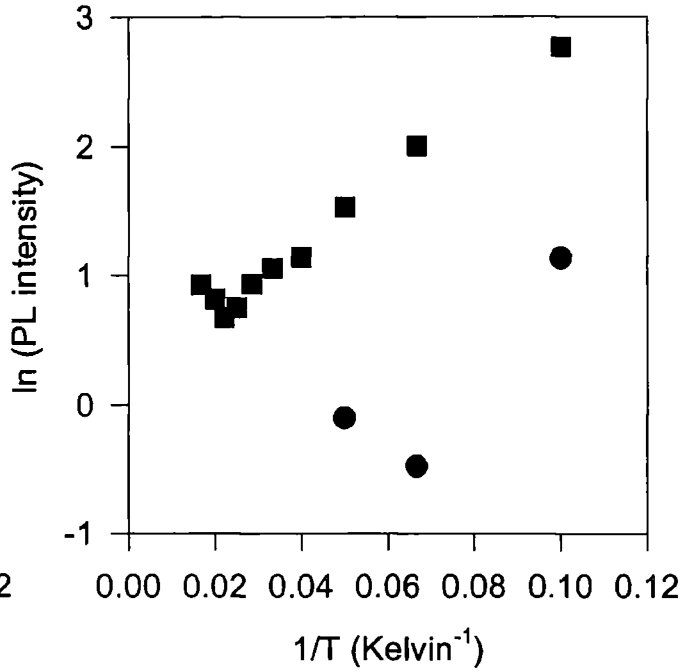
Chlorine 1.59eV
Chlorine 1.593eV
ln (PL intensity)
1/T (Kelvin$^{-1}$)

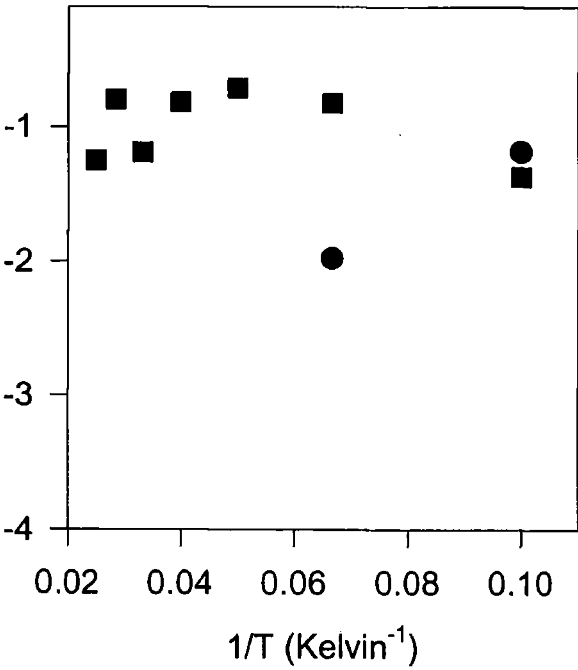
Copper 1.59eV
Copper 1.593eV
ln (PL intensity)
1/T (Kelvin$^{-1}$)

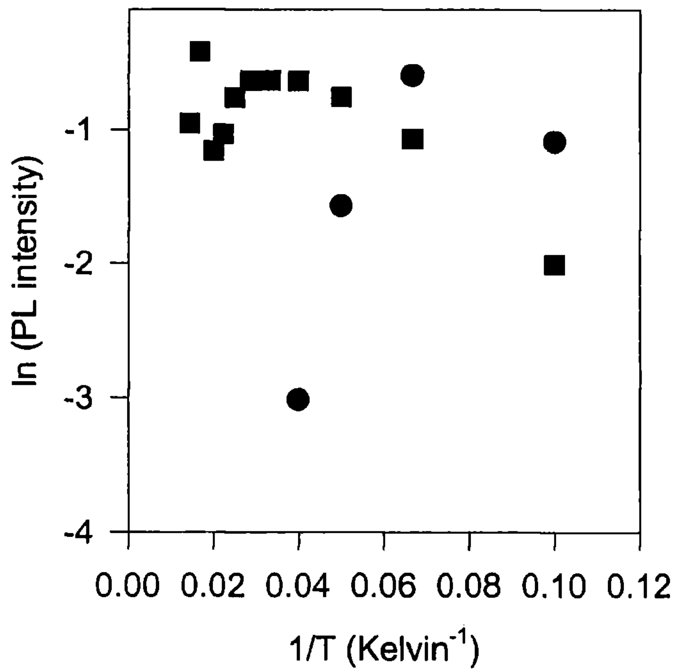
Sodium 1.59eV
Sodium 1.593eV
ln (PL intensity)
1/T (Kelvin$^{-1}$)

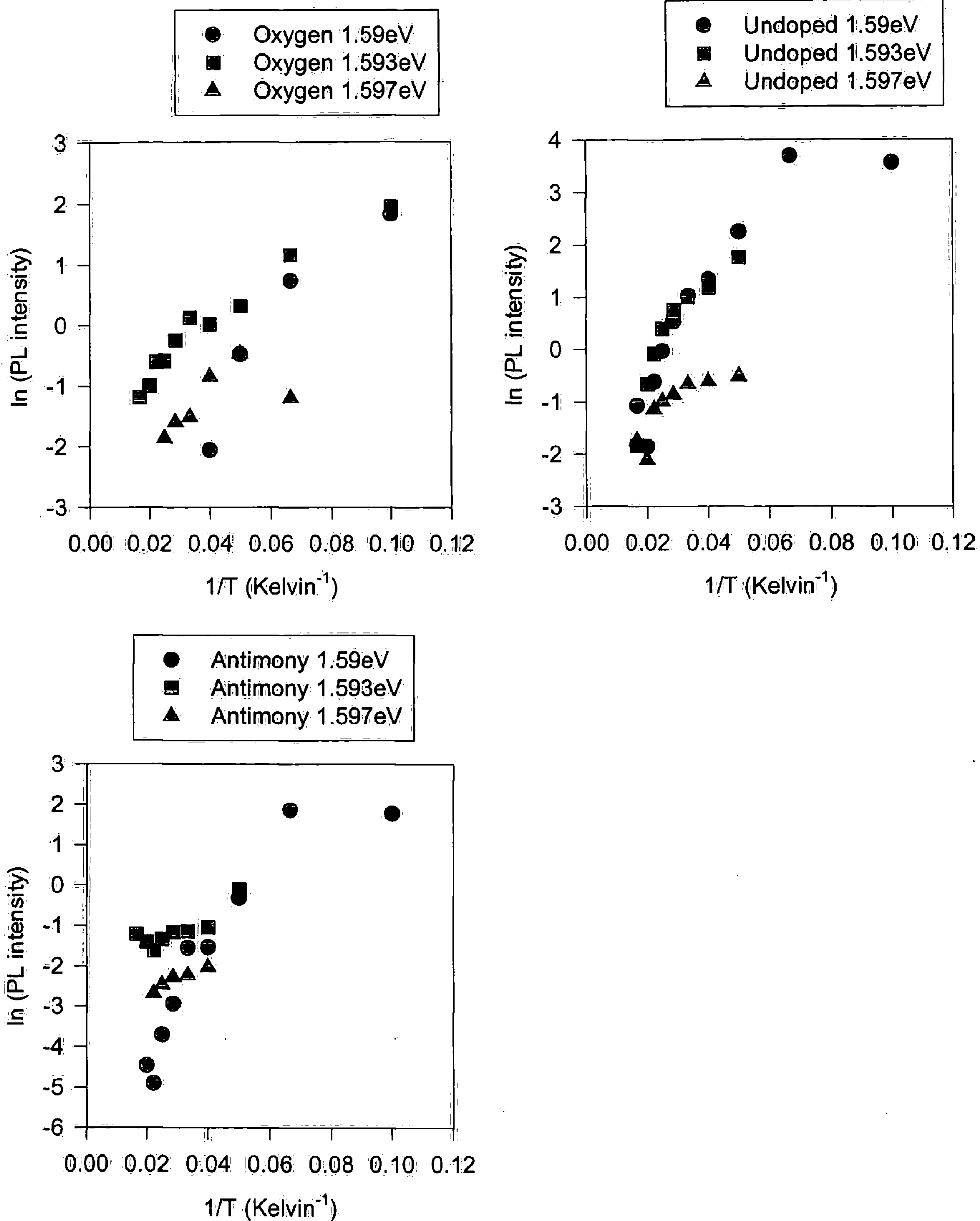


Figure 6.10: Temperature dependence of all near band edge peaks

Table 6.3: Thermally deduced activation energies.

| Sample | Peak | Activation energies (meV) | Reference Energies | Reference |
|---|---|---|---|---|
| Cl | 1.59eV | 2.414 | | |
| Cl | 1.593eV | 2.164 | | |
| Cu | 1.59eV | 2.05 | 6.54 | [21] |
| Cu | 1.593eV | 0.7178 | | |
| Na | 1.59eV | 7.548 | 6.94 | [21] |
| Na | 1.593eV | 5.52 | | |
| O | 1.59eV | 8.712 | | |
| O | 1.593eV | 6.734, 3.113 | | |
| O | 1.597eV | 4.932 | | |
| Undoped | 1.59eV | 14.61, 7.069 | 1.8, 4.9, 14 | [22] |
| Undoped | 1.593eV | 23.19, 4.325 | | |
| Undoped | 1.597eV | 3.735 | | |
| S | 1.59eV | 3.111 | | |
| S | 1.593eV | 2.502 | | |
| Sb | 1.59eV | 11.96 | | |
| Sb | 1.593eV | 3.997 | | |
| Sb | 1.597eV | 2.901 | | |

Both Cl and Cu exhibit relatively low activation energies for both the 1.59eV and 1.593eV peaks. The Na doped sample and the undoped sample exhibit some energies broadly in agreement with the reports of other authors. The undoped sample, in which lattice site vacancies are expected to play the greatest role in influencing the PL spectrum, has by far some of the highest activation energies. Both samples doped with group I metals, Cu and Na, display a similar distinctive temperature dependent profile: A rapid drop off of the 1.59eV peak while the 1.593eV peak gradually increases with temperature and then suddenly drops off between 30K and 50K, with a small spike in intensity as the temperature increases further. This profile can be assumed to be characteristic of group I dopants, whereas the samples doped with group V-VII elements showed a steady decrease in the intensity of the 1.593eV peak with temperature, as does the undoped sample. The reason for this behaviour is as yet unknown.

### 6.4 Conclusions

Photoluminescence spectroscopy has been used to successfully study the effects of known concentrations of various impurities on the spectra obtained from high quality monocrystalline CdTe. While PL analysis with the resolution and temperature limitations imposed here does not allow exclusive identification of impurity species from their PL spectra, distinctive spectral features have been obtained from several of the doped samples. Variation in the constants of intensity and temperature dependence have also been observed in all samples, as well as distinctive temperature dependence profiles dependant on the dopants group. Evidence of self compensation has been observed from the PL spectra. The data obtained here will prove useful in future PL characterisation of high quality CdTe crystals.

### 6.5 References


1. Francou, J.M., K. Saminadayar, and J.L. Pautrat, *Shallow donors in CdTe.* Physical Review B-Condensed Matter, 1990. **41**(17): p. 12035-12046.
2. Zanio, K., *Cadmium Telluride.* Semiconductors and Semimetals, ed. A.C. Beer and R.K. Willardson. Vol. 13. 1978: Academic Press.
3. Castaldini, A., *et al.*, *Comparison of electrical and luminescence data for the a-center in CdTe.* Applied Physics Letters, 1996. **69**(23): p. 3510-3512.
4. Chamonal, J.P., E. Molva, and J.L. Pautrat, *Identification of Cu-acceptor and Ag-acceptor in CdTe.* Solid State Communications, 1982. **43**(11): p. 801-805.
5. Chamonal, J.P., *et al.*, *Complex behavior of Ag in CdTe.* Journal Of Crystal Growth, 1982. **59**(1-2): p. 297-300.
6. Molva, E., *et al.*, *Photoluminescence studies in N, P, As implanted cadmium telluride.* Solid State Communications, 1983. **48**(11): p. 955-960.
7. Cooper, D.E., J. Bajaj, and P.R. Newman, *Photoluminescence spectroscopy of excitons for evaluation of high- quality CdTe crystals.* Journal Of Crystal Growth, 1988. **86**(1-4): p. 544-551.
8. Hildebrandt, S., *et al.*, *Localization of Y luminescence at glide dislocations in cadmium telluride.* Journal De Physique III, 1997. **7**(7): p. 1505-1514.

9. Seto, S., *et al.*, *Defect-induced emission band in CdTe.* Journal Of Crystal Growth, 1994. **138**(1-4): p. 346-351.

10. Gallant, A.J., *Final year project report.* 1999-2000: University of Durham.

11. Tang, C.W. and F. Vazan, *Effect of oxygen on the photoluminescence of CdS/CdTe thin-films.* Journal Of Applied Physics, 1984. **55**(10): p. 3886-3888.

12. Akimoto, K., *et al.*, *Oxygen doping in CdTe, CdS and ZnS.* Journal Of Crystal Growth, 1992. **117**(1-4): p. 420-423.

13. Chu, T.L., *et al.*, *Thin-film junctions of cadmium telluride by metalorganic chemical vapor-deposition.* Journal Of Applied Physics, 1992. **71**(8): p. 3870-3876.

14. Shin, H.Y. and C.Y. Sun, *Photoluminescence spectra of Cl-doped CdTe crystals.* Journal Of Crystal Growth, 1998. **186**(3): p. 354-361.

15. Korbutyak, D.V., *et al.*, *Growth and characterization of high-resistivity CdTe<Cl>.* Journal of Crystal Growth, 1999. **197**(3): p. 659-662.

16. Giles, N.C., *et al.*, *Photoluminescence of n-type CdTe-i grown by molecular-beam epitaxy.* Journal Of Applied Physics, 1993. **73**(9): p. 4541-4545.

17. Hofmann, D.M., *et al.*, *Identification of the chlorine-A center in CdTe.* Physical Review B-Condensed Matter, 1992. **45**(11): p. 6247-6250.

18. Taguchi, T. and C. Onodera, *Shallow acceptor bound excitons in CdTe epitaxial layers on (100) GaAs.* Materials Science Forum, 1990. **65-66**: p. 235 - 240.

19. Dhese, K.A., *et al.*, *Photoluminescence and p-type conductivity in CdTe-n grown by molecular-beam epitaxy.* Journal Of Applied Physics, 1994. **76**(9): p. 5423-5428.

20. Schmidt, T., K. Lischka, and W. Zulehner, *Excitation-power dependence of the near-band-edge photoluminescence of semiconductors.* Physical Review B-Condensed Matter, 1992. **45**(16): p. 8989-8994.

21. Zimmermann, H., R. Boyn, and K. Piel, *Thermal quenching of bound exciton emission due to phonon-induced nonradiative-transitions - experimental-data for CdTe and InP.* Journal Of Physics-Condensed Matter, 1992. **4**(3): p. 859-868.

22. Brink, D.J. and H.W. Kunert, *Photoluminescence of CdTe thin-films containing a mixed-crystal orientation.* Journal Of Applied Physics, 1995. **78**(11): p. 6720-6725.

# 7 Summary

### 7.1 Polycrystalline material

Optical photoluminescence spectroscopy has been successfully used to characterise the polycrystalline closed space sublimation deposited CdTe used in solar cells. The lack of near band edge emission suggests that the material is large grained with high defect densities. The effects of varying lengths of $CdCl_2$ anneal on the solar cells were investigated as this is a vital manufacturing step to increase the cell efficiency. An important correlation was observed:

1) A short (10 minute) $CdCl_2$ anneal at 400°C produced optimum cell efficiency, with efficiency generally dropping off for longer or shorter anneal times.

2) The most efficient cells also exhibited a gradual shift in the position of the broad 1.43eV PL emission peak (ascribed in literature[1] to a recombination between a shallow chlorine donor and a cadmium vacancy acceptor complex) from 1.43eV to 1.35eVas the CdTe/CdS interface was approached from the back surface.

3) The same set of most efficient cells showed significantly longer time resolved PL decay times near the CdTe/CdS interface, indicative of longer minority carrier lifetimes.

On the basis of these results, it is believed that the $CdCl_2$ annealing process promotes sulphur diffusion from the CdS layer into the CdTe layer, which diffuses preferentially along the grain boundaries of the material, passivating carrier recombination routes and thus increasing carrier lifetimes and device efficiency. The extent of the sulphur diffusion can be estimated from the perceived bandgap shift of the CdTe (see figures 5.15 and 5.16).

Comparison of the PL spectra from polycrystalline CdTe with the ion beam implanted reference samples studied in chapter 6 is of limited use, since the spectra from polycrystalline material are of much lower resolution without the fine near band edge detail of the single crystal spectra. However, in the chlorine ion beam implanted sample a broad feature is observed at 1.46eV, which is close to the position of the broad PL emission peak seen in the polycrystalline material. Electroluminescent emission was also obtained from

some devices, and while the technique plainly needs refining it shows potential as a characterisation/assessment tool for CdTe/CdS solar cells.

### 7.2 Single crystal material

The monocrystalline CdTe grown by the multi-tube seeded vapour growth technique was found to be highly pure with minimal defects and dominant near band-edge PL emission. Crystal quality varied spatially throughout the crystal but was found to be highest midway between the top and bottom surfaces, midway between the centre and the outer radius. A figure of merit for the crystal quality according to photoluminescence spectroscopy can be obtained by taking the ratio of near band edge emission to lower energy emission. The summary of this ratio in the form of a contour graph is shown in figure 4.9.

Diffusion of Zinc from the growth substrate was identified and found to be limited to the bottom millimetre of the crystal. The effects of various specific elemental impurities on the PL spectrum of monocrystalline CdTe were observed by study of the ion beam implanted samples. Comparison between the ion implanted samples and the CdTe grown by the multi-tube seeded vapour growth technique yields the following observations:

1) The spectrum of the undoped sample supplied with the ion beam implanted samples closely matches the spectrum of the crystal grown at Durham, confirming that both crystals are of similar high quality.

2) The 1.577eV peak observed in the Durham grown crystal, which was not identified, is relatively stronger in the majority of the ion beam implanted samples, particularly Oxygen and Chlorine doped ones. While it remains impossible at 10K to accurately deconvolute the donor bound, acceptor bound and free exciton recombinations it is clear at least in the case of the chlorine implanted material that this peak is related to a more intense donor bound or free exciton recombination peak (as was mentioned in chapter 4, it is of the correct energy to be a LO phonon replica of the free exciton recombination peak).

3) 1.476eV "Y" luminescence is observed in both the ion beam implanted and vapour grown crystals, suggestive of the presence of defects in the crystal lattice in both cases. One would presume that ion bombardment would be more likely to cause point defects than glide dislocations in the crystal lattice.

### 7.3 Suggestions for future study

Throughout this thesis, photoluminescence spectroscopy has proved a useful tool for materials characterisation. However, there is plenty of scope for further work to be done. In the case of monocrystalline material, it would prove helpful to study further samples doped by a thermal technique of some kind, which would allow the dopants to move to their natural lowest energy states in the crystal lattice. The development of polycrystalline CdTe based solar cells is an ongoing process of great importance to industry. Further variations on the processing techniques are worthy of study, such as different $CdCl_2$ anneal temperatures, the effect of the presence of oxygen during the anneal and the effect of varying CdTe grain size. Use of an electron beam rather than a laser beam to excite luminescence would allow explicit study of emission from the grain boundaries and grain centres of the CdTe, which are both simultaneously probed in PL. Lastly, electroluminescence both at low and room temperatures is worthy of further study and refinement as an analytical technique. It is capable as we have seen of producing well defined spectra with distinct features, and is intrinsically sensitive to the position of the electrical junction in the device.

### 7.4 References

1. Okamoto, T., *et al.*, *Characterization of highly efficient CdTe thin film solar cells by low-temperature photoluminescence.* Japanese Journal of Applied Physics Part 1-Regular Papers Short Notes & Review Papers, 1998. 37(7): p. 3894-3899.

## Acknowledgements

Many thanks are in order to loads of people who helped make this thesis possible. Firstly to Douglas Halliday, my supervisor, whose patient help both practical and theoretical has been nothing short of amazing.

To my family, Mum, Dad, Andrew, Bien and Russell, for constant support and being there for me.

To Corin, lab partner and friend, and Emily. Also to Mike, Paul, the Legendary David Smyth-Boyle, Ken, Anna, Ben, John, Mounir, Maria and other bizarre physicists I shared office space, equipment, thoughts and beer with over the last three years.

To Anna Wesson for additional PL work.

To Phil Dawson, Chris Bridge and Phil Buckle for help with the time resolved spectroscopy

To all the staff of Durham University, especially Norman and Davey, for unlimited help with the practical aspects of life as a research student.

To Bill, Mary, Luke, Eve and everyone from Ushaw Moor Baptist Church.

To Ali, Marios and "scary" Jessica for being my friends, especially near the end when things almost went off the rails.

To Rose, for two and a half years of our lives.

And to Robert Smith, for writing the songs.

This work was financially supported by the EPSRC. The work on bevelled solar cells was also supported by the EU.

## Appendices

### Tables


Table 6.1: The doped single crystal CdTe samples used 103
Table 5.1: Electrical characteristics of solar cells 74
Table 6.2: Peak Positions (eV) 112
Table 6.3: Thermally deduced activation energies. 118


### Figures


Figure 5.7: I-V curves for samples under standard illumination with example of fill factor shown. 74
Figure 4.14: The 1.476eV "Y" luminescence peak and LO phonon replica spectrum 59
Figure 5.2: The AM1.5 solar spectrum with some semiconductor bandgaps shown 65
Figure 2.11: Auger recombination. 26
Figure 2.5: The bandstructure of Gallium Arsenide 18
Figure 5.5: the bevel etching arrangement 71
Figure 2.4: Bloch solutions in a periodic lattice with a weak periodic potential. 17
Figure 2.3: Bloch solutions to the Schrodinger equation in a periodic lattice with no periodic potential. 15
Figure 4.1: A CdTe crystal gamma ray detector 44
Figure 5.3: A CdTe/CdS solar cell (not to scale) 67
Figure 6.9: Change of dominant NBE emission peak with temperature, example: Oxygen 114
Figure 3.3: The Cryostat head 40
Figure 2.8: Direct and indirect bandgap semiconductor absorption. 23
Figure 3.4:Dispersion on 1200 line grating as a function of wavelength 42
Figure 2.6: Donor and Acceptor impurity levels in a semiconductor. 20
Figure 5.23: EL spectra for samples annealed for different lengths of time. 95
Figure 2.13: E-q diagram for phonons 28
Figure 5.15: estimated sulphur diffusion in polished samples 85
Figure 5.16: estimated sulphur diffusion in unpolished samples 86
Figure 4.9: Fraction of PL intensity of photon energy E>1.583eV 51
Figure 5.21: Front surface room temperature time resolved PL at 820nm for a variety of cells. 92
Figure 2.12: Generic J-V characteristics of a p-n junction. 31
Figure 5.17: Intensity dependence of some PL peaks. 88
Figure 6.8: Laser intensity dependence of near band edge (NBE) peaks 113
Figure 2.7: Optical absorption in a semiconductor. 22
Figure 3.1: Optical Layout for Photoluminescence 37
Figure 3.2: optimising light collection 38
Figure 4.11: PL peak intensity as a function of illumination intensity. 54
Figure 4.2: PL points on wafer cut from the CdTe crystal boule. 45
Figure 4.6: PL spectra as a function of position 12mm along the boule 49
Figure 4.7: PL spectra as a function of position 16mm along the boule 49
Figure 4.8: PL spectra as a function of position 22.5mm along the boule 50
Figure 4.4: PL spectra as a function of position 4mm along the boule 48
Figure 4.5: PL spectra as a function of position 8mm along the boule 48

Figure 5.8: PL spectrum as a function of depth into a typical sample 75
Figure 6.7: PL spectrum for antimony doped sample 111
Figure 6.3: PL spectrum for chlorine doped sample 107
Figure 6.4: PL spectrum for copper doped sample 108
Figure 6.2: PL spectrum for oxygen doped sample 106
Figure 6.6: PL spectrum for sodium doped sample 110
Figure 6.5: PL spectrum for sulphur doped sample 109
Figure 6.1: PL spectrum for undoped sample 104
Figure 2.11: A p-n junction from an energy band viewpoint 30
Figure 5.1: Principle of a p-n junction solar cell. 64
Figure 5.9: a selection of back surface spectra 77
Figure 5.10: a selection of mid bevel spectra 78
Figure 5.11: a selection of near interface spectra 80
Figure 5.4: the setup used for electrical characterization (not to scale). 70
Figure 2.9: Spontaneous emission in a semiconductor 24
Figure 2.10: Stimulated emission in a semiconductor. 25
Figure 5.22: summary of time resolved PL data for 10 minute annealed sample 93
Figure 6.10: Temperature dependence of all near band edge peaks 116/117
Figure 5.18: Temperature dependence of PL peak intensities. 89
Figure 4.10: Total PL intensity across the wafer 53
Figure 4.3: Typical PL spectrum from the crystal boule 46
Figure 5.6: Typical profile of a bevelled CdTe/CdS solar cell (untreated sample) 72
Figure 4.13: variation in the 1.548 and 1.540eV peaks with temperature. 58
Figure 4.12: Variation of near band edge peak intensity with temperature. 56
Figure 5.19: Variation of net PL intensity with CdTe thickness in polished samples 91
Figure 5.20: Variation of net PL intensity with CdTe thickness in unpolished samples 91
Figure 5.12: Variation of peak positions with depth in polished samples 82
Figure 5.13: Variation of peak positions with depth in unpolished samples 83
Figure 5.14: Variation of the CdSxTe1-x bandgap with composition 84
Figure 2.12: vibrating linked atoms causing phonons. 26
Figure 2.2: The Wigner-Seitz cell in 2 dimensions (hexagonal point lattice). 12
Figure 2.1: A zincblende crystal lattice 11

## Equations

Eqn 5.2: Bandgap variation of CdTe with sulphur content 84
Eqn 2.1: The basis of a repeating lattice 12
Eqn 2.18: The Beer-Lambert law 21
Eqn 2.10: The Bloch wavefunction 14
Eqn 2.4: Definition of reciprocal lattice vectors 13
Eqn 2.5: Definition of reciprocal lattice vectors 13
Eqn 2.6: Definition of reciprocal lattice vectors 13
Eqn 2.25: Diode equation 30
Eqn 2.17: Effective masses of electrons and holes 19
Eqn 5.1: Efficiency of a solar cell 73
Eqn 2.24: Exciton binding energy 29
Eqn 2.2: Fourier representation of a periodic function 13
Eqn 2.3: Fourier representation of a periodic function 13
Eqn 2.29: Gaussian lineshape broadening 33
Eqn 3.1: Grating calibration formula 41
Eqn 2.30: Intensity relationship between exciting and emitted intensities 33
Eqn 4.1: Intensity relationship between exciting and emitted intensities 53
Eqn 5.3: Intensity relationship between exciting and emitted intensities 88

Eqn 2.28: Lorentzian lineshape broadening 33
Eqn 2.31: Maxwell-Boltzmann statistics for population of an excited state. 34
Eqn 2.26: Minority carrier drift current 30
Eqn 2.19: Motion of a diatomic chain of atoms 27
Eqn 2.20: Motion of a diatomic chain of atoms 27
Eqn 2.9: Periodicity requirement of reciprocal lattice 14
Eqn 2.23:Phonon energy-wavevector solutions 27
Eqn 2.27: Phonon replica spectrum 32
Eqn 4.5: Phonon replica spectrum 59
Eqn 2.7: The Schrodinger equation 14
Eqn 2.11: The Schrodinger equation with a periodic potential 16
Eqn 2.32: Solutions to Maxwell-Boltzmann equation for excited states. 34
Eqn 2.33: Solutions to Maxwell-Boltzmann equation for excited states. 34
Eqn 2.21:Solutions to motion of a diatomic chain of atoms 27
Eqn 2.22:Solutions to motion of a diatomic chain of atoms 27
Eqn 2.13: Solving the Schrodinger equation with a periodic potential 16
Eqn 2.14: Solving the Schrodinger equation with a periodic potential 16
Eqn 2.15: Solving the Schrodinger equation with a periodic potential 16
Eqn 2.16: Solving the Schrodinger equation with a periodic potential 16
Eqn 4.4: Temperature dependence of "Y" luminescence 58
Eqn 4.2: Temperature dependence of PL intensity. 56
Eqn 2.34: Temperature dependence of PL intensity. 34
Eqn 5.4: Temperature dependence of PL intensity. 90
Eqn 4.3: Thermal release of an exciton 57